ABSTRACT

Title of Document: PERFORMANCE PREDICTION OF SCALABLE FUEL CELL SYSTEMS FOR MICRO-VEHICLE APPLICATIONS.

Jeffrey Glen St. Clair, M.S., 2010

Directed By: Associate Professor Christopher P. Cadou
Department of Aerospace Engineering

Miniature (< 500g) bio-inspired robotic vehicles are being developed for a variety of applications ranging from inspection of hazardous and remote areas to environmental monitoring. Their utility could be greatly improved by replacing batteries with fuel cells consuming high energy density fuels. This thesis surveys miniature fuel cell technologies and identifies direct methanol and sodium borohydride technologies as especially promising at small scales. A methodology for estimating overall system-level performance that accounts for the balance of plant (i.e. the extra components like pumps, blowers, etc. necessary to run the fuel cell system) is developed and used to quantify the performance of two direct methanol and one NaBH4 fuel cell systems. Direct methanol systems with water recirculation offer superior specific power (400 mW/g) and specific energy at powers of 20W and system masses of 150g. The $NaBH_4$ fuel cell system is superior at low power (<5W) because of its more energetic fuel.

PERFORMANCE PREDICTION OF SCALABLE FUEL CELL SYSTEMS FOR MICRO-VEHICLE APPLICATIONS.

By

Jeffrey Glen St. Clair

Thesis submitted to the Faculty of the Graduate School of the
University of Maryland, College Park, in partial fulfillment
of the requirements for the degree of
[Master of Science]
[2010]

Advisory Committee:
Associate Professor Christopher P. Cadou, Chair
Associate Professor Kenneth Yu
Professor Gregory Jackson

© Copyright by
Jeffrey Glen St. Clair
[2010]

Dedication

There is no one else I would dare dedicate this document to. Thank you, Jenete, for your constant support, patience, and confidence in me. I love you now and for eternity.

Acknowledgements

I would like to express my thanks and appreciation to the other graduate students in my research group, namely Shyam Menon, Dan Waters, and Daanish Maqbool. They provided good advice and discussion with this thesis and even proofread some of it.

I would like to acknowledge Dr. Greg Jackson and the time he invested in helping me understand the physics and complexities behind fuel cells in general. I hardly knew what a fuel cell was when I began this research, and hopefully I have changed from that state. Dr. Jackson also provided guidance in how the research should proceed, which was appreciated. I also acknowledge his student Jenny Hu, who also provided time and patience in tutoring me with fuel cell system modeling.

I am very grateful for those at the Army Research Laboratory that took me in when things were looking grim. Dr. Brian Morgan and Dr. Ivan Lee have been great mentors and friends in the past year and have provided me with new areas of interest in a never-ending search for knowledge.

Last but not least, I would like to thank Dr. Chris Cadou, my advisor. Thank you for believing that I was smarter than I often felt and for giving me the chance to tackle a subject relatively new to both of us. Your patience and diligence will always be appreciated by me and my family.

Table of Contents

List of Tables

List of Figures

Chapter 1: Introduction.

1.1 Motivation, challenge, and the advantage of fuel cells.

The United States Army has increased its interest in robotic platforms that fly and /or crawl in recent years due to the platforms' successes in war zones. These remotely-operated platforms often aid the warfighter in areas such as sensing and scanning, communications, and defense or weaponry. They are especially useful in terrain that is difficult for human exploration, such as caves or under urban debris. Recently, the U.S. Army initiated a program with the objective of providing the warfighter with smaller, multifunctional platforms, which can act autonomously when desired. Three search and surveillance missions were presented that are of particular interest to the Army [1]: exploring a potentially hostile building, exploring a cave or demolished building, and perimeter defense. These scenarios place severe demands on the vehicles power and energy systems. In addition to the general need to maximize range/endurance, the movement of the platform may be intermittent and include sustained periods of perching and hovering or compensation for gusty winds. Thus, power requirements are also intermittent and the system would rarely reach a "steady state" operating condition. In addition, complex terrain requires crawling platforms to overcome obstacles that may be as large as the platform itself. This could require asymmetric power distribution, as well as large amounts of energy for minimal distance.

Most of the individual components of an unmanned autonomous vehicle (UAV) are electrically powered, and so it is natural that they are often designed and tested with batteries in mind [2]. However, in spite of years of improvements, batteries' energy densities remain low and as a result, fully integrated vehicles cannot meet the needs of missions described above [3]. For example, the endurance of one small (~100g) flying vehicle that could be a candidate for the missions described above is only about 10 minutes – without accounting for increased power demands associated with changing flight conditions. This short life span is inadequate for mapping a single floor of a typical office. Also, the short endurance endangers the warfighter by requiring them to place the platform directly on site as opposed to dispatching the vehicle from a safe distance.

The hovering endurance of a rotor-powered vehicle is given by the following expression:

$$E = \eta_r \eta_{pwr} \left(\frac{Q_r}{g} \right) \left(\sqrt{\frac{8\rho_{air} A}{M\ g}} \right) \left(1 - \frac{1}{\sqrt{1+\zeta}} \right) \tag{1.1}$$

where η_p is the propulsive efficiency of the rotor, A/Mg is the rotor disc loading (M is the empty weight, A is the swept area of the rotor and g is gravitational acceleration), ζ is the fuel mass fraction (fuel mass/empty weight), Q_R is the energy/mass of the fuel, and η_{th} is the overall thermodynamic efficiency of the powerplant. A derivation of Eq. 1.1 is presented in Appendix A.

Figure 1 shows how the hovering endurance of a typical 100 g micro air vehicle (MAV) – in this case Micor, a battery powered co-axial rotor vehicle [4] – depends on the energy density and overall thermodynamic efficiency of its power system. The

horizontal axis is the energy density of the fuel and the vertical axis is the overall thermodynamic efficiency of the power plant. The diagonal dashed lines are contours of endurance computed based on the Brequet range equation given in Eq. 1.1. The figure shows that the key attributes of the power system that set the hovering endurance are the energy density of the fuel and the efficiency with which it is converted. The figure demonstrates the power challenge clearly: Batteries convert their stored energy very efficiently but don't store it very efficiently (i.e. they have relatively low energy densities) and Micor's endurance is limited to about 15 minutes. While replacing batteries and electric motors with a model aircraft engine operating on 'glow fuel' (a mixture of methanol, nitromethane, and oil) greatly increases the energy density of the system, the efficiencies of heat engines at the scales necessary for the class of vehicles considered here are very low (~5%), [5] and so switching to heat engines leaves endurance virtually unchanged. Similarly, a direct methanol fuel cell (DMFC) system that meets the DARPA target energy density of 1000 W-hr/kg [6] has higher conversion efficiency than a miniature engine (~26%) and higher energy density than batteries, but neither is enough to appreciably change vehicle endurance. Therefore, the main challenge is to find a power and energy system that can deliver an order of magnitude increase in energy density over batteries in an approximately 20 g package that still delivers 'reasonable' (> 20%) overall thermodynamic efficiency.

However, other fuel cell technologies are more promising. For example, H_2-Proton Exchange Membrane (PEM) fuel cells can achieve thermodynamic efficiencies > 50% and energy densities of 1200 W-hr/kg if H_2 is stored in $NaBH_4$ [7].

Direct ammonia solid oxide fuel cells offer only slightly lower thermodynamic efficiencies (~50%) but much greater energy/mass than $NaBH_4$ and this leads to levels of performance increase (approximately a factor of 10) that justify further research. Potentially even better are solid oxide fuel cells capable of consuming liquid hydrocarbons like JP8. However, the critical question in all of these analyses is what levels of energy storage and conversion efficiency are attainable at the *system* level.

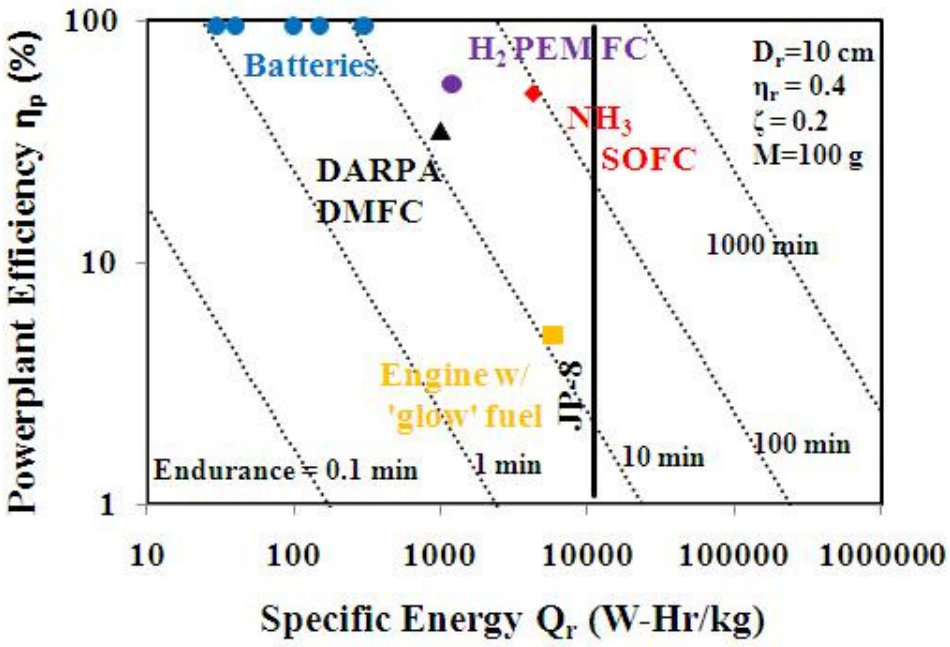

Figure 1: Performance of various batteries, fuel cells, and an engine as power and energy systems for Micor, a micro hovering vehicle (100 g). The solid black line is the energy density of JP-8.

Determining system-level performance is a complex problem – especially at scales relevant to sub-kilogram flying, crawling, and jumping sensor platforms. First, the unit cells usually must be bundled together in series or parallel to achieve the desired voltage and power. These 'bundles' are called 'stacks'. This packaging adds

weight and losses. Second, while the stack is the heart of the fuel cell system, it requires many other additional components to service it. Some examples include pumps and blowers, condensers, heat exchangers, membranes, valves, and other parts necessary for thermal management and power conditioning. The net result is that the volume, mass, and sometimes the overall efficiency of the fuel cell system can be set by the size, mass, and performance of the additional components required to service the stack.

The power/energy consumed by these subsystems is termed 'balance of plant' (BOP) and can become increasingly important as the size of the fuel cell system is reduced. The conversion efficiency of the overall fuel cell system is determined by the operating voltage, fuel utilization in the cell stack and by the parasitic losses associated with fluid pumping, fuel pre-processing (as needed), thermal management, and power conditioning. These parasitic losses become more significant with decreasing fuel cell size because of the aforementioned increased surface area/volume ratio and can reduce or even eliminate the advantage of using high energy density fuels in small-scale systems [8]. As a result, power densities reported in the literature - which are usually of MEAs or stacks - do not translate directly into system-level power density, and overall efficiency and balance of plant must be accounted for in order to make meaningful comparisons between different fuel cell technologies. The objective of this work is to provide a methodology and computational tool for predicting the performance (power density and energy density) of miniature fuel cell systems by considering the performance of the fuel cell stack as well as the overall balance of plant.

1.2 Previous work.

There are a number of example analyses including balance of plant in kW-scale power systems like a high temperature PEM fuel cell system that operates on reformed diesel fuel [9], a bus powered using a fuel cell/battery system [10], and a stationary, residential PEM fuel cell system that uses reformed methane [11]. Some simulations look into individual issues inside the system, such as anode CO tolerance [12] or water balance [13] of the MEA. Doss et al. used a model that was built in-house that simulates a gasoline reformer system coupled with fuel cells for automotive applications [14, 15]. The investigation was a parameter study to provide insight into how the autothermal reformer (ATR) temperature, pressure, and fuel to air ratios affect the system and reformer efficiencies. System efficiencies up to 40% were attained with this model. However, none of these studies provides any insight into how these systems would perform if scaled down for use in the miniature sensor platforms envisioned by the U.S. Army. Another balance of plant investigation involved modeling of a reversible fuel cell system, which is a system that uses electricity to dissociate water in order to make and store H_2. When power is required of the system, the hydrogen is fed to a PEM fuel cell. This reversible system showed good agreement with its experimental counterpart, however the system appears far too complex to scale down to the Army's needs [16]. While some system studies have been performed for small-scale power applications [17], they often assume component efficiencies based on larger applications. Other studies have given insight into the fuel cell performance through mathematical modeling, but these models do not include the balance of plant that would support the fuel cell under consideration

[18, 19].

Benavides et al understood the complexity of scaling down balance of plant components, and focused their efforts on the DC to DC converter to improve system efficiency and mass [20]. While much insight can be gained from these models, they are insufficient in determining whether a fuel cell system is the solution to the Army's needs.

In summary, what is required is a thermodynamic model of a fuel cell system that incorporates the entire BOP and is designed to address the specific missions the Army envisions for its microsystems. Such a model is required to assess the relative merits of various power/energy systems being considered for these missions but at present one does not exist. This thesis seeks to create one.

1.3 Objectives and approach.

The overall objective of this thesis is to identify a fuel cell power system that is well-suited for powering the miniature flying, crawling, and hopping vehicles being developed for the three mission scenarios of the U.S. Army's Collaborative Technology Alliance (CTA) in Micromechanics [1] described in section 1.1, and whose performance exceeds that of batteries. The challenge is that what is usually reported in the literature is MEA performance whereas overall system performance (i.e. system level power and energy density) is required in order to assess suitability for the CTA applications. Unfortunately, the latter is usually not available because balance of plant considerations make it highly dependent on scale (i.e. physical size) and the particulars of the application (mission environment, profile, etc.). The objective here is to provide a methodology and computational tool that can be used

when the size and application details are known. The fuel cell system model would predict the system performance described above and can be used to analyze the advantages of a hybrid fuel cell/battery system over a battery only system. Since there are many types of fuel cells and possible implementations, it is not possible to do complete system-level analyses for each possible fuel cell-based power system. Therefore, a multi-step approach is taken.

The first step is to narrow the field of candidate technologies. This is accomplished by performing a survey of current fuel cell technologies that establishes the level of performance that is available today (at the MEA/stack level) and summarizes the advantages and disadvantages of different technologies. Hydrogen-based PEM fuel cells are not included in the survey because the specific energy of compressed or liquid hydrogen is too low; instead more research is conducted on fuel reformers that provide the PEM cell with H_2 from another fuel source. Also, some of the literature reviewed compares results with a typical PEM fuel cell, providing a good baseline for comparison. Solid oxide fuel cells are also not included in the survey because the high temperature operation could mean an excessive system complexity for MAV applications. Items of interest include what type of fuel and oxidizer are used, power density, efficiency, operating temperatures, and an estimate of the overall complexity of the entire system in a real application. The results of this survey are used to generate a semi-quantitative ranking of each candidate technology's suitability for the three CTA mission scenarios and to identify two or three technologies worthy of further study.

The second step is to perform a more detailed system-level analysis of the

promising technologies identified in step one. This is accomplished by assembling a system model from physics-based models of each component. Particular attention is paid to properly representing how the performance of all system components - not just the fuel cell - changes with size.

The third step is to use the system models to compare fuel cell to battery-based power systems using a baseline mission of a micro-air vehicle that weighs 225 g or less. The influence of mission profile is investigated by repeating the comparison for alternate missions. The outcome will be an improved understanding of the capabilities and limitations of fuel-cell based power systems in small unmanned air vehicles.

1.4 Thesis structure

This chapter has explained the overall motivation for developing miniature fuel cell-based power systems and the challenges associated with assessing fuel cells' suitability for various autonomous sensor platforms being developed by the U.S. Army. Balance of plant is identified as the critical parameter governing fuel cells' applicability at these scales and a research program is outlined for addressing the gaps in the literature.

Chapter two presents an overview of fuel cell fundamentals, as well as a survey of fuel cell technologies that appear to be most relevant/suitable for the miniature vehicle application. Hydrogen storage and some current reforming technologies are also discussed. The critical parameters of interest for the survey are power density, operating temperature, efficiency, system complexity and type of oxidizer used. Chapter three discusses the survey results presented in chapter two and

develops a semi-quantitative methodology for ranking each fuel cell system based on its suitability to the CTA missions. Three technologies worthy of additional consideration are identified.

Chapter four presents the system model used to simulate one of the promising candidates, a direct methanol fuel cell. Detailed models of each component are developed and water recirculation is incorporated.

Chapter five presents results from the system simulations. Power densities and efficiencies are computed and the influence of water recirculation is quantified. A case study is presented to compare the mission performance of a battery-only power system to a hybrid fuel cell/battery system. The advantages of a hybrid system are discussed.

Chapter six summarizes the major conclusions of the thesis and makes recommendations for future work.

Chapter 2: Survey of Advanced Fuel Cell Technologies.

The objective of this chapter is to survey current fuel cell technologies that have been researched at the component level (reformer or fuel cell stack only) and to summarize the advantages and disadvantages of each. Items of interest include what type of fuel and oxidizer are used, power density, efficiency, operating temperatures, and an estimate of the overall complexity of the entire system in a real application. The discussion begins with energy storage and continues with a survey of reformer technology. Fuel cell technologies are then presented with an overview on the basic principles of operation followed by summaries of the state of the art for each type of fuel cell. A summary of the findings is then presented.

2.1 Energy storage media: capabilities, advantages, and challenges.

The most energetic fuel per unit mass for fuel cells is the same as for standard combustion: hydrogen. Pure hydrogen has a large specific energy (120 MJ/kg) when it reacts with oxygen, and its waste product is water. A major concern with using hydrogen directly for fuel cells is storage and transportation of the fuel. Storing gaseous hydrogen can be hazardous because of its high pressure and propensity to leak. This is especially a concern for the automotive industry and portable devices. Another concern is that hydrogen is a gas at normal temperatures and pressures so its energy density is very low, and it is not possible to store a significant amount without a large or heavy (i.e. high pressure) tank. This is illustrated in Figure 2. As the

pressure is increased to achieve a energy density closer to liquid hydrocarbon (LHC) fuels, the specific energy drops to inadequate levels.

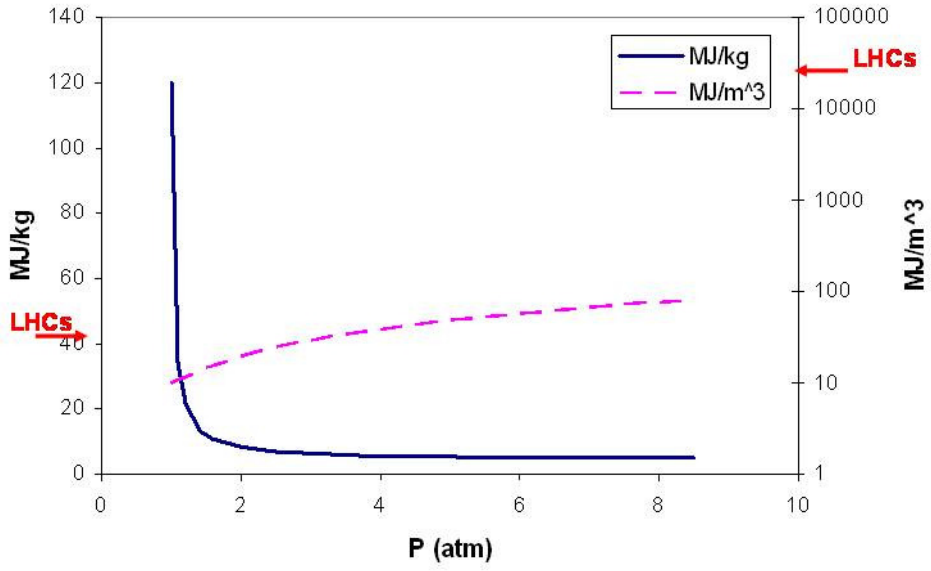

Figure 2: Specific energy and energy density vs. pressure for a H_2 gas tank

An alternative to storing pure hydrogen is storing it within a larger, more complicated molecular compound like liquid hydrocarbons. While this lowers the overall energy density, it can make storage more efficient and safe. The removal of hydrogen from a carrier is generally called reforming, and the process generally has strict conversion requirements when combined with a hydrogen based fuel cell. Often unreformed fuel can damage the membrane and lower performance to undesirable levels.

Ammonia can also be viewed as a hydrogen carrier but it poses some safety challenges due to its toxicity. Less-hazardous ammonia-carriers have been investigated. One option is storing the ammonia in metal ammine salts. For example, $Ca(NH_3)_8Cl_8$ can store hydrogen at a relatively high gravimetric hydrogen density (just under 10%) [21] and also releases the ammonia at lower temperatures than other

carriers like $Mg(NH_3)_8Cl_8$, requiring less energy. Table 1 provides a comparison of non-hydrocarbon hydrogen carriers' energy densities. Ammonia stored in metal ammines is also less toxic than gasoline. Ammonia borane (NH_3BH_3) has also been considered as an ammonia carrier. The substance is easy to transport as a solid and is non-toxic [22].

Regardless of the carrier, Ammonia decomposition to hydrogen is endothermic, and heat is also needed to extract the ammonia from the carriers. Therefore, a reformer is required for any of these storage methods and therefore the challenge of devising an efficient integration of the reformer and fuel cell remains.

Table 1: Energy Densities of Hydrogen Carriers [21]

Carrier Name	Phase	Specific Energy (MJ/kg)	Energy Density (MJ/L)
$Ca(NH_3)_8Cl_2$	Solid	11.76	13.8
$Mg(NH_3)_6Cl_2$	Solid	11.01	13.08
NH_3	Liquid	12.5	12.96
H_2	Liquid	120	8.52
Mg_2NiH_4	Solid	3.06	4.8
$LaNi_5H_6$	Solid	1.64	4.32
$NaAlH_4$	Solid	4.2	3.12
H_2 (200 bar)	Gas	2	1.68

Another class of hydrogen storage compounds is the borohydrides. These solid state storage compounds can be reformed in a decomposition reactor to produce H_2 like the metal ammines or they can be used directly in a fuel cell when placed in an aqueous solution. The metal ammine salts are generally lighter in weight than metal hydrides. Ponce de Leon et al. wrote a review of progress being made and challenges to consider for these direct borohydride fuel cells in 2006 [23]. Borohydrides produce higher open circuit voltages than methanol and can attain

similar power densities at lower operating temperatures. A recent review of hydrogen storage carriers [24] included borohydrides and compared them with nitrogen based hydrides. It also found that sodium and lithium borohydrides have lower hydrogen yields (on a gravimetric basis) than ammonia or ammonia borane. In 2007, Millennial Cell Inc. was developing a hydrogen source based on the hydrolysis of sodium borohydride [25]. This process is exothermic giving it an advantage over ammonia and the metal ammines described above. A systems study showed that a heat exchanger could be used to recover the heat of decomposition thereby doubling the hydrogen production rate of their reactor to 400 SLPM/L. Operating temperatures were moderate (around 150 °C) and the temperature distribution within the reactor was uniform which improved fuel conversion and catalytic effectiveness.

Light alcohols are of particular interest due to their relatively high energy densities (12-36 MJ/kg) and potential to be produced from bio-mass. Fuels like ethanol and methanol are like borohydrides in that they can be used directly in a fuel cell, or reformed to create H_2. However, using these fuels directly requires them to be in an aqueous solution which lowers the effective energy density. These alcohols will be discussed further in this chapter.

2.2 Reformers.

2.2.1 Ammonia

One of the earlier investigations of miniature ammonia reformers was carried out by Arana et al. at MIT [26]. The reactor used 4 silicon nitride tubes in a double-u formation that also functioned as a heat exchanger. A schematic of the reactor

geometry is presented in Figure 3. Ammonia cracking takes place in one of the tubes while the other provides the necessary heat. The catalyst was iridium amine on alumina and the tube length was a little less than 3 mm. Up to 97% of the ammonia was converted to hydrogen with a thermal input of 1.8 W – supplied using electric heaters not the other tube for the purposes of the experiment. The authors interpreted the high conversion to be almost 1.6 W of H_2, based on the LHV. In a reactor that is 0.12 cm^3 in volume, this translates to a power density of over 13 W/cm^3 before accounting for the necessary auxiliary components which take up the better part of the system volume. The author noted that common hurdles for miniature "generators" are tight fabrication and geometries, parasitic losses associated with pumps, blowers, and power management, and thermal losses. Insulation can actually be bad for small systems, depending on the conduction and convection coefficients of the insulation and air respectively. For example, the authors found that adding insulation to a channel with a radius smaller than 1 mm would increase thermal losses by increasing its exterior surface area. That being said, an improvement in performance was expected when other improvements in thermal management were made like vacuum packaging and adding heat shields. Finally, the effect of improved thermal management will be limited if the parasitic losses associated with pumps and/or other components are comparable to or larger than the thermal losses.

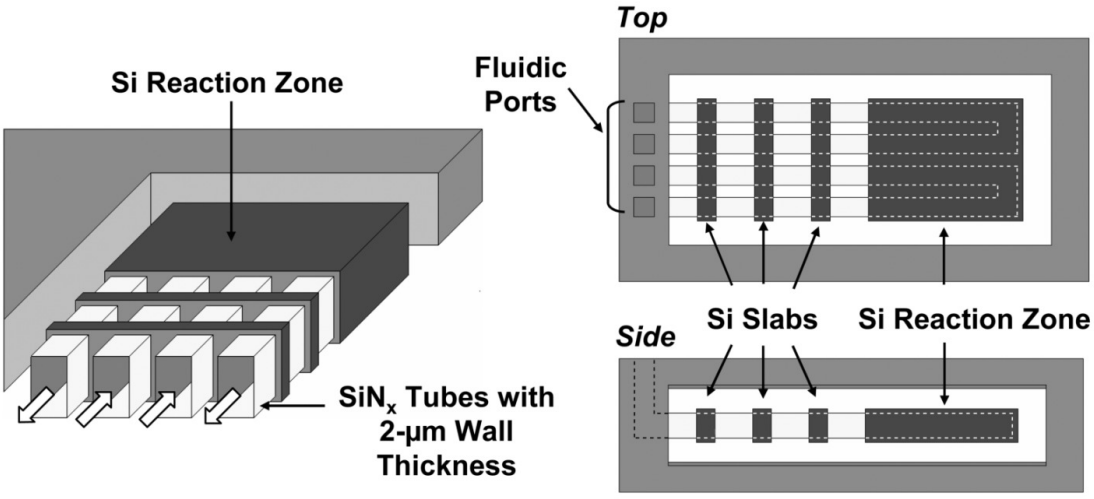

Figure 3: Schematic illustration of the suspended-tube reactor [26]. In the fabricated device, each tube is 200 μm wide by ~ 480 μm high. A 3-slab reactor is shown in the figure. Reactors with up to 7 slabs have been fabricated.

Another group at MIT developed a system model of a SOFC operating on ammonia. [27] The model included butane-fueled catalytic burners to maintain the SOFC's operating temperature. The goal of the model was to maximize energy density while meeting a specific power demand. The authors noted that ammonia was not fed directly to the SOFC so as not to form large amounts of NO. Yttria stabilized zirconia (YSZ) was assumed for the electrolyte, nickel (Ni) +YSZ cermet for the anode, and strontium doped lanthanum manganite (LSM) +YSZ cermet for the cathode. Ruthenium (Ru) was used to decompose the ammonia in the reactor. The specifications made in the model produced around 1 W at 0.65 V. It was found that increasing the electrolyte thickness increased efficiency and also improved mechanical stability. As the thickness increases, so does the active electrochemical surface and the current density through the electrolyte decreases, causing a reduction in activation overpotential. Other conclusions were drawn about the SOFC, which

was the primary interest of the research. However, the most relevant conclusion for the purposes of this thesis was reiteration of the fact that thermal management will be a critical issue when designing an optimal ammonia based system. The authors indicated that radiation shields and vacuum packing could be necessary to reduce heat losses.

In 2004, a few publications by J.C. Ganley focused on ammonia reformers that were not coupled with any fuel cells [28-30]. The first publication focused on finding cheaper alternatives to Ru for an ammonia reformer catalyst [28]. The authors argued that there are many catalytic activity correlations in the literature that are meant to encompass most types of catalysts, but these analytical results differ from one another. Therefore, the research focus was to evaluate each catalyst experimentally and to determine if a single correlation could be found that accurately describes the performance of all of these catalysts. The catalysts were deposited onto alumina foam pellets, and the foams were used in a quartz tube reactor. The reactor was heated by a temperature-controlled tube furnace. The results indicated that Ru gave the highest reaction rates by far with Ni taking second place at 61% the reaction rate of Ru. Based on these results, Ru was selected for all subsequent experiments.

The first of these studies considered monolithic anodized alumina posts for supporting the Ru catalyst in a microreactor [29]. The large surface area of this array of posts modestly increased activity compared to other supports while avoiding issues like fluid bypassing (clogs), thermal non-uniformity, and mechanical strength/stability. The results were relatively promising in that 50 sccm of NH_3 in a penny-size reactor produced 46 sccm of H_2 which translates to about 13 W of power

in a 'typical' PEMFC. This is enough power to run small electronic devices. Ammonia conversion decreased with flowrate and increased with temperature making it difficult to increase power density without increasing operating temperature. The authors concluded that more work needed to be done on the reactor geometry and this was one of the items considered in the next study.

The geometry study included a comparison of various post and channel-based flow arrangements as well as various methods for altering the chemistry including hydrothermal treatment of the supports, whether or not to use a potassium promoter, and changing the type of catalyst precursor [30]. Similar to the previous study, Ru deposited on anodized alumina served as the catalyst. The authors found that channels worked better than posts and smaller channels increased the conversion of ammonia. Hydrothermal treatment and potassium promoters also improved performance, and the original design for a catalyst precursor, $RuCl_3$, was the better option. Incorporating all of these improvements into one reactor led to 99% conversion at 600 °C and a flow rate of 0.25 sccm which corresponds to roughly 60 W worth of H_2. Given that the size of the reactor was 0.35 cm^3, this gave a volumetric power density of about 180 W/cm^3 which is quite impressive for a small scale reformer. It was concluded that although the reformer is only a part of the entire system, it could meet or exceed the requirements of a typical portable power applications which require approximately 20 W within a 0.5 cm^3 volume.

Ammonia decomposition for H_2 production was also being investigated by researchers in Denmark [31]. One study focused on using porous graphite for catalyst supports. The activity of Ru on graphite was found to be orders of magnitude higher

than Ru on alumina for the same reactor geometry. Promotion using Ba or Cs could further enhance the performance of the reformer. However, high Cs loading also lowers the required operating temperature causing a shift in equilibrium back to NH_3. Therefore, removing either the NH_3 or H_2 during the process is necessary. The two options suggested by the author were to divide the reactor into two stages and remove the NH_3 to a second smaller, hotter reactor, or bleeding the H_2 through a Pd membrane thereby increasing the fraction of NH_3 in the reactor and causing it to decompose. The membrane would also provide the fuel cell with pure H_2 fuel.

The U.S. Army has also investigated technologies using ammonia as fuel [32]. Hydrogen Components Inc. had their Ammonia Hydride Hydrogen Generators (AHHG) tested by the Army (CERDEC). The ammonia is stored in vapor form in a cartridge which plugs into the lithium aluminum hydride ($LiAlH_4$) reactor bed. The hydride and ammonia produce H_2 which is fed through a filter, or 'getter', to remove the NH_3 before entering the fuel cell stack. The hydrogen is generated on-demand as it is consumed using a pressure check valve system. The fuel cell is a Proton Exchange Membrane (PEM) system by Ball Aerospace. The reactor was tested at different power demands. The system operated stably at lower power levels (5W), but 50 W demanded too much of the system. Higher power levels led to more unconverted ammonia leaving the reactor, saturating the ammonia getter, and restricting hydrogen flow. At the 5W level, an energy density of 483 W-hr/kg was provided, and the reactor could run autonomously for 50 hrs. However, the reforming system alone weighed almost 1 kg, which is much larger than the desired system weight for MAVs.

Incomplete conversion of ammonia can have more serious consequences than simply clogging a getter. For example, Uribe studied the effects of unreformed ammonia on a Nafion proton exchange membrane with catalyst layers prepared from carbon supported 20% Platinum (Pt) [33]. The cell size was 5 cm^2. His results showed that traces of ammonia in the anode cause a decrease in cell current while larger amounts (130 ppm) can damage the membrane irreversibly limiting operation to only a few hours. As a result, great care must be taken when using ammonia with PEM cells to ensure that conversion is complete.

In summary, PEM cells coupled to NH_3 decomposition reactors have great potential assuming the ammonia doesn't find its way to the PEM cell. However, the main problem with ammonia-based systems is that whatever route is taken, direct or indirect, there will be an extremely hot (above 600 °C) component in the system. As a result, thermal management will be the critical barrier to implementing miniature NH_3-based fuel cell power systems for 100 gram-scale vehicles.

2.2.2 Liquid hydrocarbons

Hydrocarbon fuel reformers have received much attention for hydrogen production. One such reformer has microchannels on each side with different catalysts to utilize two different ethanol reforming reactions at the same time [34]. Ethanol autothermal steam reforming takes place with a Co/ZnO catalyst at lower temperatures (500 °C). The process is endothermic. On the bottom side, total oxidation of ethanol using a CuMnOx catalyst takes place, which is an exothermic process. Thus the bottom side provides heat for the top side reactions to occur. Complete ethanol conversion was observed at operating temperatures higher than 400

°C. Hydrogen selectivity, which is the amount of hydrogen atoms from the reactants that form H_2, hovered around 60% for the temperatures tested. These high selectivities amounted to a reformer efficiency of 71%, or 0.9 STP mL/min of H_2 was formed from 0.36 STP mL/min of ethanol.

Ethanol can also be partially oxidized to for H_2 through catalytic combustion. Behrens et al. investigated different operating regimes of their reactor, focusing on equivalence ratio of the fuel [35]. When the ethanol (or butanol) was combusting at a slightly fuel rich regime, partial oxidation occurs and H_2 was formed. The hydrogen selectivity attained is only 18%. The catalyst, a slurry mixture containing rhodium (Rh) on a γ-Alumina coated surface, provides a cheaper alternative to other types of catalysts used in reforming.

Another group investigated a micro-methanol steam reformer that uses solar energy for the endothermic reforming process [36]. The reactor was first tested with a green (argon) light laser and achieved efficiencies around 5%. The carbon selectivity to CO was 11%. The catalyst was made of fine particles (CuO/ZnO/alumina) that were loaded onto the surface using pulsed laser ablation technology. The efficiency dropped by half when the technology was tested with a simulated solar light.

A three dimensional simulation was built to study the effects of operating conditions and geometry on a methanol reformer [37]. Parameters like channel size, flowrate and inlet/outlet configurations were varied and tested to see if improvements could be made on an existing reformer. The reformer with a central inlet and two outlets improved the methanol conversion ratio to 42.3% (the previous design with

the inlet and outlet on opposite sides attained 32.4%) and decreased CO production. Larger channel widths (0.9 mm) also improved the performance in these areas.

In summary, the liquid hydrocarbon reformers have great potential in providing a PEM fuel cell with the hydrogen it requires. These reformers, like ammonia reformers, require high temperatures to ensure high conversion efficiencies; therefore thermal management will also be a challenge with a system that utilizes these technologies.

2.2.3 Other types

Aluminum functions like a fuel when used to reform water to make H_2. Aluminum reacts with water over a catalyst producing H_2 and Al_2O_3. A group from Samsung investigated this concept for fuel cell reformer applications [38]. An efficiency of 78.6% with respect to the aluminum reaction enthalpy was attained when NaOH is mixed with the water and CaO promotes the aluminum. Lifetime concerns arose during testing however, because H_2 was not produced after the first hour of operation.

2.3 Fuel cells.

For the purposes of this thesis, a fuel cell is defined as a device that converts chemical potential energy stored in fuel molecules into electrical power by reacting it electrochemically with oxygen in the air. A unit cell generally consists of an electrolyte located between two electrodes - a positive anode and a negative cathode - as illustrated in Figure 4. Fuel is fed to the anode, while oxidizer (air) is supplied to the cathode. The electrolyte is impermeable to fuel and oxidizer molecules but allows

transport of certain ionic species produced by electrochemical reactions occurring at the electrodes The transport of the ions through the electrolyte is driven by the difference in chemical potential between the two electrodes. The ions create an electric potential which drives the electrons through an external load. Where reaction products are produced depends on the type of fuel cell. Since the reactants (both the fuel and oxidizer) are usually stable at normal temperatures and pressures, a catalyst is often needed to ensure that the ionized species are present in adequate quantities. Catalysts are generally rare earth metals like Pt or palladium (Pd), although researchers are constantly looking for alternatives. Electrolytes can be either solid or liquid, depending on the type of cell.

One way to classify fuel cells is based on how fuels are reformed in the cells to species that are better suited for the particular type of cell. Indirect means that the fuel is reformed in a separate component before it enters the fuel cell. Often the reformate is hydrogen which is required for use in PEM fuel cells. In direct fuel cells, the reforming process occurs within the MEA. An example is the direct methanol fuel cell (DMFC).

Another classification is based on how the reactants enter the fuel cell. An actively-fed fuel cell uses pumps, blowers, or fans to introduce the reactants, whereas a passive system uses diffusive or naturally convective methods like CO_2 bubbles in the effluent flow. Passive fuel cells may have higher system efficiencies because they have fewer parasitic processes; however they often suffer in other areas such as power density and low flow rates. They also can be more expensive to produce. For

example, while an actively pumped DMFC requires 10 times the catalyst loading of a PEM cell, a passively fed DMFC requires even more [39].

2.3.1 Proton exchange membrane fuel cells

2.3.1.1 Operating principles

Proton Exchange Membrane fuel cells are perhaps the most well known. Figure 4 is a schematic of a PEM cell, with the fuel being hydrogen and the electrolyte being a polymer membrane, such as Nafion ®. The reactions that take place at the electrodes are:

$$\textbf{Anode: } H_2 \rightarrow 2H^+ + 2e^- \quad (2.1)$$

$$\textbf{Cathode: } 2H^+ + 2e^- + \tfrac{1}{2} O_2 \rightarrow H_2O \quad (2.2)$$

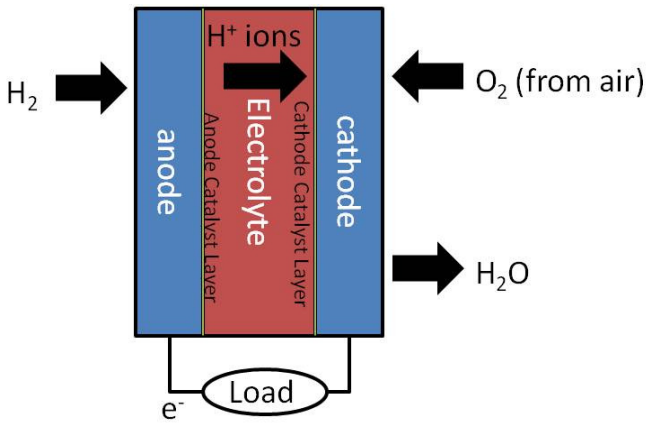

Figure 4: Proton exchange membrane fuel cell schematic.

Because the fuel is H_2, the system is carbon free and the only product is water. Hydrogen has a high gravimetric energy density, can produce high voltages, and is quite diffusive so it can produce high power densities. PEM cells also operate at relatively low temperatures and have relatively short start-up times. The greatest disadvantage of this type of cell is the problem of supplying and/or storing hydrogen which has been discussed in the previous section.

To overcome the impracticality of H_2, a PEM fuel cell is often combined with a fuel reformer. The reformer takes other types of fuel and converts them to H_2 plus other byproducts, some of which will be CO if the fuel is a hydrocarbon. Since the anode catalyst is easily poisoned by CO, great care must be taken when reforming hydrocarbon fuels to ensure that only H_2 enters the fuel cell. The separation hardware adds size, mass, and complexity. Water and thermal management are also concerns for PEM fuel cells. The membrane must remain hydrated in order to conduct H^+ ions, but cannot be flooded either. The narrow, low operating temperature range of the cell often requires additional components like heat exchangers to be added to the system. This increases complexity and balance of plant losses.

2.3.1.2 State of the art

The state of the art in PEM fuel cells was not reviewed because it was beyond the scope of this thesis. This technology has also been around for quite some time. There is an extensive amount of research done in improving this technology, yet it is felt that little progress has been made. This suggests that the solution should be looked for elsewhere. The other technologies that are presented occasionally provide a comparison with H_2 fed PEM fuel cells as a point of reference. These have been considered sufficient for the current work.

2.3.2 Solid oxide fuel cells

2.3.2.1 Operating principles

Solid Oxide Fuel Cells (SOFC) operate at high temperatures, usually above 600 °C so that ionic conduction of oxygen ions through the electrolyte can take place. Whereas researchers of PEMFCs are trying to increase operating temperatures to

improve performance, SOFC researchers are trying to lower the temperature in order to expand the types of materials that can be used and to reduce problems with coefficient of thermal expansion (CTE) mismatches that constrain how components can be connected to each-other without failing during thermal cycling. Complexity is increased because means to heat the stack and control its temperature must be provided. The thermal time constant of the stack also limits transient performance. On the other hand, high temperature operation also has some very important advantages. First, kinetics can be fast when compared to other FC types. Second, hydrocarbons can be directly used as fuel which eliminates the need for a reformer and CO poisoning is not an issue. A schematic of an SOFC is given in Figure 5. When methane is used as a fuel in a SOFC, the following overall reactions occur at the electrodes:

$$\textbf{Anode: } CH_4 + 4O^{2-} \rightarrow CO_2 + 8e^- + 2H_2O \quad (2.3)$$

$$\textbf{Cathode: } 8e^- + 2O_2 \rightarrow 4O^{2-} \quad (2.4)$$

So far, the high temperature requirement has restricted applications to relatively large-scale stationary power. Improvements in thermal management, however, could make SOFCs more attractive for small-scale portable power applications.

2.3.2.2 State of the art

Solid oxide fuel cells were also considered beyond the scope of this thesis, with the exception below. This decision was made due to the concerns associated with high temperature operation. Fournier et al. studied solid oxide fuel cells using ammonia as the fuel [40]. The objectives were to determine which stabilized zirconia electrolyte performed best and to compare anode materials. It was concluded that among Pt, Ag, and Ni cermet anodes, Ni cermet was the most suitable. It was also

found that yitria stabilized zirconia electrolytes performed better than the calcium type. A maximum power density of approximately 75 mW/cm^2 was achieved at 800 °C, which is comparable to other small fuel cell designs. At high temperatures (above 700 °C), ammonia performed better than hydrogen with an 11 mW/cm^2 increase in power density. This is explained by the orders of magnitude difference between the equilibrium constants for dissociation of H_2 vs. NH_3, which results in different cell potentials.

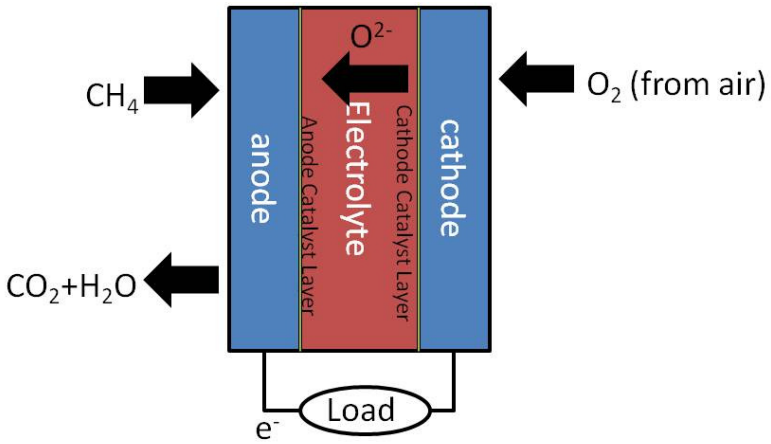

Figure 5: Schematic of a solid oxide fuel cell using methane as fuel.

2.3.3 Direct methanol or ethanol fuel cells

2.3.3.1 Operating principles

A variation on using hydrogen with a PEM fuel cell is using light alcohols directly without a reforming process. The most common fuels under consideration for use in this way are methanol and ethanol. Figure 6 is a schematic of a direct alcohol fuel cell, using either ethanol or methanol. Using the fuel directly can reduce system complexity as well as eliminate the concern for hydrogen storage. These fuels can also be produced from biomass, or "out in the field" sources, which could

improve replenishment time. However, the fuel must often be heavily diluted in water (~10% by weight) in order to protect the electrolyte from carbon build up which leads to poisoning of the cathode. The dilution drastically reduces the effective energy density of the entire system unless the water is recirculated. In addition, water recirculation carries the penalty of increased system complexity. The direct methanol fuel cell (DMFC) suffers from two major problems: slow oxidation and methanol crossover through the membrane. Methanol crossover refers to the diffusion of methanol through the membrane to the opposite electrode side. This can damage the membrane and block sites intended for proton conduction. The reactions that occur at the electrodes are:

$$\textbf{Anode: } CH_3OH + H_2O \rightarrow CO_2 + 6H^+ + 6e^- \quad (2.5)$$
$$\textbf{Cathode: } 6H^+ + 6e^- + 1.5O_2 \rightarrow 3H_2O \quad (2.6)$$

Ethanol has the following overall reactions occur at the electrodes

$$\textbf{Anode: } C_2H_5OH + \mathbf{3}H_2O \rightarrow 2CO_2 + 12H^+ + 12e^- \quad (2.7)$$
$$\textbf{Cathode: } 12H^+ + 12e^- + 3O_2 \rightarrow 6H_2O \quad (2.8)$$

A problem with ethanol fuel cells is that ethanol has slow oxidation kinetics with Pt-based catalysts, which are typically used for PEM fuel cell anodes. Partial oxidation of ethanol produces acetic acid. This lowers the electron count from the ideal case of 12 electrons per ethanol molecule when the products are CO_2 and H_2O to only 4 per molecule. The power densities obtainable with ethanol have been shown to be about 1/7 of what could be obtained with a direct methanol fuel cell. And, power densities of alcohol-based fuel cells are often an order of magnitude smaller than a PEM cell running on pure H_2 [41].

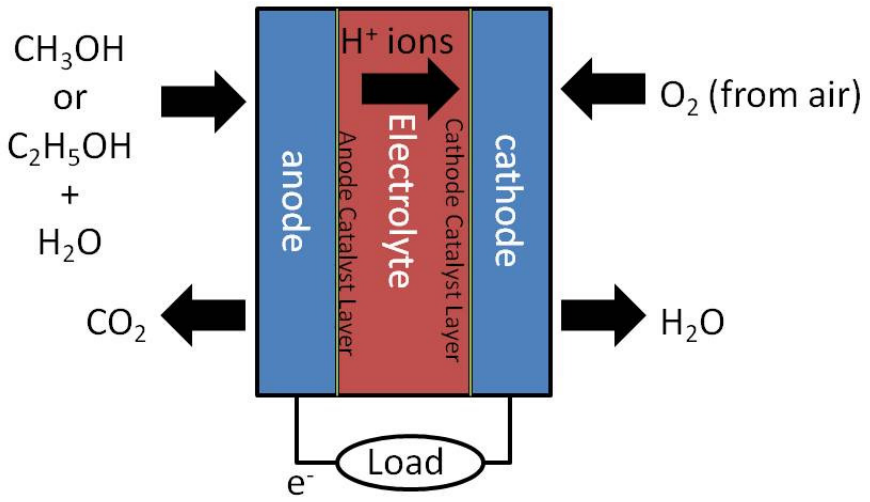

Figure 6: Schematic of an acidic-based direct alcohol fuel cell using either methanol or ethanol for fuel.

2.3.3.2 State of the art

A study was conducted in 2006 to investigate the performance of a passive direct methanol fuel cell under different operating conditions. The effects of fuel concentration, catalyst loading, membrane thickness, reactant supply mode, and long term operation were investigated [39]. The maximum power density of 45 mW/cm^2 was achieved with 5 M methanol and a catalyst loading of 8 mg/cm^2. The methanol concentration associated with maximum power was found to be higher in a passive cell than in an active one. This is because slower mass transport in passive cells leads to higher cell temperature because less heat is carried away by the reactant supply flow. The higher temperature leads to higher kinetic rates at the anode and cathode. However, it is noted that methanol crossover must be reduced and fuel feed concentration must be increased in order to achieve acceptable system-level energy and power densities.

Kim, in 2006, considered a vapor fed passive fuel cell where the pure methanol is vaporized before it enters the anode [42]. Liquid fed passive DMFCs have higher methanol crossover than vapor fed DMFCs, but achieve better power densities because of higher catalytic activity and water back diffusion from the cathode that helps maintain anode humidity. The higher catalytic activity was due to higher operating temperatures caused by greater methanol crossover; however, performance degradation was observed after a few hours. The authors found that the vapor fed system had a higher fuel efficiency as well as energy density, compared to a liquid fed system. The power density of the membrane was around 30 mW/cm^2. Similar conclusions were reported by a different group, although their power densities for a passively fed system were in the tens of mW/cm^2 [43]. The author of this study also noted that passive approaches improve system efficiency, durability and reliability, and that a planar serial connection is more desirable than stack geometry.

A study by Ye et al. investigated a methanol fuel cell driven by natural circulation [44]. This involved using the buoyancy of CO_2 gas produced at the anode to draw in fresh reactants instead of a pump. The authors found that longer inlet tubes improved performance but limited applicability at small scales. For example, power densities in the range of 30 mW/cm^2 are achievable but require an inlet tube length of 2.4 m. A convenient aspect of this arrangement was that the feed flow rate increased naturally with current density which means that this DMFC was self-regulating and could operate in a load-on-demand mode.

Another variation on the direct methanol fuel cell involved using carbon nanotubes as supports for the Pt/Ru catalyst [45]. A power density of 62 mW/cm^2 at

60 °C was achieved using pure oxygen at the cathode. The power density was about 20 mW/cm^2 lower using regular carbon supports. Even though performance would be lower using air at the cathode, it appeared that carbon nanotubes could increase the performance of other DMFC designs that have achieved high performance using air.

The catalyst isn't the only component within the cell that could benefit from the use of nanomaterials. Nanocomposite membranes have also been considered for use in DMFCs [46]. They are less expensive than Nafion ® and allow less crossover and better proton conduction. While this study focused on the characterization of the membrane, the authors did conduct a performance comparison test. At lower concentrations, the membrane performed worse than the standard Nafion ® membrane. At a concentration of 5 M methanol however, the nanocomposite membrane performed better. At 90 °C, a power density of 125 mW/cm^2 was attained with oxygen as the oxidizer. It was not clear whether the membrane could be operated at higher fuel concentrations and the degree to which the higher performance is due to the high temperature and pure O_2 oxidizer. However, the results are promising and confirm the belief of many researchers that changing the membrane could increase performance.

Tain et al. in 2008 attempted to improve the performance of a Nafion® membrane by impregnating it with a poly(1-vinylimidazole)/Pd composite [47]. The modification improved performance at lower temperatures mostly by decreasing methanol crossover. At 80 °C however, crossover became problematic again. At 5 M fuel concentration, a maximum power density of about 130 mW/cm^2 was achieved

using oxygen as the oxidizer. This seems to be an improvement over the nanocomposite membrane.

Another study to note used a combination of catalyst coated membranes (CCM) and catalyst coated substrates (CCS) for the electrodes [48]. The combination of the CCM anode and CCS cathode performed better than having both electrodes of the same type. One reason was that there was less fuel crossover. The authors also showed how temperature can have a substantial effect on power density. The mixed system produced 130 mW/cm^2 at 70 °C but decreased down to around 80 mW/cm^2 at 50 °C. The oxidizer was air and not pure O_2, and the results show this mixed coating technique could be a promising idea for DMFCs.

The last study considered for direct methanol fuel cells focused on how the cathode channel depth could change the performance of the cell [49]. Hwang et al. found that changing this geometric parameter had a significant impact on the performance because it changed the linear velocity and the internal pressure distribution. Decreasing the depth from 1 mm to 0.3 mm could increase power densities by approximately 20 mW/cm^2. The pressure drop and linear velocities were calculated and simulated with CFD software to confirm the cause for the increase in power density. Increasing the internal pressure increased performance - most likely because of the increase of oxygen partial pressure. The maximum power density achieved at 80 °C was an impressive 140 mW/cm^2, a value that makes this study stand out among the DMFC technologies investigated.

In 2006, an anode study was performed for a DEFC that combined tin with a ruthenium/ platinum catalyst [50]. The fuel cell produced 50 mW/cm^2 with an OCV

of 0.75 V that was stable over many days. The oxidizer was pure oxygen like another ethanol study. This DEFC study used a double layer anode catalyst using a Pt/Sn mixture for the outer layer, and Pt/Ru for the inner layer. At 90 °C, power densities around 90 mW/cm^2 were achieved. [51]

Another study investigated the use of nanowires as the electrolyte integrated on a silicon substrate of a micro fuel cell [52]. The wires are Nafion/poly(vinyl pyrrolidone) (PVP). The catalysts were PtRu/C and Pt/C, and the fuel tested was methanol with air as the oxidant. A single 2.1 micrometer diameter wire produced 1.54 μW. While this power level is very small, one could increase the number of wires (the author gives 10^5 wires as an example) in stacks of 10's. The author claims that in a space of 7cm x 2cm x 2cm, one could fit a small fuel cell assembly that would be capable of powering portable electronic devices.

In summary, direct fuel cells using alcohols like methanol and ethanol seem to provide a promising combination of performance, simplicity, and compactness. Without the need of a reformer or high temperatures for operation, the direct alcohol fuel cell system appears to be an attractive option for powering small, electronic platforms used by the warfighter.

2.3.4 Alkaline fuel cells

2.3.4.1 Operating principles

Alkaline fuel cells (AFCs) have been used since the 1960's in spacecraft to generate power for the vehicle and to generate drinking water for the astronauts. Alkaline fuel cells have several advantages. First, the kinetics of oxygen reduction in an alkaline media is faster than those in an acidic media (PEM). Second, a wider

variety of catalysts may be used for AFCs, making them less costly. [53] Third, a variety of fuels may be used (including alcohols) but like the direct methanol/ethanol PEM fuel cells, dilution of the fuel is required. AFCs require higher levels of dilution due to the fact that many alkaline cells use a liquid electrolyte that flows with the fuel. They also require pure air and can be poisoned by CO_2, which is why they have been mostly used in spacecraft applications where pure H_2 and O_2 are available. A portable terrestrial device would require additional hardware to separate the CO_2 in the air and so would be more complex than other types of FCs. However, the crossover in an alkaline methanol fuel cell is lower than in acidic media, perhaps making higher flow rates more feasible [54]. Figure 7 is a schematic of an alkaline fuel cell using methanol, ethanol, or sodium borohydride (NaBH4) as fuel. The overall reactions that occur on the electrodes of an alkaline methanol fuel cell are

$$\textbf{Anode: } CH_3OH + 6OH^- \rightarrow CO_2 + 5H_2O + 6e^- \quad (2.9)$$
$$\textbf{Cathode: } 6e^- + 3H_2O + 1.5O_2 \rightarrow 6OH^- \quad (2.10)$$

And for ethanol:

$$\textbf{Anode: } C_2H_5OH + 2OH^- \rightarrow CH_3CHO + 2H_2O + 2e^- \quad (2.11)$$
$$\textbf{Cathode: } 2e^- + H_2O + 0.5O_2 \rightarrow 2OH^- \quad (2.12)$$

And for sodium borohydride:

$$\textbf{Anode: } NaBH_4 + 8OH^- \rightarrow NaBO_2 + 6H_2O + 8e^- \quad (2.13)$$
$$\textbf{Cathode: } 8e^- + 4H_2O + 2O_2 \rightarrow 8OH^- \quad (2.14)$$

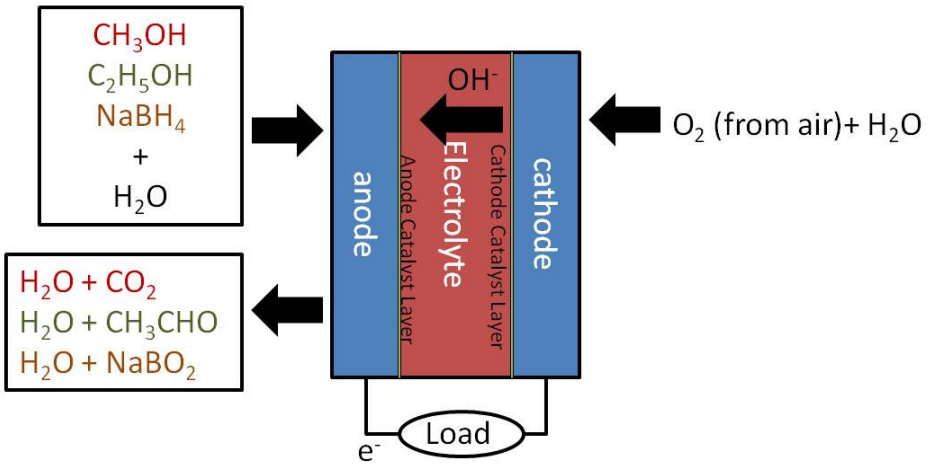

Figure 7: Direct alkaline fuel cell using methanol, ethanol or sodium borohydride as fuel.

2.3.4.2 State of the art

A feasibility study was performed in 2003 to determine if methanol and perhaps other non-traditional fuels could be used in alkaline fuel cells [55]. A comparison was then made between the alkaline fuel cell and its acidic counterpart, the direct methanol fuel cell. They pointed out that an alkaline equivalent to Nafion has not become available as yet in that an alkaline membrane still requires the fuel in its aqueous solution to be at least slightly alkaline to perform as well or better than DMFCs. The authors found that as the voltage increased as the operating temperature increased. However, higher temperatures can degrade and damage the alkaline membranes just as is the case with acidic membranes. However, alkaline media with pH > 7 are great for oxygen reduction, and methanol can be fully oxidized to CO_2. Therefore, the authors concluded that an alkali methanol fuel cell would be feasible if improved membranes were developed. The improvements necessary included higher conductivity and stability at higher temperatures. The author noted that new catalysts and alternative fuels were also worth looking into.

An alkali fuel cell capable of operating on multiple types of fuels was built and tested by Verma et al. in 2005. [56] The fuel cell ran successfully on aqueous solutions of methanol, ethanol, or sodium borohydride. At room temperature, the sodium borohydride performed the best both in terms of current density and power density, but the maximum power density was low, peaking at only 16.5 mW/cm^2. At a higher temperature (60 °C), the methanol cell performed better achieving a maximum power density of 31.5 mW/cm^2. Sodium borohydride was slightly lower due to the loss of H_2 via hydrolysis. At both temperatures, the open circuit voltage (OCV) of sodium borohydride was the highest of all fuels.

Next, the same authors performed an anode study comparing the performance of this multi-fuel cell with Pt black, Pt/Ru, or Pt/C anode catalysts. [53] The catalyst loading was also varied for comparison. An important problem with methanol operation is that the electrolyte reacts with carbon dioxide produced on the anode and is gradually consumed. The proposed solution was to recycle the electrolyte to remove the carbonate, and to periodically recharge with fresh KOH. However, this would lead to a larger system. Ethanol does not have this problem because acetaldehyde is generated instead of CO_2. For both methanol and ethanol, it was found that Pt/Ru was the best catalyst but only slightly. Ruthenium is not the most active catalyst for these particular fuels, but it enhances activity by supplying OH species to aid in the oxidation of adsorbed CO. It is also reasonably CO tolerant. The use of Ruthenium increases the power density from 13.86 to 15.8 mW/cm^2 for methanol and from 11.42 to 16 mW/cm^2 for ethanol. The performance of the sodium

borohydride cell varied little with catalyst loading and type; the typical power density was 20 mW/cm^2 using Pt black.

A mathematical model of this cell was also created [57]. Because of the nature of the study, more details were given on the reaction mechanisms and kinetics than the other two papers. These details will not be covered here; however it is worthwhile to note a few items. The activation overpotential is more significant at the anode than the cathode with this alkaline configuration. The authors found that there is an optimal electrolyte concentration and that increasing fuel concentration above 2 M did not improve performance. Cell voltage did increase with temperature for the alcohols, but the increase in temperature lowers the performance of a sodium borohydride cell. This study quoted a power density of 22.5 mW/cm^2 for $NaBH_4$ at room temperature, while the methanol and ethanol maximums produced 24.3 and 14.5 mW/cm^2 at 65°C, respectively.

Bunazawa and Yamazaki studied the effect of neglecting an alkaline in the fuel solution with an alkaline fuel cell [58]. The difference in adding 0.5 M NaOH to the 1 M methanol aqueous solution increased the power density by an order of magnitude to 58.9 mW/cm^2. The operating temperature was 80 °C and pure O_2 was used as the oxidizer. A different direct alkaline methanol fuel cell built by Scott et al. performed even worse using oxygen, but the temperature was at 60 °C [54]. The power density was given as 16 mW/cm^2 and around 6 mW/cm^2 when air was used as the oxidizer at near ambient conditions.

Yang et al. looked into improving methanol alkaline fuel cells by using a composite polymer membrane [59]. The membrane, which was poly(vinyl

alcohol)/hydroxyapatite (PVA/HAP), was tested using an 8 M KOH and 2 M methanol solution. Using air at the cathode at ambient conditions, a power density of 11.48 mW/cm^3 was achieved. The authors noted that this is a great improvement over other alkaline DMFC results because the membrane is less expensive than Nafion ®, and the manganese cathode catalyst was also less expensive than precious metals like platinum. Yang et al. also tested a poly(vinyl alcohol)/titanium oxide (PVA/TiO2) membrane [60]. The KOH concentration of the electrolyte solute was lowered to 4 M due to better alcohol solubility in that solution. Ethanol and isopropanol were also tested but methanol performed the best due to its higher open circuit voltage. Methanol produced a power density of 9.25 mW/cm^2. While this is a somewhat lower performance than that of the PVA/HAP membrane, the PVA/TiO2 membrane required half as much KOH solute. Therefore, it is difficult to tell which of the composite membranes is actually better.

Another alkaline-methanol study used the idea of laminar, parallel flow of the anode and cathode streams. Laminar flow, when combined with microfluidic geometry, can be used to create a barrier between the reactants within a single channel while still allowing ionic transport to take place. This design removes the necessity of a membrane [61, 62]. The authors found that when comparing alkaline and acidic fuel mixtures, alkaline mixtures generated higher OCV and power density. The power density of the 1 M methanol with 1 M KOH solution at room temperature was 17.2 mW/cm^2, and the OCV was 1.05 V. It was concluded that the better performance of the alkaline mixture over acidic mixtures stemmed mainly from lower anode overpotentials and improved kinetics of methanol oxidation and/or oxygen

reduction. Another feature of the design was that although carbonates were formed like in traditional alkaline fuel cells, they were washed away with the flow because there were no membrane pores to clog.

Hayes et al. investigated a similar geometry, in which the oxidant enters the fuel cell orthogonally from the plane of reactant flow through the electrodes [63]. The orthogonal flow convects the effluents forward, and like above, a membrane is not required. Instead the fuel is reduced and diffuses into an empty gap between the electrodes where it reacts with the oxidizer at the cathode to form the final products. This design focuses on optimization of the fuel and catalysts, not on membrane limitations. There are limitations with this design, such as lower fuel utilization caused by channel length constraints. The design was tested with H_2 and methanol in an alkaline aqueous solution, using O_2 as the oxidizer. With .01 M methanol in 1 M KOH at 90 °C, a power density of 46 mW/cm^2 was achieved. Similar power densities were claimed using H_2 as fuel. That is a fairly low power density for such a high temperature and is probably due to the low concentration of fuel. The fuel utilization at this maximum power density was near 42% meaning that more than half of the fuel is wasted.

In 2007, Tsivadze et al. performed a catalyst study using ethanol as the fuel and NaOH as the electrolyte in the solution [64]. The fuel solution was 2 M ethanol and 6 M NaOH. The catalyst that performed the best was cobalt based giving a power density of about 40 mW/cm^2 at 60 °C. This is more than double the power density Scott et al. achieved using methanol and pure O_2. Another ethanol study by a different group attained a maximum power density of 58 mW/cm^2 at ambient

conditions but it was achieved using pure O_2 as the oxidizer. The fuel solution was 1 M ethanol and 0.5 M KOH [41].

In summary, alkaline fuel cells consuming alcohols or sodium borohydride appear to be reasonable alternatives to direct types or PEM cells with external reformers. The fuel crossover in an alkaline fuel cell is lower than its direct, acidic counterpart and similar power densities are achievable. However, means must be provided for recirculating the water/alkaline fuel carrier solution in order to achieve reasonable system-level energy density. The necessity of CO_2 removal remains a logistic challenge.

2.3.5 Other fuel cells

2.3.5.1 Proton Conducting Ammonia Fuel Cell

Maffei et al. in 2005 reported a planar ammonia fuel cell with a proton conducting electrolyte: $BaCeO_3$ doubly doped with gadolinium and praseodymium [65]. The fuel was switched between hydrogen and ammonia over a 96 hour time period, and it was found that there was little deterioration in performance. In other words, the ammonia performed just as well as the hydrogen, although power densities using either fuel were somewhat low (30-40 mW/cm^2) for high temperature fuel cells. The special doping did help performance, but the large thickness of the electrolyte resulted in a relatively low current density. The advantage of proton conducting electrolytes over oxide types is that no NO_x formation occurs. This was confirmed using gas chromatography on the products. Zhang et al. were able to achieve much higher power densities (147 mW/cm^2) using thinner, slightly differently doped electrolytes layers [66]. While pure oxygen was used as the oxidizer, the high open

circuit voltage and current densities still show great potential for a proton conducting ammonia fuel cell.

2.3.5.2 Molten Alkaline Fuel Cell

Ganley reported results from a molten alkaline type fuel cell using ammonia directly as the fuel [67]. The nickel cathode had to be doped with lithium to prevent polarization or deactivation. He found that ohmic losses are significant, even with the doping, and that the potential dropped as the temperature increased. The maximum power density of the membrane was 40 mW/cm^2 at 450 °C. It was concluded that if the electrodes were placed closer together (they were at 2 cm distance) and their surface area were increased, higher performance would be achieved. While the ability to use ammonia directly (i.e. without a separate reformer) is promising, the 40mW/cm^2 is relatively low for a high temperature fuel cell.

2.3.5.3 Direct Formic Acid Fuel Cell

Most of the literature that was collected on direct formic acid (HCO_2H) fuel cells originates from Dr. Richard Masel's research group from the University of Illinois at Urbana-Champaign, as well as his partners. Direct formic acid fuel cells (DFAFCs) are similar to other direct types using no reformer but directly oxidizing the formic acid at the anode of a PEM fuel cell. Formic acid in its natural state is found in the venom of bees and ant stings, but its uses in the chemical industry include being a preservative for livestock hay, as well as a food additive that has been approved by the U.S. Food and Drug Administration (FDA) [68].

Dr. Masel and his group started investigating formic acid fuel cells around the turn of the century, with high expectations due to certain properties of the acid.

Reduced surface poisoning reactions were also expected. The theoretical open circuit voltage of formic acid is 1.45 V - a great improvement over other direct fuels like methanol. With their first attempt, however, an OCV of only 0.7 V was attained [68]. The anode catalyst was Pt with noble metal additives, which was used to ensure minimal amounts of CO were produced. The cell area was 5 cm^2 and Nafion 117 was used as the membrane. Electrodes were made from graphite blocks. The optimal feed concentration was in the range of 10-20 M. Below this range there was a limitation due to mass transport, and above the range dehydration of the membrane was the probable cause. The formic acid fuel cell was shown to excel compared to an in-house direct methanol fuel cell. Operating at 0.4 V, the DFAFC at 12 M reached a power density of 48.8 mW/cm^2 compared to 1 M methanol producing 32 mW/cm^2. Methanol did have a higher maximum power density at 51.2 mW/cm^2. Lastly it was found that DFAFCs were not dominated by fuel crossover losses like DMFCs because the sulfur within the membrane repels the formic acid. This was later confirmed by the team in a study specifically observing fuel crossover through a Nafion membrane [69].

Shortly following this initial study, another study looked into different variations of Pt for the anode catalyst [70]. With Pt alone as the baseline, the variations included adding palladium or palladium with ruthenium. Pt/Pd catalyst's catalytic reactivity outperformed the other two by two orders of magnitude. A current density of 1 $\mu A/cm^2$ at 0.27 V was attained. Another advantage of Pt/Pd was that it favored the production of carbon dioxide directly, unlike the other catalysts that made CO in an intermediate stage.

Instead of comparing ruthenium on palladium, an alternate study was done to compare Pt/Pd with Pt/Ru, a popular catalyst for fuel cells like DMFCs [71]. The OCV was found to have a strong dependence on the catalyst. Pt/Pd had an OCV of 0.91 V compared to Pt/Ru which had an OCV of 0.59 V. However, the voltage dropped relatively quickly with increasing current density with the Pt/Pd catalyst. In consequence, at high voltages (>0.5 V) Pt/Pd was the better choice, whereas at low voltages Pt/Ru produced a higher power density. Unfortunately, Pt/Ru favors the production of CO, which makes Pt/Pd a better candidate for electro-oxidation of formic acid. The authors also noted that the reactivity of Pt/Pd was not nearly as high as the previous study and the cause was unknown. The authors hypothesize that the process by which the catalyst is made and deposited made the noticeable difference. A kinetic study was also performed to confirm that Pt/Pd performs better than Pt black, and that the former catalyst is CO tolerant [72].

Pre-treatment of the anode was also considered. This conditioning process lowers the cell resistance, thus increasing the current. [73] Typically for a DMFC, hydrogen is used as the conditioner, but with formic acid, it was found that methanol had a positive effect, and hydrogen actually had a negative effect. The authors were unsure why conditioning with methanol increases the power density, but they were sure that the conditioning is only beneficial if a load is being applied simultaneously. Loading can cause pore alignment within the Nafion membrane, so that may have been the cause for the increased performance. The conditioning provided an increase of power density (through improved current density) of 33 mW/cm^2 to 119 mW/cm^2.

Following these advancements, a passive miniature air breathing direct formic acid fuel cell was built and tested. [74] Interestingly, no methanol conditioning was used, and the anode catalyst was Pt. Perhaps the cell was being tested before the previous insights had surfaced. The size of the fuel cell was 2 cm x 2.4 cm x 1.4 cm, and the cell operated at room temperature. Oxygen plasma treated carbon cloth had the best performance when compared to other cloths considered. The maximum power density achieved was 33 mW/cm^2 and the cell ran better at lower concentrations between 1.8-10 M. This range is lower than the range quoted for the actively pumped fuel cell from before [67], and the authors felt that dehydration was the limiting factor for achieving higher concentrations. Regardless, the effective energy density of a 10 M solution of formic acid is higher than 2 M of methanol, which the authors claim as the upper limit of each, respectively. A similar study was also performed on an actively pumped system, where none of the recent findings were implemented [75]. A comparison with a stack running on methanol was made, and the results re-affirmed the advantages of formic acid. Power densities using formic acid as the fuel achieved were 84 and 110 mW/cm^2 for 18 and 30 °C, respectively, while methanol attained 45 and 67 mW/cm^2 at those temperatures. These higher power densities were attributed to the higher concentrations at which formic acid can run.

Another passive formic acid fuel cell system was built and tested slightly later, this time with a Pd black anode and no conditioning [76]. The concentration range that was tested increased to 12 M with satisfactory results. The passive cell at 10 M concentration could attain a power density of 177 mW/cm^2 at 0.53 V at ambient

temperatures. According to the authors, this surpasses the best current passive DMFC technologies. Because the fuel cell was passively fed, the mass transport through the cathode was considered the limiting factor of performance.

Because the Pt/Pd catalyst performed well in previous research, the group next investigated an anode catalyst that was purely Palladium [77]. Formic acid was also used as the pre-conditioner. The concentration of formic acid in the aqueous solution was varied, including concentrations which were higher than typical for alcohols in direct fuel cells (3-20 M). Performance increased substantially. The fuel cell generated power densities between 230 and 255 mW/cm^2 at voltages between 0.4-0.5 V within the concentration range of 3-15 M at 20 °C. This impressive accomplishment is compared with methanol (50 mW/cm^2) and hydrogen (320 mW/cm^2) at room temperature. When the temperature was increased, the power density also increased, such as 375 mW/cm^2 at 50 °C. A concentration of 20 M did produce good results (110 mW/cm^2 at room temperature) but not as well as lower concentrations. Thus it was assumed that this is the breaking point for the hydration of formic acid. Decay in performance after several hours was reported, but it was proposed that anode polarization would restore performance after such extended use.

In order to overcome this decay, the researchers investigated supports to use with the palladium [78]. Many metals were considered, and it was found that a few could stabilize the activity, vanadia (V) being the best option. The electric current produced per mass of precious metals for Pd-V was 3 orders of magnitude higher than a typical Pt/Ru catalyst. Other materials were investigated including carbon. The study confirmed previous findings that carbon was more “efficient” in that it could

reach power levels with lower amounts of catalyst, but the power densities (with respect to surface area) were lower than those obtained with Pd black as the catalyst/support. The authors expressed hope, however, that this weakness could be improved with future research, thus making the catalyst efficient and power dense. Gold was also mentioned as an option to improve the activity of the anode. [79, 80]

Formic acid was also considered as a fuel for use in silicon based micro fuel cells, for chip-scale uses [81]. The silicon was etched with sulfuric acid for the membrane, giving a thickness of less than 100 microns. The etched silicon is used as the electrolyte because Nafion is difficult and less robust when bonding to the silicon substrate. In some cases, the silicon membrane had higher proton conductivity and lower crossover leading to better performance than a Nafion membrane. On a per unit area basis (because these membranes are thinner than Nafion), only the lowest anodization current density sample (20 mA/cm^2) was lower in proton conductivity.

Two identical silicon MEAs were later tested, and a difference of 10 mW/cm^2 was observed between the two maximum power densities [82]. In addition to this discrepancy in reproducibility, both cases showed higher crossover than Nafion. Doping the fuel with sulfuric acid was necessary to achieve desirable power densities of about 30 mW/cm^2. Improvements were made to the fuel cell to increase performance consistently, including alterations to the substrate and structure, insulating materials, and catalyst layers [83]. These improvements increased proton conductivity and transport while reducing crossover to triple the power density to 94 mW/cm^2. The fuel was still doped with sulfuric acid, however. More specific reasons for the increase in performance were attributed to how the substrate was dry-

etched, adding gold palladium to the catalyst layer, and removing titania nanoparticles from the design that were previously deposited between the membrane and anode catalyst [84]. These results show a more substantial potential for formic acid fuel cells in micro power applications.

The Korean Institute of Science and Technology built a formic acid fuel cell system to power a laptop computer [85]. It was a stack of 15 cells that could provide 30W with a power density of 60mW/cm^2. The entire system was 1440 cm^3 and 1.8 kg, including the stack, a full fuel tank, tubing, a mini pump, a mini compressor, 3 cooling fans, a small battery, and a power conditioning control board. This system is quite large compared to a typical 12 V laptop battery that is 95 cm^3 in size and weighs only 0.16 kg. The mini pump and compressor run on the battery, making it a hybrid system. Platinum was used as the catalyst and Nafion 115 ® as the membrane. The highest efficiency attained was 23%, which decreased as the fuel flow rate increased. However, it should be noted that this efficiency was attained at a concentration of 11 M (50%wt) so lowering the concentration might have improved performance. After three months of operation, performance was reduced but still stable.

After this extensive study of direct formic acid fuel cells, it was determined that the advantages of these systems do not outweigh the safety concerns associated with formic acid itself. While it is used for preservatives and food additives, the acid itself can cause severe burns to skin and eyes - even in the vapor phase - and the recommended maximum exposure is 5 PPM. Higher concentrations, which most researchers used in these studies, can be corrosive or cause blindness similar to methanol poisoning. Also, the formic acid fuel cells showed stability concerns after

many hours, requiring a type of recharge for the fuel cell to achieve optimal performance. Therefore, the formic acid fuel cell was not believed to be a viable replacement for batteries in miniature autonomous systems.

2.3.5.4 Non-conventional fuel cells

L-ascorbic acid, more commonly known as vitamin C, was considered by a group in Japan as a possible fuel. Various catalysts were tested, and one test case included no catalyst, just carbon cloth [86]. The fuel cell did function without a metal catalyst, although the performance was worse than most of the catalysts tested. The theoretical OCV for L-ascorbic acid is 0.758 V, but actual OCVs varied between 0.5 and 0.6 V. The cell area was 10 cm^2, and the experiment was run at room temperature with air at the cathode. The overpotential of L-ascorbic acid oxidation was relatively small, as was the crossover. At a concentration of 1 M, Pd gave the best power density at 6 mW/cm^2, compared to the 2.3 mW/cm^2 attained with the anode absent of a metal catalyst. A later study indicated improvement in the L-ascorbic acid cell, citing 15 mW/cm^2 using carbon black at the anode [87]. However, the oxidant was oxygen, which makes a proper comparison with previous results difficult.

Another design uses nuclear power to drive a closed loop system. H_2 and O_2 are formed from water using the decay energy of a radioisotope [88]. As long as the isotope is active, the products of the fuel cell resupply the system with reactants. The fuel cell uses an alkaline-based electrolyte. The catalysts are silver at the cathode and platinum at the anode. The author mentions that breakthroughs in thermal insulation design would be necessary if small sizes are desired. The goal was to achieve 10 mW

in a volume of 1 cm^3, but the current design produced only 0.45 mW, with an efficiency quoted between 10 and 20%.

2.4 Summary.

Pure hydrogen would be an ideal fuel for fuel cells, absent storage and safety issues. Other forms of hydrogen storage, such as ammonia, metal ammines and borohydrides provide safer alternatives at the expenses of complexity (because reforming is required) and energy density. Four fuels stand out as alternatives to pure H_2: ethanol, methanol, ammonia, and sodium borohydride. The alcohol-based fuel cells can also be separated into two categories – alkaline and acidic. Table 2 provides some highlighted fuel cell technologies discussed in this chapter. Each fuel and type has its advantages and disadvantages. Fuel crossover in an alkaline fuel cell is less than in an acidic fuel cell. DEFCs show poor performance compared to DMFCs because of higher overpotentials of ethanol oxidation at low temperatures. Ammonia is carbon free and is not required to be diluted in water for use, but high temperatures are required for direct or indirect fuel cell operation. However, no technology clearly stands out over another. Therefore a more detailed ranking system is required to determine which type of fuel cell system is best suited for powering the miniature autonomous systems described in Chapter 1. These will be developed and discussed in the next chapter. Finally, tables summarizing all of the fuel cells considered when preparing this chapter and their defining features are presented in Appendix B.

Table 2: Sample fuel cell technologies

Type	Ox.	Catalyst(s)	Max Power Density (mW/cm^2)	Temp. (°C)	Ref #
Direct Methanol	air	A: Pt/Ru, C: Pt	140	80	[49]
Alkaline Methanol	air	A: Pt/Ru, C: MnO_2	11.48	25	[59]
Direct Ethanol	O_2	A: Pt-Sn-Ru/C	50	80	[50]
Alkaline Ethanol	air	A: Pt, C: MnO_2	16	25	[53]
Alkaline Borohydride	air	A: Pt, C: MnO_2	22.5	25	[57]
Direct Ammonia	O_2	A; $Ce_{0.8}Gd_{0.2}O_{1.9}$	147	600	[66]

Chapter 3: Survey Results.

The literature review provided key insights into current fuel cell technologies, and what advantages and disadvantages are associated with them. In order to determine which technology would be the best candidate for the U.S. Army's CTA objectives, a scoring system to rank these technologies is developed. This semi-quantitative methodology is presented as well as the results.

3.1 Categories for consideration.

The first category for the scoring process is perhaps the most apparent when reading the literature: the energy density of the fuel. This quantitative value, being the amount of energy stored in the fuel per unit volume or mass, depends on nothing more than what type of fuel is being used. Power density is also a quantitative category of interest that is generally not difficult to find for each particular case considered. For most fuel cell MEA research, the power density is the foremost result of the experimental study or modeling. Another category of interest is the operating temperature. One of the concerns of utilizing reformers and ammonia-based FCs is high operating temperature and the effect it could have on the vehicle system. In order to minimize extra weight and volume necessary for thermal isolation, as well as ensuring that the fuel cell stack would not melt other electronics on the platform, lower temperatures are more desirable. Oxidizer type is another category of interest. As was discussed in chapter two, many researchers used air for the oxidizer, but some used pure O_2 for the experiment. This can have important ramifications on the results

given, especially if the fuel cell is alkaline. AFCs are CO_2 intolerant and would require increased system complexity when running on air to remove the unwanted constituent. Conversion efficiency, or how much fuel was converted into useful power, is another category. This value was not found as often as the power density of the fuel cell so estimates are made when a specific number was not published. The basis for these estimates is described in the following section. System simplicity is based on a qualitative assessment of the balance of plant. The more complex the system appeared, as far as what type of components it contained and how many of them, the lower the score it received.

3.2 Conversion efficiency.

Efficiency in a fuel cell system is generally broken into three parts: The reforming efficiency, the fuel cell efficiency, and the balance of plant efficiency. The reforming efficiency is a measure of how effectively the chemical potential energy in the original fuel is converted to chemical potential energy in the fuel of choice which is usually H_2:

$$\eta_{FP} = \frac{\dot{m}_{ref} h_{ref}}{\dot{m}_{in} Q_r} \tag{3.1}$$

In Eq. 3.1, $\dot{m}$ is the mass flow rate and *h* is the heat of combustion. The subscripts *in* and *ref* refer to the fuel entering the reformer and reformate, respectively. Efficiency in a fuel cell is a measured by the amount of electrical power the cells produce divided by the power brought into the cells via the reformate:

$$\eta_{FC} = \frac{n_{cells} A_{cell} i V_{cell}}{\dot{m}_{ref} h_{ref}} \tag{3.2}$$

where n_{cells} is the number of cells in the stack, A_{cell} is the cross sectional area, i is the current density, and V_{cell} is the voltage the cell operates at. Lastly, the balance of plant efficiency takes into account the parasitic losses, $\dot{W}_{lost}$, due to the components necessary for functionality:

$$\eta_{BOP} = \frac{n_{cells} A_{cell} i V_{cell} - \dot{W}_{lost}}{n_{cells} A_{cell} i V_{cell}} \tag{3.3}$$

The overall thermodynamic efficiency is the product of the previous three efficiencies:

$$\eta_{th} = \eta_{FP}\eta_{FC}\eta_{BOP} = \left(\frac{\dot{m}_{ref} h_{ref}}{\dot{m}_{in} Q_r}\right)\left(\frac{n_{cells} A_{cell} i V_{cell}}{\dot{m}_{ref} h_{ref}}\right)\left(\frac{n_{cells} A_{cell} i V_{cell} - \dot{W}_{lost}}{n_{cells} A_{cell} i V_{cell}}\right) \tag{3.4}$$

This methodology is used to find the conversion efficiencies of the systems chosen for consideration. When values for certain parasitic losses (like pumps, blowers, and power conditioning) were not provided in the text, estimates were made based upon previous experience using these components. The 'effective' energy density of a fuel is the product of the overall thermodynamic efficiency of the cell with the fuel's heating value:

$$h_{eff,sys} = \eta_{th} Q_r \tag{3.5}$$

Eq. 3.5 also shows how using an energy dense fuel has little advantage if the overall conversion efficiency is low. Table 3 summarizes the efficiencies of three fuel cell systems each of which utilizes a different fuel. In each case, the reforming efficiency is unity because the original fuel is used directly in the fuel cells. The last two columns show how these efficiencies affect the effective energy density of the fuel.

Table 3: Conversion Efficiency and Effective Energy Density

System	η_{FP}	η_{FC}	η_{BOP}	η_{th}	h_{in} (kJ/g)	Eff. h_{sys} (kJ/g)
Direct $NaBH_4$ AFC with 2M solution feed and water recycling.	1.00	0.46	0.61	0.27	33.5	9.05
$NaBH_4$ without recycling					7.62	2.06
Direct Methanol FC with 2M solution feed	1.00	0.38	0.71	0.28	21.1	5.91
Ammonia PCFC with high-T membrane	1.00	0.50	0.74	0.37	18.8	6.96

3.3 Scaling methodology.

First the categories are assigned weights proportional to their relative importance. The values of the weights reflect the author's personal assessments of what was important in a micro UAV application. Both energy density and conversion efficiency receive the highest weights of five in light of the conclusions of Figure 1 in Chapter 1 and Eq. 3.5 above. Oxidizer is assigned a weight of four, to capture the very unrealistic possibility of using pure O_2. Overall simplicity is also given a weight of four because complexity is something that should be minimized to ensure reliability. Operating temperature is assigned a weight of three, and power density a

weight of two. Power density is lower on the scale because the fuel cell membrane is not the direct object of improvement per se; rather it is the power density of the system as a whole.

A score between zero and one is assigned to each technology considered for each category, based on the following qualifications: The score for energy density is found by dividing the energy density of the technology in question by the energy density delivered by the best technology in the set. Thus, the most energy dense fuel in the set gets a score of one. The same concept is used for conversion efficiency and power density. Oxidizer and operating temperature are Boolean in nature. If the oxidizer is air, the technology score is one; otherwise a zero score is given. If the operating temperature is below 250 °C, a one is given; otherwise the score is zero. The score for overall simplicity is based upon the current author's understanding of how complex the system would be. For example, if the system uses a reformer, the maximum score it can receive is 0.5 because the reformer makes it twice as complex, if not more, than a system without a reformer. The overall score of the technology is computed by summing the product of the weight and score of each category of interest:

$$S = \sum_i w_i s_i \tag{3.6}$$

The scoring methodology is summarized in Table 4. An uncertainty score is also assigned to each category and technology. This value represents how much estimation is used for that technology. The overall uncertainty was computed in a root-mean-square fashion:

$$U = \sqrt{\sum_i (w_i u_i)^2} \tag{3.7}$$

Table 4: Fuel Cell Technology Scoring System

Criteria (i)	Weight (w_i)	Scoring (s_i)	
		Range	Explanation
Energy Density of fuel	5	0-1	$h_i/h_{max\ of\ set}$
Conversion efficiency	5	0-1	$\eta_i/\eta_{max\ of\ set}$
Oxidizer	4	0-1	1 if Air, 0 otherwise
Overall simplicity	4	0-1	Max 0.5 if uses separate reformer
Operating Temperature	3	0-1	1 for T < 250 C, else 0
Power Density (membrane)	2	0-1	$\rho_i/\rho_{max\ of\ set}$

3.4 Scaling results.

The results of the scoring exercise are presented in Figure 8. The number label provided for each bar gives the number of the reference to the publication where data used to compute the score came from, the first author's last name, and the first letter of the fuel name (A-ammonia, E-ethanol, M-methanol, S-sodium borohydride). The results show no clear winner as far as what type of fuel to use. Ethanol, methanol, sodium borohydride, and ammonia based systems each have at least one technology with a score higher than 15 (top score possible is 23). Fuel cell systems using sodium borohydride have a higher uncertainty level (see Figure 9) than other fuel types because of the importance of water recovery in these cells. If $NaBH_4$ is stored in stoichiometric proportions and is used in a non-looping system, the effective energy density of the system is low. However, if water can be recovered from the exhaust, then the system could deliver the highest effective energy density (as shown

in Table 3). The adjacent bars representing the same sodium borohydride technology illustrate the advantage of a water recovery system.

Figure 8 separates the overall score into the different scoring categories, to show the effect of each. When comparing the top performers in each fuel category, there are observations that can be made. Ethanol has a higher energy density, but the methanol system has a higher conversion efficiency. Ammonia has a higher simplicity score, but the operating temperature brings the score down. The sodium borohydride system performs well in all categories, but only if the water is recovered. Without water recovery, the technology drops from having the top score, to the 13th highest score. The water recovery causes a slight decrease in simplicity of the system, which is also represented. Also note that because of the significance of the category, all technologies using pure O_2 as the oxidizer are lower in the overall score.

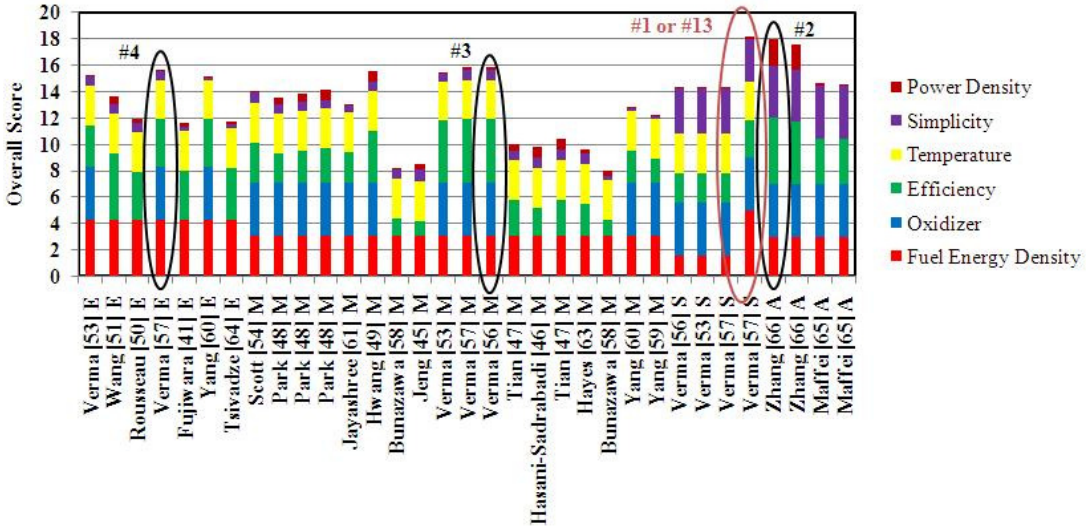

Figure 8: Individual category scores for each fuel cell technology. Numbers in brackets are references and letters the type of fuel used.

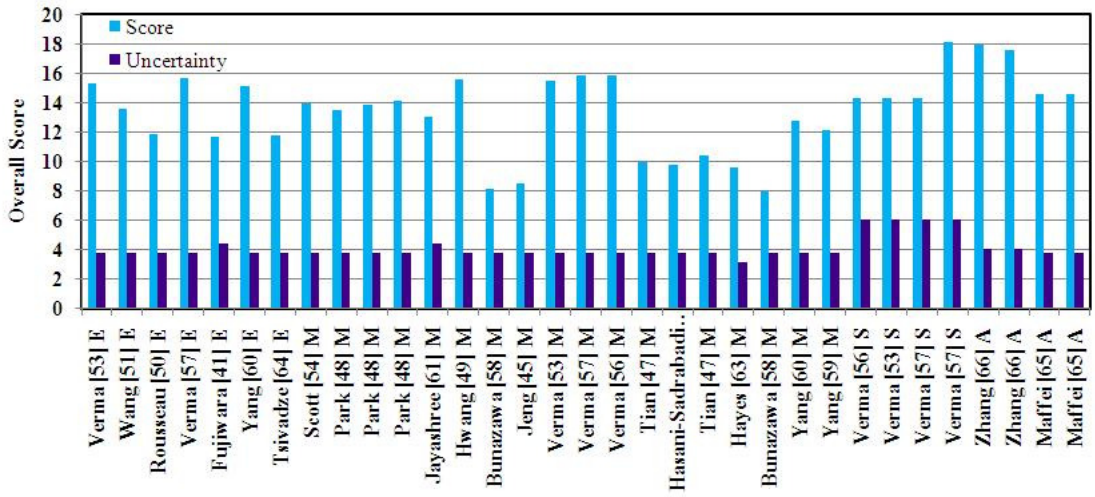

Figure 9: Overall Scores and uncertainties of fuel cell technology rankings.

3.5 Summary.

The purpose of the literature survey and scoring system is to identify which technology type should be considered for the system modeling and future research. Although some insight was developed, no fuel appears to outdo the others. Although there are many low scoring methanol systems, there are still some that show great potential. Ammonia system scores in general appear high, even with the temperature disadvantage. All of the sodium borohyride systems could be ranked high with water recovery integrated into the system. Ethanol has the lowest high score compared to the others. Because of this, methanol, ammonia, and sodium borohydride systems appear to be the best ones to focus on in the quest to develop high energy density power supplies for the miniature crawling, hopping, and flying vehicles envisioned by the U.S. Army.

Chapter 4: System Model for Direct Methanol or Sodium Borohydride Fuel Cells.

The results of the previous chapter suggest that direct methanol and alkaline direct sodium borohydride systems appear to be particularly well-suited for powering the small vehicles envisioned by the U.S. Army. A DMFC system is selected for detailed modeling (and comparison to batteries) because simple configurations are possible while still achieving high efficiencies. Simplicity tends to result in relatively low system mass suitable for use in miniature ground vehicles and aircraft. A direct sodium borohydride fuel cell (DBFC) system is also selected for detailed modeling and comparison because the energy density is comparable to ammonia and its lower temperature operation greatly facilitates integration with the vehicle structure.

4.1 Selection of simulation environment.

The system model derives from one developed for a larger system that incorporated a liquid hydrocarbon reformer that produces hydrogen for a PEM fuel cell [87]. The model is implemented in MS Excel using a Visual Basic program running as a macro. This provides some advantages to the user. First, very little experience in programming is necessary as most of the changes necessary can be implemented directly in the spreadsheet. The programming that is required is done in Visual Basic. Second, MS Excel provides a visual picture of what is happening to each variable when another variable or equation is modified. While the equations are not as easy to follow as other programming languages, debugging can be easier

because each cell provides the value of its variable in real time. If blaring mistakes are made in the code, they can be seen before the code is initiated. Also, Excel enables one to create worksheets that make the system modular without the necessity of declaring variables as global. It also makes it easy to ensure that the functions have the correct variables listed. Third, individual macros can be run without the necessity of running the entire program. This is ideal for when only one component has been modified and the user would like to check the functionality of that component prior to investing time in a full system calculation. Generally speaking, a complete system simulation takes up to 30 minutes.

4.2 System overview.

4.2.1 Non-recirculating methanol system

Figure 10 is a schematic illustration of the complete non-recirculating direct methanol fuel cell power and energy system (NRDMFCPES)[*]. A pump feeds fuel to the anode and a fan supplies air to the cathode. The air performs three functions. First, it is the oxidizing agent for the electrochemical reaction. Second, since a lot of water is created at the cathode, excess air is used to remove the water to prevent cathode flooding [46]. Third, the cathode air flow is also used to cool the stack and the air flow rate is controlled to maintain the fuel cell at a stable operating

[*] The term 'fuel cell power and energy system' (FCPES) refers to the complete power system that includes the fuel cell stack, all balance of plant components, the fuel and fuel tank. This is what goes in a vehicle and is ultimately the goal of this study to predict. However, it will also be convenient at times to focus on the energy conversion components of the FCPES which are the fuel cell stack plus all balance of plant components. This will be referred to as the 'fuel cell system' (FCS).

temperature of 57 °C. The net result is that the cathode functions with a large excess of air.

The fuel is stored in an external fuel tank as a concentrated solution of methanol in water (5 M or 8.3% by mole). The anode and cathode flows discharge directly to the atmosphere. A DC-DC converter boosts the low voltage DC power from the DMFC stack to a higher bus voltage (12 VDC) used to run the auxiliary components and provide external load power. The efficiency of the DC-DC converter efficiency (η_{inv}) is assumed to be 93% for all power and energy systems (PES) considered here.

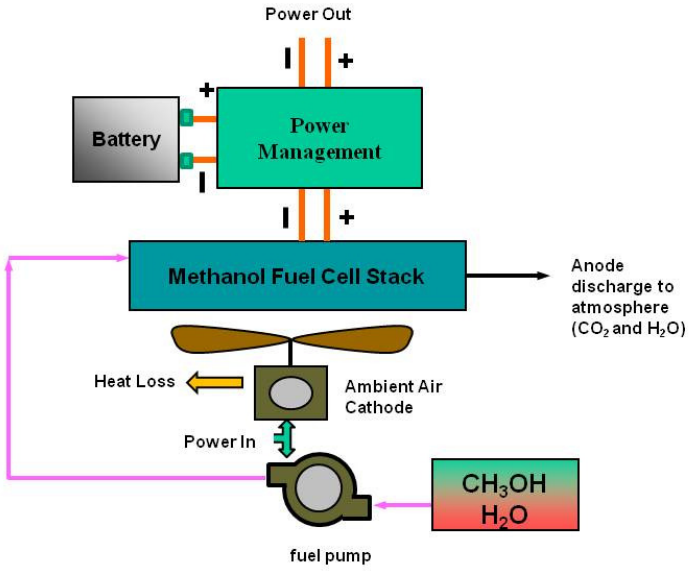

Figure 10: Direct methanol fuel cell system with pre-diluted fuel and direct discharge of anode and cathode feeds to atmosphere.

4.2.2 Recirculating methanol system

Figure 11 is a schematic diagram of a water recirculating direct methanol fuel cell power and energy system (RDMFCPES). This system is similar to the NRDMFCPES but has some modifications to make it more favorable and realistic.

The most important modification is the incorporation of a recirculation loop that recovers the water at the anode and returns it to a tank where it is mixed with pure methanol to create the 5 M solution needed at the anode. This greatly increases the overall energy density of the system because pure methanol instead of diluted methanol can be stored in the fuel tank and a much smaller amount of water needs to be stored on board. However, this advantage comes at the cost of increased complexity and system mass. The water created at the cathode is not recirculated because most of the cathode exhaust is oxygen. Oxygen in the mixer is not desirable, and removal would introduce more system complexity.

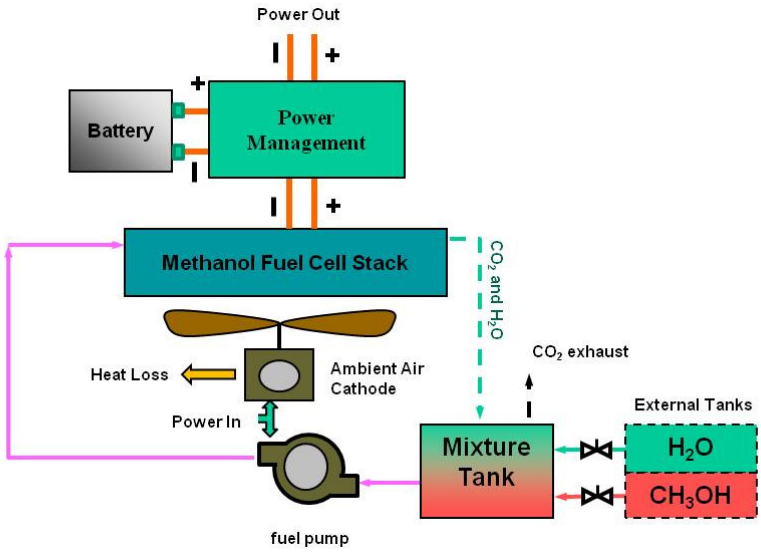

Figure 11: Direct methanol fuel cell model system with recirculation of the anode products, separate tanks for pure methanol and water, and a mixing/CO_2 separation tank.

4.2.3 Recirculating alkaline $NaBH_4$ system

Figure 12 is a schematic illustration of the alkaline sodium borohydride fuel cell power and energy system (ANaBH4FCPES). It is similar to the RDMFCPES in that water is recirculated from the anode and reactants are stored separately. Some of

the differences, however, will pose significant challenges should one actually try to build a prototype. One difference is the need for a third tank that stores enough of the KOH electrolyte to get the system started. Since KOH is recirculated with the water, it shouldn't need replenishment. Another difference is the mechanism for feeding $NaBH_4$ – a solid - into the mixing tank. While such a metering mechanism is simple to implement in a simulation, achieving this in practice will be more difficult as alternatives to the simple metering valve used in the liquid methanol systems will need to be developed. Finally, the oxidation product $NaBO_2$ is also a solid and means also will need to be developed to separate it from the recirculation loop. This separation is achieved in the simulation using a membrane but something else might have to be devised in practice.

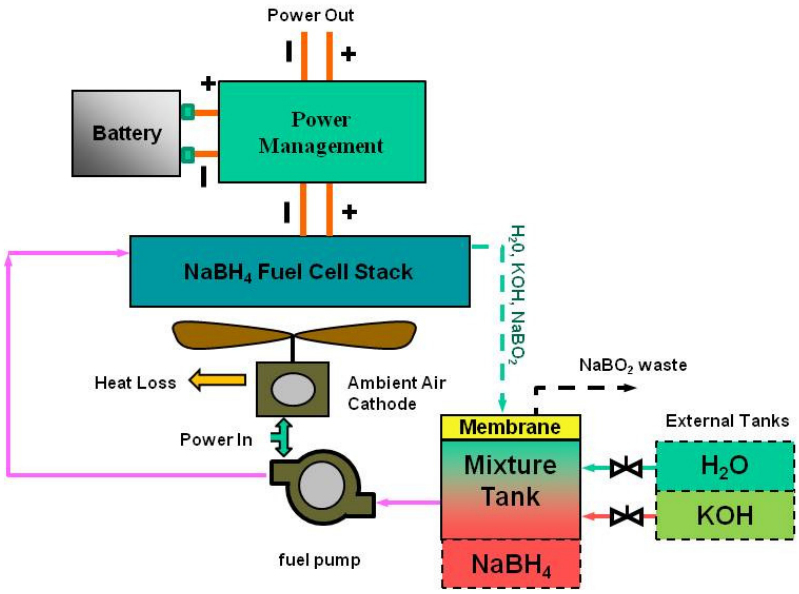

Figure 12 Direct Sodium Borohydride system diagram with anode product recirculation and solid waste removal.

4.3 System component models.

4.3.1 Methanol fuel cell stack

The overall power the fuel cell stack is required to produce depends on the desired power level (P_{user}), parasitic loads (P_{loss}), and electrical inverter efficiency:

$$P_{FC} = \frac{P_{user}}{\eta_{inv}} - P_{loss} \tag{4.1}$$

where:

$$P_{loss} = \frac{P_{fuelpump} + P_{fan}}{\eta_{inv}} \tag{4.2}$$

The fuel flow rate and current associated with P_{FC} are given by:

$$\dot{n}_{fuel} = \frac{P_{FC}}{eFV_{cell}} \tag{4.3}$$

$$I = \frac{P_{FC}}{n_{cells}V_{cell}} \tag{4.4}$$

In these expressions, the flow rate, $\acute{n}_{fuel}$, is in units of mole/s, current, I, is in Amperes, V_{cell}, is the voltage through each cell, e is the number of electrons shed per fuel molecule (which is 6 from Eq. 2.5), n_{cells} is the number of cells in the stack, and F is Faraday's constant. The performance of the MEA is modeled assuming that the cell voltage (V) is linearly proportional to the current density (i):

$$V_{cell} = V_l - V_{slope}i \tag{4.5}$$

The current density is found simply by dividing the current by the area of a single cell. The Tafel slope (V_{slope}) and the baseline limiting voltage (V_l) are inferred from the data

of Hwang et al [49]. Eq. 4.5 is a reasonable approximation of MEA performance for current densities between 50 and 500 mA/cm^2 and pressures around 1 atm. Operating conditions outside this space are not considered. The methodology used to compute the pressure losses associated with the anode and cathode flows is explained in Appendix C. Multiplying the actual operating voltage by the current density provides the power density of the individual fuel cell. The fuel cell stack design/architecture is also loosely based on the work of Hwang et al. [49]. The cell area is held fixed at 10.9 cm^2. Cell thickness and weight were not given for this design and are estimated to be 5 mm and 2 g, respectively.

Species conservation is enforced at the anode and cathode sides per the chemical reactions taking place there - Eqs. 2.5 and 2.6 for a DMFC. Methanol and water are consumed at the anode side, while CO_2 is produced. The anode stoichiometric ratio equals the inverse of the stack fuel utilization, meaning the amount of fuel used in relation to the amount of fuel needed to satisfy Eq. 2.5. The anode flow is run fuel rich in order to make sure that adequate fuel remains near the end of the flow path. Inadequate concentrations drop the open circuit voltage of the local cells to the operating voltage of the stack, and no current is produced. If this occurs at lower voltages, carbon can be oxidized in the catalyst layer which could damage the stack. Therefore, an anode stoichiometric ratio (ψ) of 1.3 was used in the non-circulating model while 1.1 was used in recirculating case. The species mole fractions at the anode are given by:

$$X_{fuel} = \frac{\dot{n}_{fuel,in} - \dot{n}_{fuel,in}/\psi}{\dot{n}_{atout}} \tag{4.6}$$

$$X_{CO2} = \frac{\dot{n}_{CO2,in} + \dot{n}_{fuel,in} / \psi}{\dot{n}_{atout}} \tag{4.7}$$

$$X_{H2O} = \frac{\dot{n}_{H2O,in} - \dot{n}_{fuel,in} / \psi}{\dot{n}_{atout}} \tag{4.8}$$

where $\dot{n}_{atout}$ is the total mole flow out of the anode. The total flow out is the flow in ($\dot{n}_{atin}$) plus the changes due to the reaction at the anode:

$$\dot{n}_{atout} = \dot{n}_{atin} + (-\dot{n}_{fuel,in} / \psi)_{fuel} + (\dot{n}_{fuel,in} / \psi)_{CO2} + (-\dot{n}_{fuel,in} / \psi)_{H2O} = \dot{n}_{atin} - \dot{n}_{fuel,in} / \psi \tag{4.9}$$

Since the stack is air cooled, the total air flow rate is determined by the species balance on the cathode side and an energy balance on the entire stack.

The species mole fractions on the cathode side are given by:

$$X_{O2} = \frac{\dot{n}_{O2,in} - 1.5\left(\dot{n}_{fuel,in} - \dot{n}_{fuel,out}\right)}{\dot{n}_{ctout}} \tag{4.10}$$

$$X_{N2} = \frac{\dot{n}_{N2,in}}{\dot{n}_{ctout}} \tag{4.11}$$

$$X_{H2Oc} = \frac{\dot{n}_{H2O,cin} + 3\left(\dot{n}_{fuel,in} - \dot{n}_{fuel,out}\right) + \dot{n}_{CO2,in} - \dot{n}_{CO2,out} + \dot{n}_{H2O,in} - \dot{n}_{H2O,out}}{\dot{n}_{ctout}} \tag{4.12}$$

The air flow required to feed the electrochemistry and cool the stack is calculated by performing an energy balance on the stack:

$$\dot{m}_{a,out} h_{a,out} + \dot{m}_{c,out} h_{c,out} - \dot{m}_{a,in} h_{a,in} - \dot{m}_{c,in} h_{c,in} + P_{FC} = 0 \tag{4.13}$$

Eq. 4.13 is solved iteratively by varying $\dot{m}_{c,in}$ so as to maintain a stack exit temperature of 57 °C (330 K).

The fuel cell stack solver iteratively solves for three main values, the MEA voltage (V_{act}), the power produced by the fuel cell (P_{FC}), and the flow rate of the cathode air flow ($\dot{m}_{c,in}$). A residual is for the purpose of this work is defined as the difference between the guess values and actual values or a measure of convergence to a solution. With the voltage, the guess value is used for Eqs. 4.3 and 4.4, which then produces an actual value in Eq. 4.5. The residual of the two values is taken and multiplied by 10^4 to ensure greater refinement towards convergence. The power guess and actual value are related in much the same way, but in a larger scale due to the changes associated with system parasitics. The residual between the two power values is multiplied by 10^2 for refinement purposes. The cathode flow guess value is varied until Eq. 4.13 is equal to zero, a non-zero value being the residual. The solver will continue to refine these residuals towards convergence until the sum of the three residuals is less than the tolerance of 10^{-3}.

4.3.2 $NaBH_4$ fuel cell stack

The physics of the $NaBH_4$ cell are identical to that of the methanol version except that the reactions at the cathode and anode are different. The fuel cell architecture is based loosely on the research of Verma et al. [51]. The cell area for the $NaBH_4$ system is 9 cm^2. As with the recirculating methanol system, ψ = 1.1. Given the reaction in Eq. 2.13, the mole ratios at the anode side are

$$X_{fuel} = \frac{\dot{n}_{fuel,in} - \dot{n}_{fuel,in}/\psi}{\dot{n}_{atout}} \tag{4.14}$$

$$X_{NaBO2} = \frac{\dot{n}_{NaBO2,in} + \dot{n}_{fuel,in}/\psi}{\dot{n}_{atout}} \tag{4.15}$$

$$X_{H2O} = \frac{\dot{n}_{H2O,in} + 6 \cdot \dot{n}_{fuel,in} / \psi \cdot (1-\gamma)}{\dot{n}_{atout}} \tag{4.16}$$

where γ is the fraction of water produced that seeps to the cathode. In previous renditions of the model, this is a property that is known based on previous experience with the electrolyte. Because this information was not provided for the current design, this value was set at 2/3, which would be optimum for the cathode reactions (see Eq. 2.14). The total flow out is the flow in, plus the changes made due to the reaction at the anode:

$$\dot{n}_{atout} = \dot{n}_{atin} + (-\dot{n}_{fuel,in} / \psi)_{fuel} + (\dot{n}_{fuel,in} / \psi)_{CO2} + (6 \cdot \dot{n}_{fuel,in} / \psi \cdot [1-\gamma])_{H2O} \tag{4.17}$$

Given Eq. 2.14, the cathode mole ratios are

$$X_{O2} = \frac{\dot{n}_{O2,in} - 2\left(\dot{n}_{fuel,in} - \dot{n}_{fuel,out}\right)}{\dot{n}_{ctout}} \tag{4.18}$$

$$X_{N2} = \frac{\dot{n}_{N2,in}}{\dot{n}_{ctout}} \tag{4.19}$$

$$X_{H2Oc} = \frac{\dot{n}_{H2O,cin} - 4\left(\dot{n}_{fuel,in} - \dot{n}_{fuel,out}\right) + 6\gamma\left(\dot{n}_{fuel,in} / \psi\right)}{\dot{n}_{ctout}} \tag{4.20}$$

And the energy balance at the cathode is the same as Eq. 4.13. The same residuals and tolerance are used for the fuel cell stack solver of both fuel cell designs.

4.3.3 Mixer

Figures 11 and 12 show the mixer as simply a volume where water from its tank, unconsumed fuel and water from the anode exhaust, and the alkaline electrolyte

KOH in the NaBH4 system, are combined and mix[†]. The mixing process itself is not modeled and it is simply assumed that the stream leaving the volume on its way to the fuel pump is homogeneous and, in the case of the direct methanol cell, does not contain any CO_2. The desired fuel concentration at the anode of the direct methanol system is 5M or 0.09 moles methanol per mole H_2O. This gives a methanol mole fraction of

$$X_{CH3OH} = \frac{mol_{CH3OH}}{mol_{tot}} = \frac{\text{methanol/H}_2\text{O}}{\text{methanol/H}_2\text{O}+1} = \frac{0.09}{0.09+1} = 0.0826 \tag{4.21}$$

and a water mole fraction of 0.9174. The amount of water needed to be drawn from the water tank in order to maintain X_{CH3OH}=0.0826 is the difference between the amount required for the fuel cell and the amount recirculated:

$$\dot{n}_w = \dot{n}_{w,out} - \dot{n}_{w,anode} = X_w \frac{\psi \dot{n}_{fuel}}{X_{fuel}} - \dot{n}_{w,anode} \tag{4.22}$$

It is assumed that CO_2 is able to bubble out completely in the mixer so the mass flow of CO_2 exiting the mixer equals the mass flow of CO_2 into the mixer via the anode exhaust. The temperature of the exit flows are determined by performing an energy balance assuming that the mixer is adiabatic:

$$\dot{m}_{fuel}h_{fuel} + \dot{m}_{water}h_{water} + \dot{m}_{rec}h_{rec} = \dot{m}_{mix}h_{mix} + \dot{m}_{bub}h_{bub} \tag{4.23}$$

In Eq. 4.23, the subscript *rec* means recirculated products (i.e. from the anode flow) and *mix* refers to the reactants that are sent to the anode. Pure methanol and water

[†] Note that there is no mixer in the pre-diluted direct methanol system. Also, mixer volume and mass were not considered for performance.

enter the mixer at room temperature and pressure from their respective tanks, and the CO_2 exits the mixer at the same temperature as the fuel mixture. Power laws relate the enthalpy and entropy of each species to the temperature:

$$h = a_1 T + \frac{a_2}{2} T^2 + \frac{a_3}{3} T^3 + \frac{a_4}{4} T^4 + \frac{a_5}{5} T^5 + a_6 \tag{4.24}$$

$$s_{Po} = a_1 \ln(T) + a_2 T + \frac{a_3}{2} T^2 + \frac{a_4}{3} T^3 + \frac{a_5}{4} T^4 + a_7 \tag{4.25}$$

The enthalpy or entropy of a mixture is the sum of the product of the species enthalpy or entropy and the respective mass fraction (y_i):

$$H_{mix} = \sum_i y_i \cdot h_i \tag{4.26}$$

$$S_{Pomix} = \sum_i y_i \cdot s_{Po\,i} \tag{4.27}$$

The mixer solver iteratively solves for the temperature of the exit mixture using Eqs. 4.23 and 4.24. The residual is calculated as the difference between both sides of Eq. 4.23, and the tolerance for the mixture is the same as the fuel cell stack and all other components (10^{-3}).

For the $NaBH_4$ model, the electrolyte makes the mole fraction calculations slightly different:

$$X_{NaBH4} = \frac{mol_{NaBH4}}{mol_{tot}} = \frac{\mathrm{NaBH4/H_2O}}{\mathrm{NaBH4/H_2O + KOH/H_2O + 1}} \tag{4.28}$$

$$X_{KOH} = \frac{mol_{KOH}}{mol_{tot}} = \frac{\mathrm{KOH/H_2O}}{\mathrm{NaBH4/H_2O + KOH/H_2O + 1}} \tag{4.29}$$

The energy balance of the $NaBH_4$ mixer is then

$$\dot{m}_{fuel}h_{fuel} + \dot{m}_{water}h_{water} + \dot{m}_{KOH}h_{KOH} + \dot{m}_{rec}h_{rec} = \dot{m}_{mix}h_{mix} \qquad (4.30)$$

Because there is no carbon in the system, no bubbling is required. However, the fuel cell produces $NaBO_2$, a solid that requires removal from the system. This is the purpose of the membrane in Figure 12 which is assumed to work with 100% efficiency[‡].

4.3.4 Fuel, water, KOH tanks and ambient air

In the NRDMFCPES, the fuel concentration is fixed and the solver works by controlling the mole flow rate exiting the fuel tank. With recirculation, the individual fuel mole flow rates are determined in the mixer and the solver works by controlling amount of fuel entering the system from the fuel tank. The residual for the fuel solver is the difference between the guess value in the fuel tank and the calculated value in Eq. 4.3. The tolerance for this residual is 10^{-7}. The water needed from the tank is determined by the fuel concentration in the anode return flow and the target anode supply concentration.

The fuel cell system model does not incorporate fuel and fuel tank mass and volume, since these will vary depending on mission requirements. So, calculation of the total mass and volume of the complete PES occurs in post-processing and will be described in more detail in section 5.2. Note that the total mass of the PES ($m_{\text{tot, PES}}$) is the sum of the fuel cell components mass (m_{FCsys}) plus the mass (m_{fuel}) of the fuel

[‡] This assumption, as well as perfect CO2 removal, is adequate for its current purposes. However, perfect membranes do not exist, and this result may cause a decline in performance. Further study of the membranes is required.

and fuel tank. Similarly, the total volume of the PES is the sum of the volumes of the fuel cell components plus the volume of fuel plus tank.

4.3.5 Fuel pump

The fuel mixture exits the mixer and enters the fuel pump where its pressure is raised to overcome pressure losses through the flow system and fuel cell stack. The isentropic efficiency of a pump is defined as [89]:

$$\eta_p = \frac{H_{isen} - H_{in}}{H_{act} - H_{in}} \tag{4.31}$$

where H_{in} is the enthalpy at the inlet, H_{isen} is the enthalpy at the outlet if the pressure rise is accomplished isentropically and H_{act} is the actual enthalpy at the pump exit. The isentropic efficiency of the pump is assumed to be 1%, based on the volume flow rate and pressure provided by the manufacturer. Rearranging Eq. 4.31 enables one to solve for the actual enthalpy leaving the pump. A solver is used to find the temperature to match the isentropic enthalpy, and then the solver finds the temperature that gives the actual enthalpy. The residual of the first step is the difference between the mixture entropy values considering isentropic flow, and the second step has a residual based on energy conservation like the previous components. The summed residual must be less than the 10^{-3} tolerance to be considered converged. The electrical power required to run the pump (P_p) is given by:

$$P_p = \frac{(H_{in} - H_{act})}{\eta_{motor}} \tag{4.32}$$

The motor efficiency is assumed to be 90% (electrical to mechanical), and the pump is assumed to be adiabatic [12]. The power is negative to show that energy is being consumed. Because the conditions (pressure, temperature, and parasitic power required for operation) of the pump change very little with different power demands and fuel cell stack sizes, only a single pump was considered for all the simulations. It is made by TCS Micro Pumps Ltd. [90].

4.3.6 Cathode fan

The fan model is very similar to the fuel pump model. An isentropic efficiency of 1% is also assumed but some heat loss is considered in order to keep the simulation stable. The operation is very different however, due to the fact that the fluid is now a gas, not a liquid. The specific enthalpies of the fuel mixture and air are not similar. This causes quite a change in parasitic losses from one test case to the next, as opposed to the small changes observed in the fuel pump. Because of this, some heat loss is required; otherwise the parasitic values for the fan would keep increasing, causing model divergence. Since air serves as both a reactant consumed by the chemical reaction and the cooling medium, small changes in power demands can cause large changes in required air flow that require a different fan to be used. Therefore, it may be necessary to switch fans during the iteration process with one of a larger or smaller flow rate range. The code handles this automatically but the discontinuities this introduces in response along with the already high sensitivity to

air flow rate make it more difficult to get the system performance iteration process to converge if inappropriate starting conditions are selected.

At present, the code chooses between nine fans from three companies: Risun Expanse Corp [91], Jarothermal [92], and Indek [93]. Their flow rates range from <0.32 to 6.35 CFM and their mass ranges from 1.8 to 25 g. The power of the fan is varied to match the necessary flowrate for cathode/cooling operation. The volume flow rate is found using the ideal gas law. Air flow properties are predicted just like with the pump, using two temperatures guess values for isentropic and actual flow. The residual calculations and tolerances are also the same. All fan property (mass, volume, etc) and performance data come from the fan manufacturer, and are given in Appendix D. Because multiple performance curves for each power level/speed possible were not provided, the model uses the flow rates that were listed by the manufacturers.

4.4 Simulation overview.

The main screen, which is the first worksheet in the Excel workbook, provides the system level parameters and results. User input parameters include: power demand, ambient temperature, ambient pressure, humidity, stoichiometric ratio for anode flow, number of cells in the fuel cell stack, electric motor and inverter efficiencies, and the iteration tolerances. System outputs (results) include: fuel energy input, system efficiency, power produced by the fuel cell (which is larger than the system power demand), MEA power density, operating voltage, and parasitic loads. Additional results include mass and volume of the entire system

The main screen also includes a summary of each component in the system. This summary includes the electric work demand (positive if providing power and negative if requiring it), heat transfer demand, the sum of the residuals, the inlets, and the flow data. It also provides a summary of each component, including where the incoming flow is coming from and flow properties.

Within each component, which has its own worksheet, the inlet flow data is taken from the outlet data of the sheet given in the prescribed cell. The numbered outlet is also provided, since some components have more than one. Flow data, which is given for the inlet and outlet of each component, includes: the mass flow rate (g/s), total molar flow rate (mol/s), temperature (K), pressure (bar), molecular weight (g/mol) of the pure or mixed fluids, mole and mass fractions of all the constituents being considered, individual mole flow rates of the constituents, enthalpy (J/g) and entropy (J/g*K) of the constituents as well as the total amounts, the vapor pressure of water, the entropy (J/mol*K) of the constituents at ambient pressure, and the mole flow rates of the periodic elements (C,H,O). A sum of the mole fractions is also provided for each outlet for debugging. This flow data is passed from one component to the next through the main screen, like the tubing of an actual system.

A schematic illustration of the overall iteration process is provided in Figure 13. The gross power output of the fuel cell (i.e. the usable power requirement plus the parasitic power losses) is selected along with a stack operating voltage and the conditions in each component are updated by their own iterative solvers. When the components are converged, the gross power output of the fuel cell is updated, a new stack operating voltage is selected to meet this demand, and the process is repeated

until the stack voltage, power output, and the energy balances of all components have converged.

This model was used to investigate the scaling of fuel cell system performance with size by varying two parameters in the model: net power output and the number of electrochemical cells in the fuel cell stack. Increasing the number of cells for a particular system decreases the current density, increases cell voltages, and improves the stack efficiency η_{FC}. However, it also increases system mass and volume leading to tradeoffs between energy density, power density, and efficiency (specific fuel consumption). These tradeoffs and how they differ for the three fuel cell systems considered here will be discussed in the next chapter.

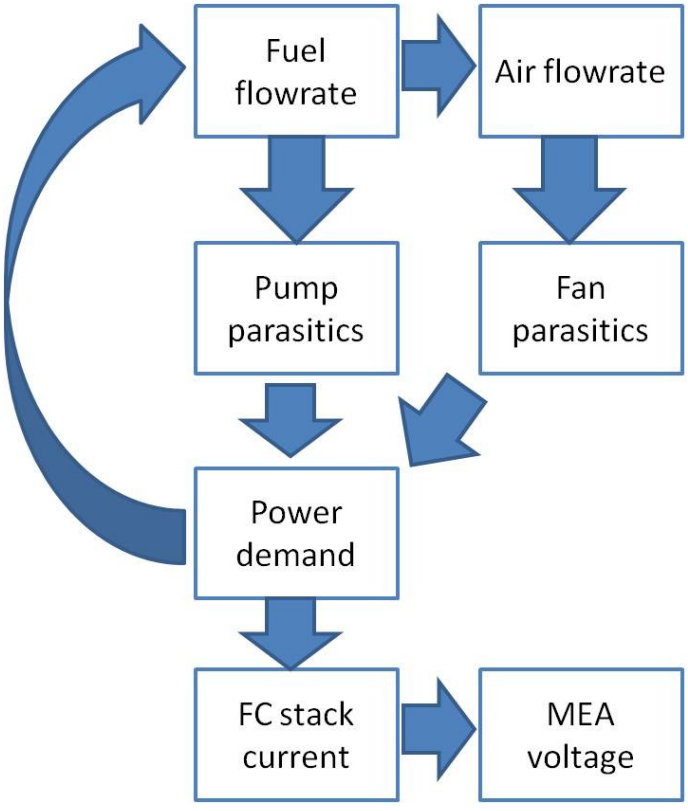

Figure 13: Iterative scheme for fuel cell system model.

Chapter 5: Model Results.

5.1 Fuel cell and BOP alone.

5.1.1 Non-recirculating DFMC system

Figure 14 shows how system efficiency η_{th} varies with the total mass m_{FCsys} of the non-recirculating DMFC systems. The numbers at the ends of each curve give the number of cells in the stack at those maximum or minimum points. The number of cells varies linearly along the curves between the end points. Since the cells are stacked in parallel, η_{th} increases with the number of cells because increasing the number of cells decreases the current density. However, the improvement in efficiency is non-linear and decreases with increasing numbers of cells.

Figure 14 also shows that decreasing the power requirement does not change the peak attainable efficiency until the power drops below 10W. At 5W, the baseline parasitic losses associated with the pump and blower are more significant than the ohmic losses and the peak attainable efficiency is lower. This is the reason that the 5W curve crosses the others. The net result is that efficiencies as high as 30% can be attained for fuel cell systems lighter than 150 g (without fuel).

Figure 15 shows efficiency as a function of power demand for three different stack sizes. It shows that there is an optimum power level associated with a particular number of cells. This is a result of the tradeoff between stack overpotential losses that increase with power and the baseline parasitic loss fraction (baseline parasitic power /system power output) that decrease with power. Both the peak

efficiency and the power level associated with this peak increase with the number of cells. Peak efficiency increases with number of cells because the relative importance of parasitic losses decreases as the system gets larger.

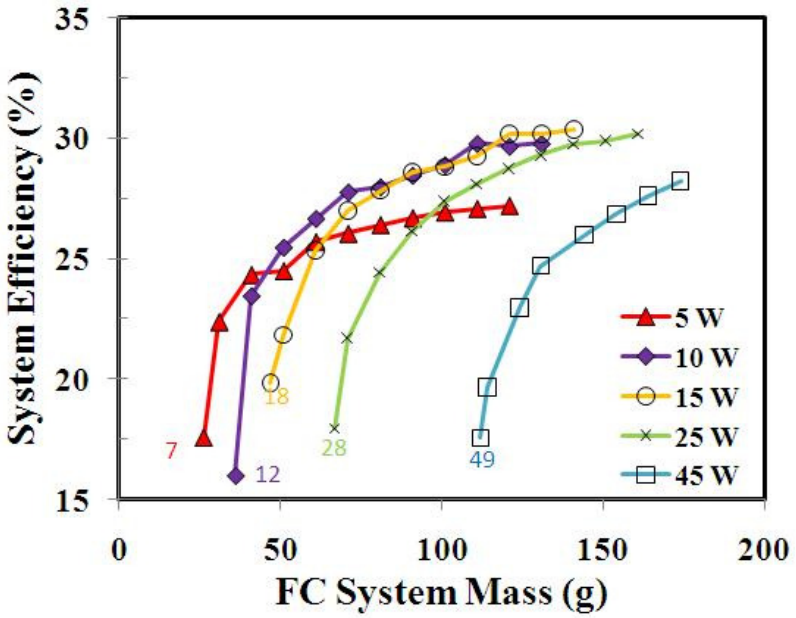

Figure 14: Fuel cell system efficiency vs. the mass of the system (m_{FCsys}) without fuel for different overall power levels. The numbers at the ends of the curves indicate the number of electrochemical cells in the fuel cell stack at those points.

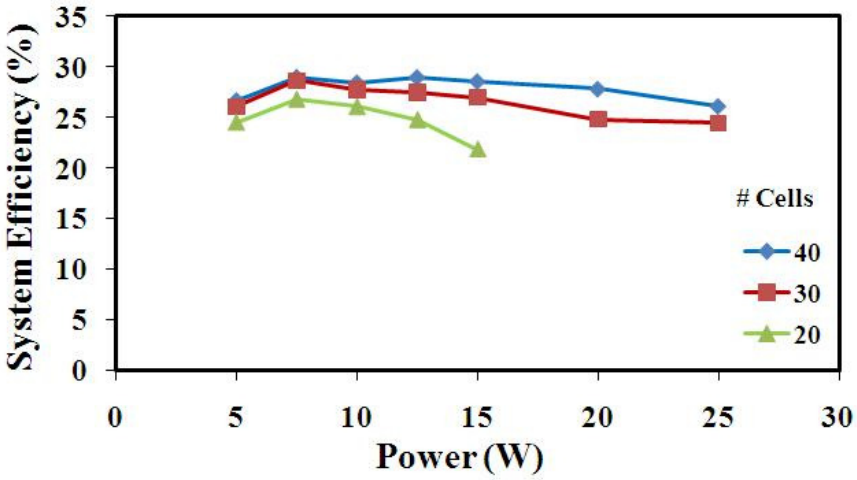

Figure 15: DMFC system efficiency vs. power output for various stack sizes.

The efficiencies achieved seem high for a fuel cell system. To better assess the cause, the individual efficiencies – fuel cell and balance of plant – are plotted in Figure 16. Fuel cell efficiencies hover above 30%, but the BOP efficiencies are high, mostly above 80%. This is most likely due to the assumed high efficiencies of the parasitic motors and power conditioning. Predicting most of the ancillary components to be adiabatic is also another possible cause.

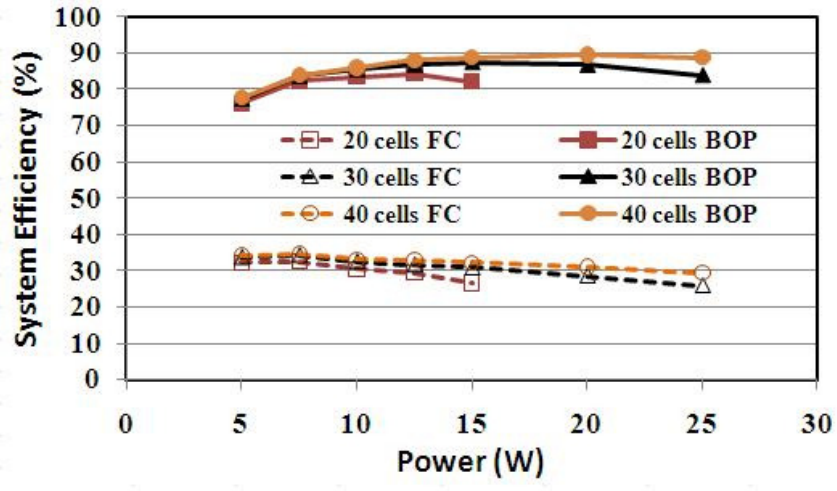

Figure 16: Fuel cell and balance of plant efficiencies for systems with various stack sizes. The dashed lines represent the FC efficiency, and the solid the BOP efficiency.

Figure 17 shows the specific power of the fuel cell system as a function of m_{FCsys} for different numbers of cells and power levels. Decreasing the number of cells increases specific power for all configurations considered. This trend is also non-linear. The lowest cell count on each curve in Figure 17 corresponds to the minimum number of cells capable of satisfying the specified power demand. The 45 W system has the highest system specific power recorded of 510 mW/g using a 49 cell stack. The high for the lowest power system (0.25W using a 1 cell stack) is 45 mW/g.

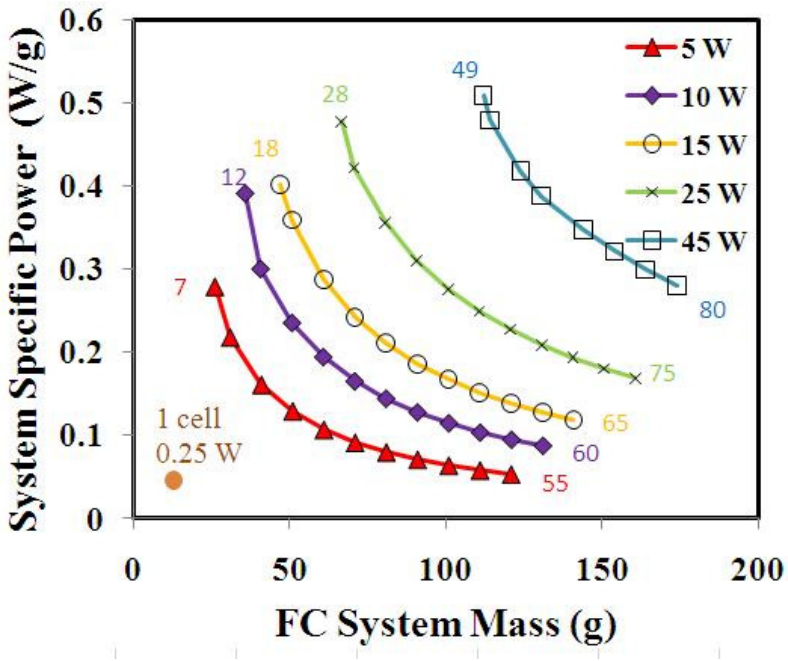

Figure 17: System specific power of non-recirculating DMFC systems at various power demands. Numbers at ends of curves give the number of electrochemical cells in fuel cell stack at those points. The specific power of a 1 cell system producing 250 mW is also provided.

5.1.2 Water recirculating direct methanol fuel cell system

The lowest cell counts shown in Figures 14 and 17 are the minimum amounts of fuel cells necessary to achieve the desired power output. These minimum amounts were found with the recirculating systems as well. Figure 18 provides these minimal stack values as well as a larger range of cell count. The point after the minimum on each curve is the next multiple of 5. The effect of increasing the number of cells can be quite dramatic when the fuel cell power is low. For example, adding 3 more cells to a 5W system boosts efficiency by almost 8 percentage points. The difference in system mass is relatively small because the system with fewer cells actually uses a slightly heavier fan. As with the non-recirculating systems, the curves also show that systems with more cells and operating at higher power levels are more efficient. This

is because the larger blowers, motors, and other components used by these systems are more efficient. Changing the power requirement does not have a significant effect on the peak attainable efficiency until ohmic losses become much less important (< 10%) compared to total parasitic losses. This occurs at approximately 10 W.

Figure 19 shows efficiency as a function of power demand for three different stack sizes. As is the case with the previous system, efficiency is maximized at intermediate power demands because of the tradeoff between stack overpotential losses that increase with power and baseline parasitic losses that decrease as a fraction of total power. The power level associated with peak efficiency increases as the number of cells increases. Efficiency is maximum in the 20 and 30 cell systems at about 7.5 W while peak efficiency in 40 cell systems occurs at about 12.5 W.

The specific power of the recirculating DMFC systems is shown in Figure 20. Specific power is maximized at a single power level and number of cells. Increasing or decreasing the power level or the number of cells decreases the overall specific power. The figure shows that the maximum specific power density is about 0.4 W/g and corresponds to 24 cells, a power output of 20 W, and a system mass of approximately 70 g.

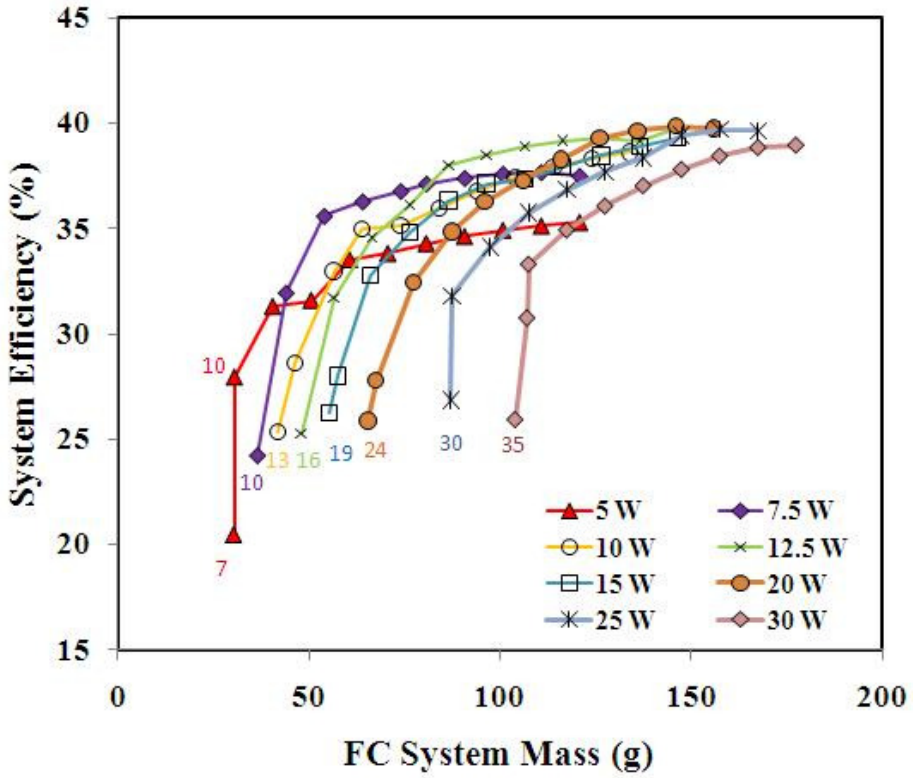

Figure 18: Fuel cell system efficiency without fuel for different overall power levels. The numbers at the ends of the curves indicate the minimum number of cells required to achieve the desired power level.

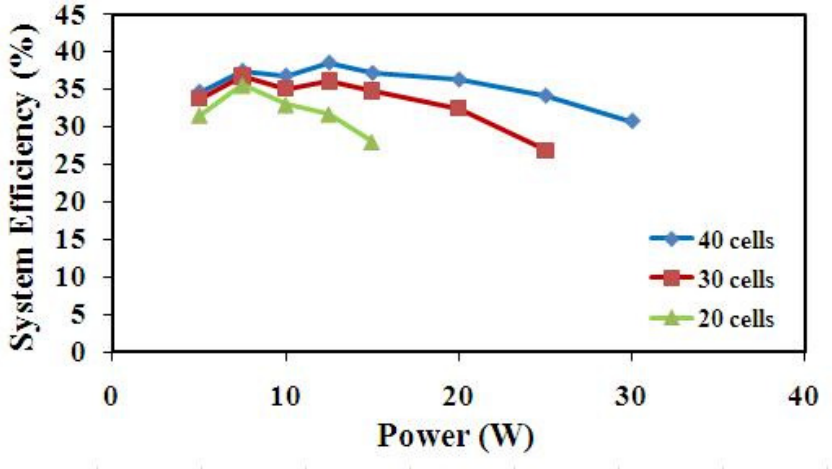

Figure 19: Recirculating DMFC system efficiency vs. power output for different stack sizes.

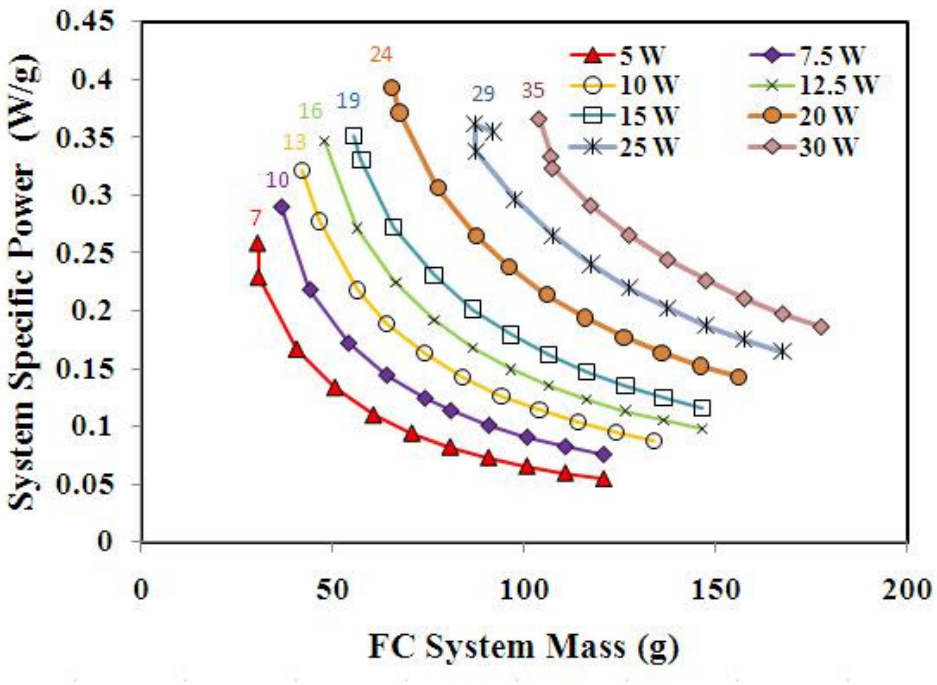

Figure 20: Specific power of recirculating DMFC systems at various power levels. Numbers show the number of cells in the fuel cell stack at the end points of the curves. The symbols correspond to increments of 5 cells.

While the results show that recirculating DMFC systems are more efficient than non recirculating ones, the greatest impact of water recovery is on the energy density of the system because less water storage is required and more of the mass budget of the system can be spent on the fuel. This advantage will be discussed further in section 5.2.

Figures 21 and 22 compare the performance of non-recirculating and recirculating systems. Figure 21 shows how the efficiency of the system at 10 W changes relative to the baseline system when water recovery and recirculation is added. Clearly, including water recirculation significantly improves efficiency. This is because non-recirculating systems run rich in order to maintain good diffusive transport of fuel to the anode and this extra fuel flows overboard and is wasted.

Water recovery and recirculation enables one to recover unreacted fuel exiting the anode. The net result is less fuel is wasted and the efficiency of the system is higher. The increase in efficiency can reach 8.5%. Figure 22 shows that while the system specific power curves overlap, when comparing similar stack sizes, the specific power of the recirculating system is slightly lower than the non-recirculating design for the same stack size. Adding recirculation decreases specific power because it adds a parasitic load. This load becomes less significant as the stack size increases causing the two curves to overlap more closely at higher cell counts.

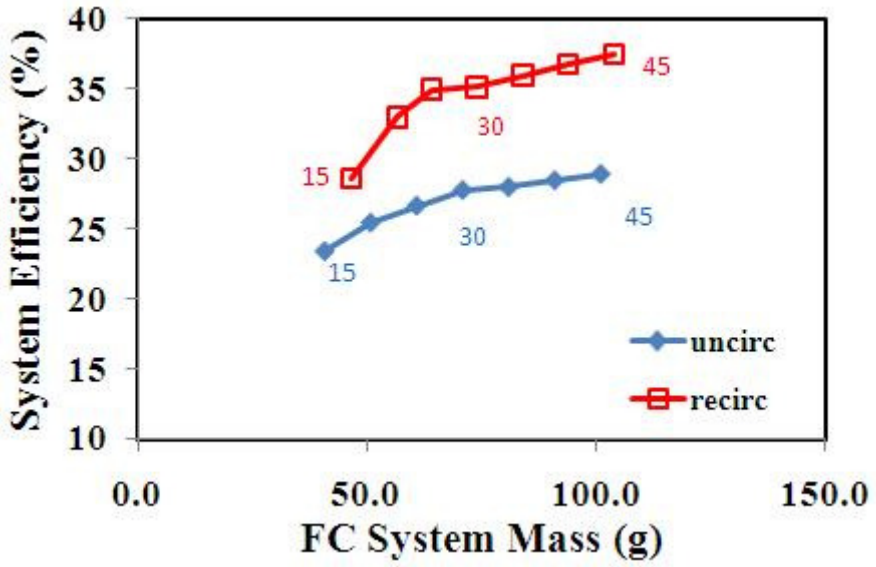

Figure 21: Fuel cell system efficiency of a DMFC system with and without recirculation of the anode exhaust for a 10 W power demand. Numbers denote cell count in the stack.

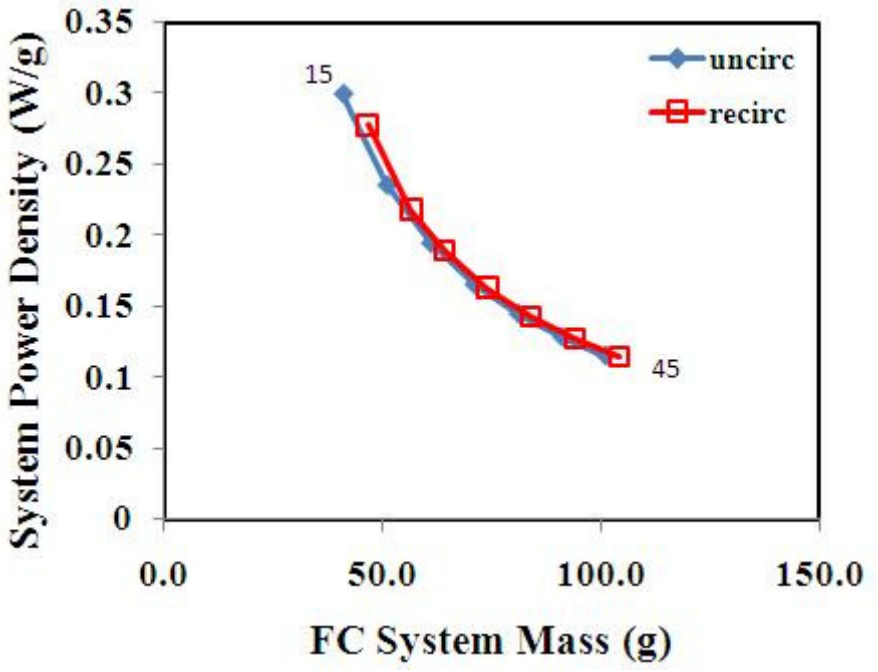

Figure 22: Specific power of a DMFC system vs. the system mass (m_{FCsys}) with and without recirculation of the anode exhaust for 10 W power demand.

5.1.3 Recirculating direct alkaline sodium borohydride fuel cell system

Although the open circuit voltage of the sodium borohydride fuel cell is higher than the methanol fuel cell, the Tafel slope of the voltage-current density (V-i) curve is much steeper. This means that MEAs current densities must be lower in order to function and therefore more stacks are required to meet a particular power demand. Figure 23 shows sodium borohydride system efficiency as a function of overall system mass. As alluded to earlier, the minimum stack size is much larger for this system than the previous DMFC system. Efficiencies are comparable to the DMFC system because it also uses water (and fuel) recovery of the anode. However, the larger required stack size leads to a significant weight penalty: Figure 18 shows that a 12.5 W recirculating DMFC could be as light as 50 grams whereas Figure 23 shows that a comparably efficient $NaBH_4$ system would weigh about 200 grams.

Because the system weight is 4 times as much as the methanol system, it is no surprise that the specific power values shown in Figure 24 are about a quarter of those attainable by the recirculating DMFC systems. Finally, the largest power level considered was 12.5 W because the results suggest that higher power systems would be far too heavy for the miniature vehicles that are of interest in this study.

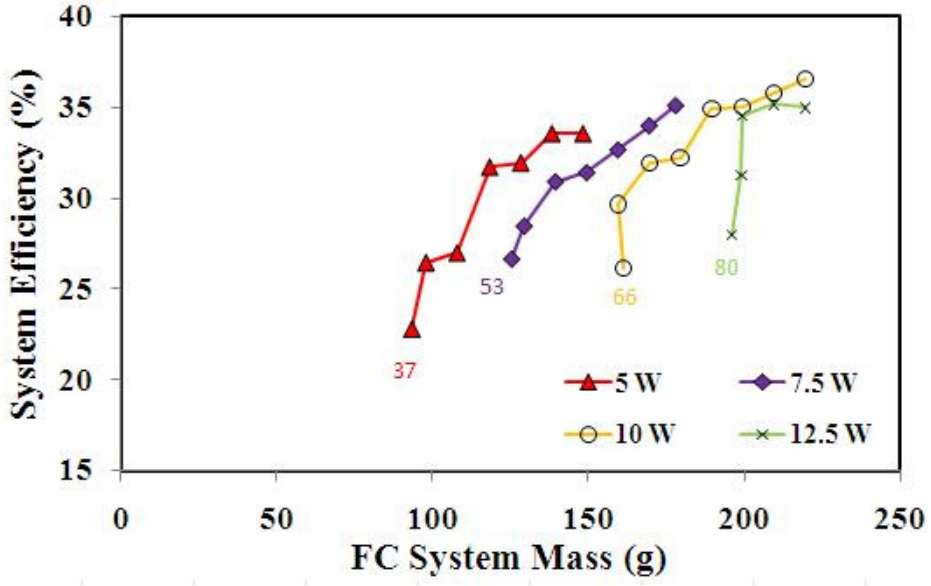

Figure 23: Sodium borohydride fuel cell system efficiency at different power levels. The numbers at the ends of the curves indicate the minimum number of cells required to achieve the specified power level.

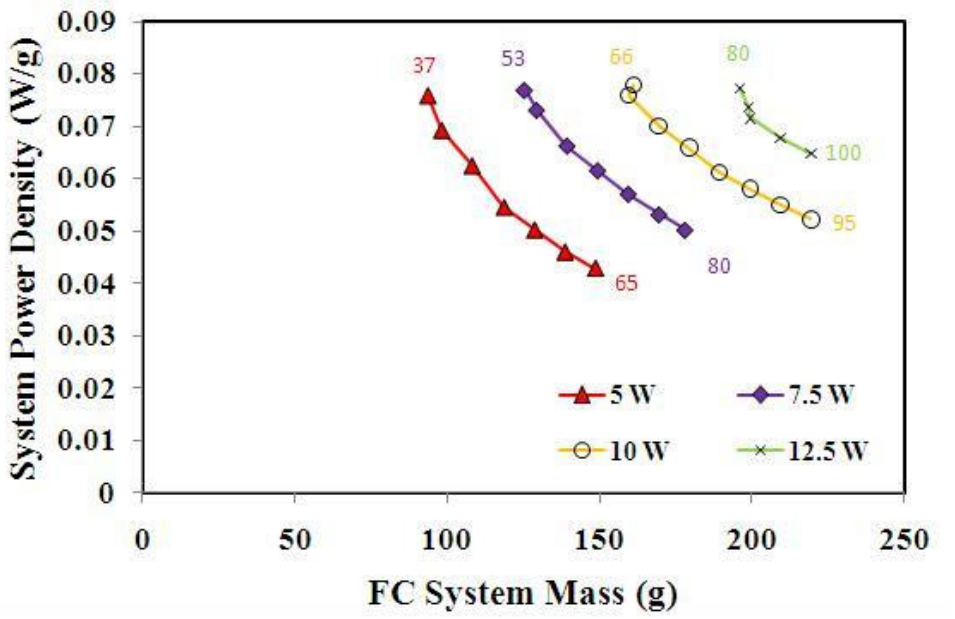

Figure 24: Specific power of sodium borohydride fuel cell system at various power demands. The numbers at the upper end of the curves show the minimum number of cells required to achieve the specified power level. The numbers at the lower ends show the number of cells in the fuel cell stack at those points.

5.2 Power and energy density comparison.

Up to this point, the discussion has focused on the fuel cell system by itself without consideration of the fuel and fuel tank. This was done in order to highlight the critical aspects of the fuel cell system (FC_{sys}) design. However, the specific power and specific energy of the overall PES are heavily influenced by the fuel mass fraction (ζ). The fuel mass fraction is defined as the ratio of the mass of fuel and tank (m_{fuel}) to the mass of the fuel cell stack plus the balance of plant components (m_{FC} + m_{BOP}= m_{FCsys}). As discussed previously, the total mass of the integrated power and energy system, $m_{tot,\ PES}$ equals m_{FCsys} + $m_{fuel.}$ This leads to the following expressions for the power and energy density of the system:

$$\frac{P}{m_{tot,PES}} = \frac{P}{m_{FCsys}}\left(\frac{1}{1+\zeta}\right) \tag{5.1}$$

$$\frac{E}{m_{tot,PES}} = \eta_{th} Q_R \left(\frac{1}{1+1/\zeta} \right) \tag{5.2}$$

In these equations, P/m_{FCsys} is the specific power of the system without fuel (reported for the various systems considered in Figures 17, 20, 22, and 24) and Q_R is the specific energy of the fuel-water mixture (2914 J/g for the 5 M methanol solution). P/m_{FCsys} is the maximum specific power achievable by the PES and $\eta_{\mathrm{th}} Q_R$ (the product of the overall thermodynamic efficiency with the specific energy of the fuel) is the maximum possible specific energy of the PES. Neither extreme is realizable in a practical PES system as peak specific power is only achieved at ζ=0 (which means zero specific energy and hence range/endurance) and peak specific energy is only achieved at ζ=infinity (which means zero power density).

The functions of ζ that modulate the peak power and energy density are plotted in Figure 25. Increasing the fuel mass fraction decreases the specific power and increases the specific energy of the complete fuel cell system. Eq. 5.1 and 5.2 show that while the performance limits are set by the fuel cell and BOP considerations only, the actual specific power and specific energy of the complete fuel cell system is also strongly affected by the fuel mass fraction. Optimizing the system requires trading specific power for specific energy (or endurance). While this trade ultimately must be driven by the mission, choosing ζ=1 is a reasonable interim strategy that maximizes the product of the two curves and represents an even-handed compromise between PES specific power and specific energy.

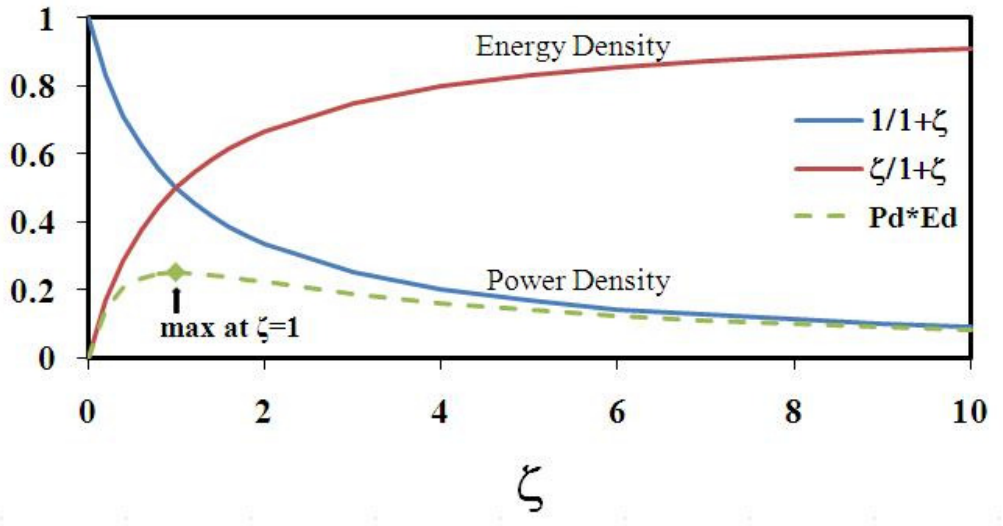

Figure 25: Functions of ζ that modulate the peak specific power and specific energy of the fuel cell system.

The complete tradeoff between specific power and specific energy is illustrated in Figure 26. It shows specific power as a function of system specific energy for three 10 Watt PES – direct methanol, direct methanol with recirculation, and direct borohydride with recirculation - each with two different cell stack sizes. The stack sizes chosen correspond to the endpoints of the fuel cell system specific power figures above. The solid circles show where systems with different values of ζ lie on the curves with the color of the circle denoting the value of ζ. Colors range from black (ζ=0.2) to purple (ζ=10). The dashed diagonal lines show contours of constant endurance. The open symbols (x, +, and *) denote $m_{tot,\ PES}$ = 100 g, 150 g, and 200 g respectively and provide an indication of the relative sizes of the various systems. The vertical line crossing the x-axis shows the DARPA specific energy target of 1000 W-Hr/kg.

The figure shows that as ζ becomes large, most of the PES's mass is contained in the fuel and the system performance curves approach the specific energy of the fuel times the conversion efficiency. As ζ becomes small, specific power approaches its maximum but this comes at the price of reduced endurance because there is less fuel available. The curves for each class of system cross each-other because systems with more cells have lower specific power but are more efficient.

The first set of curves in the lower left corner of Figure 26 corresponds to the baseline methanol system without recirculation. A symbol corresponding to a high performance Li-ion battery from A123 Systems is provided on the figure as a reference [94]. While the battery's endurance is lower than all of the fuel cell systems under consideration, its specific power is about an order of magnitude larger than the best NRDMFCPES. The second set of solid curves on the lower right side of the figure correspond to direct methanol fuel cell systems with recirculation. Adding recirculation shifts the baseline system to the right for two reasons. First, recirculation improves efficiency by recovering unreacted fuel exiting the anode. Second, and more importantly, recirculation reduces the amount of water needed to be carried on board. This frees space for more fuel thereby increasing Q_R. The net effect is nearly an order of magnitude improvement in effective specific energy and endurance over the non-recirculating system and batteries.

The third set of curves to the far right in Figure 26 shows the performance of a recirculating alkaline direct sodium borohydride fuel cell PES. Although the borohydride systems have lower specific power values, the higher specific energy of the fuel provides the opportunity for longer endurance missions using less fuel. This

is important because more weight is needed for the system itself. Notice, however, that only 200 g systems are shown for the borohydride system as 100 g and 150 g systems are not possible because BOP would consume more power than the fuel cell supplies. The 60 cell RDMFCPES and the 66 cell ANaBH4FCPES curves overlap at an overall system weight of 200 g, meaning that the same system weight provides the same endurance and system specific power and specific energy. Comparing the methanol and $NaBH_4$ systems on a mass basis, the methanol system with a 200 g weight and smaller stack size will outlast the sodium borohydride systems. While both the RDMFCPES and ANaBH4FCPES can meet the specific energy DARPA target if size is not a consideration, the RDMFCPES comes closer to meeting it at the 200 g mass limit relevant to the miniature crawling/hopping/flying vehicles of interest to the U.S. Army.

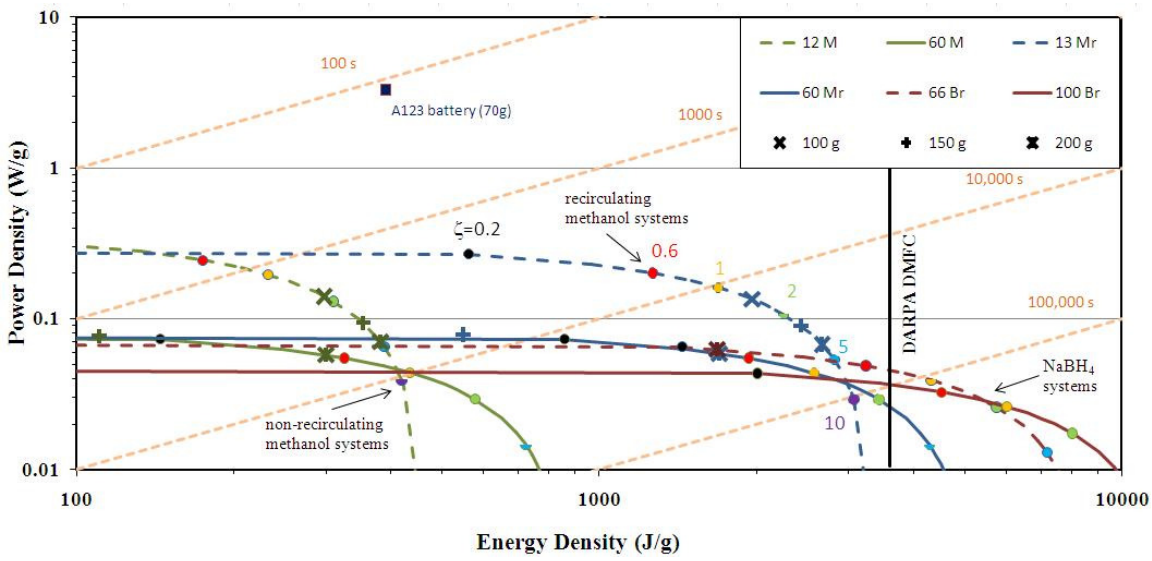

Figure 26: Ragone plot for a series of 10 W fuel cell systems. Subscripts r, B, and M refer to recirculation, borohydride, and methanol, respectively. Dashed lines indicate PES with maximum specific power, while solid lines are PES with peak efficiency. Colored circles indicate the fuel mass fraction of the PES at that point. Other colored symbols represent PES weight. Diagonal dotted lines are of constant endurance.

Figure 27 shows how the power requirement influences the relative merits of one technology over another. At 5 W, the sodium borohydride system requires fewer cells in the stack thereby lowering system weight and making the ANaBH4FCPES more competitive with the RDMFCPES. The ANaBH4FCPES outperforms the RDMFCPES for 5W systems weighing more than 150 g while the RDMFCPES continues to be best for 5W systems weighing less than 150 g. The reader is referred to Appendix E for the data in table format of all Ragone plots.

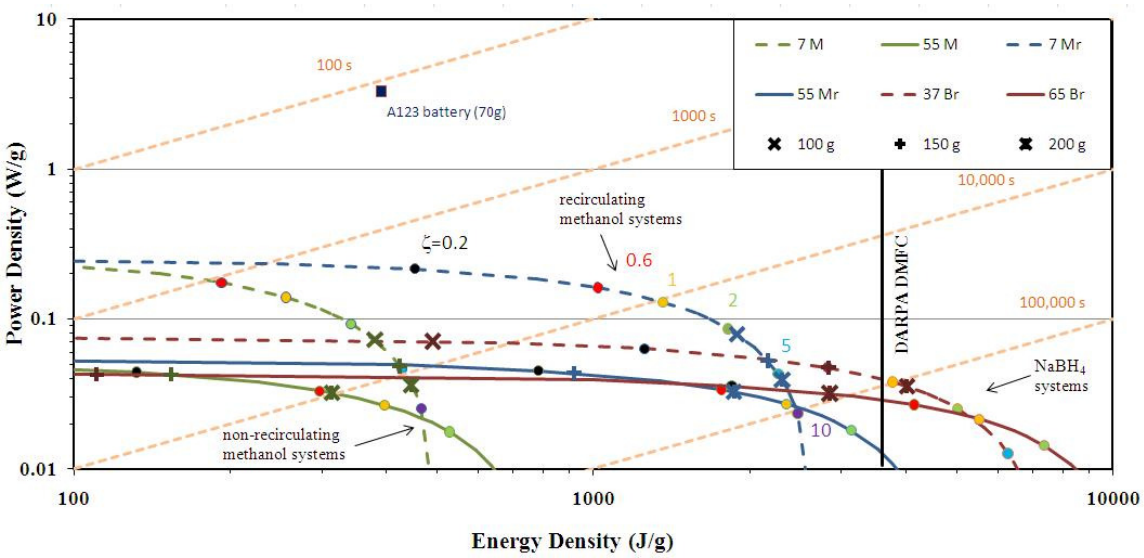

Figure 27: Ragone plot for a series of 5 W fuel cell systems. Subscripts r, B, and M refer to recirculation, borohydride, and methanol, respectively. Dashed lines indicate PES with maximum specific power, while solid lines are PES with peak efficiency. Colored circles indicate the fuel mass fraction of the PES at that point. Other colored symbols represent PES weight. Diagonal dotted lines are of constant endurance.

Figure 28 shows a comparison of performance for the baseline NRDMFCPES at different power levels. This is beneficial because if the PES mass is known, a designer can quickly see how much power is achievable at what specific power, specific energy, and endurance. Points of constant PES mass are not linear, thus

having a power demand or endurance requirement in mind would make the design decisions easier. Figure 29 is a similar plot, but with the RDMFCPES. Figure 30 provides the same comparison for the ANaBH4FCPES. The performance in these curves is very similar, but endurance per PES mass does improve with lower power levels.

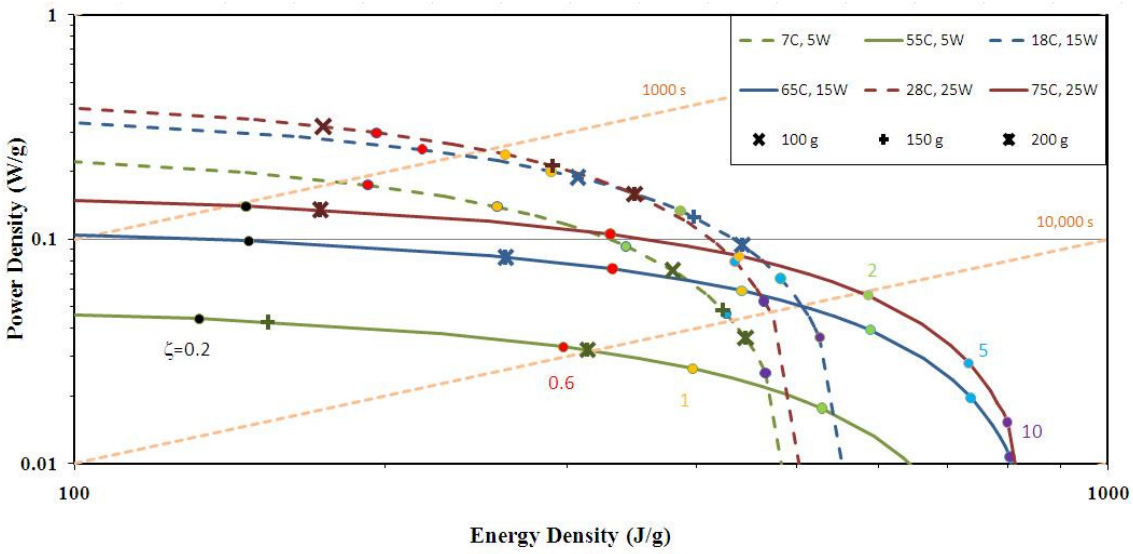

Figure 28: Ragone plot for NRDMFCPES. Curves depict stack size and power demand. Dashed lines indicate PES with maximum specific power, while solid lines are PES with peak efficiency. Colored circles indicate the fuel mass fraction of the PES at that point. Other colored symbols represent PES weight. Diagonal dotted lines are of constant endurance.

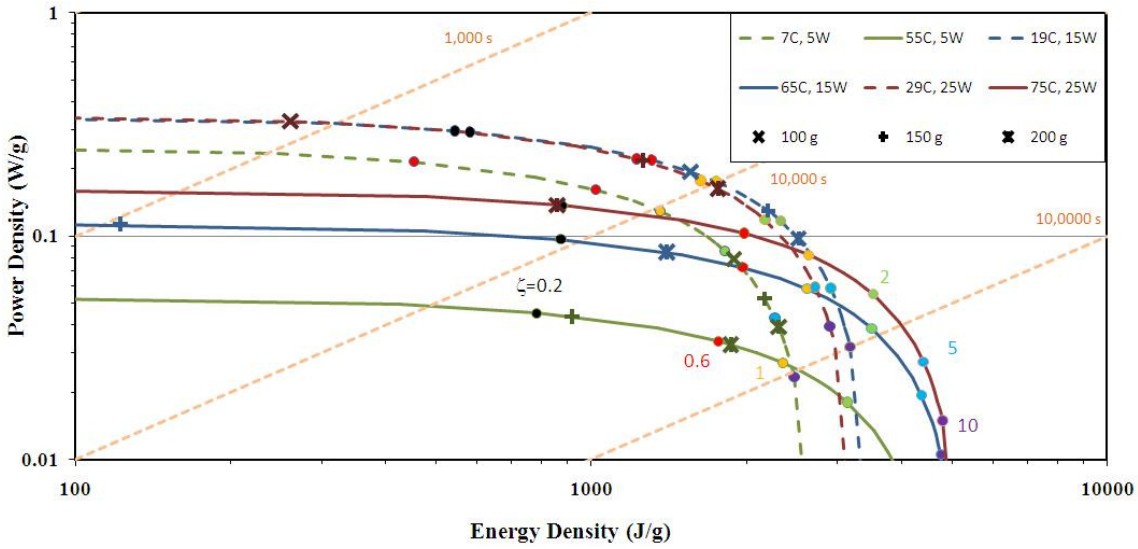

Figure 29: Ragone plot for RDMFCPES. Curves depict stack size and power demand. Dashed lines indicate PES with maximum specific power, while solid lines are PES with peak efficiency. Colored circles indicate the fuel mass fraction of the PES at that point. Other colored symbols represent PES weight. Diagonal dotted lines are of constant endurance.

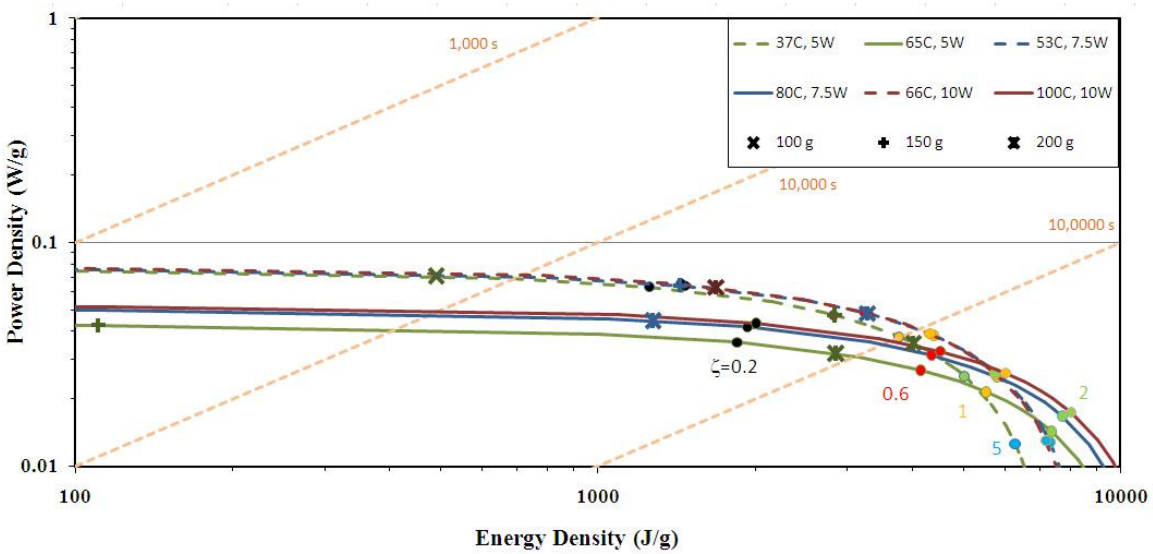

Figure 30: Ragone plot for ANaBH4FCPES. Curves depict stack size and power demand. Dashed lines indicate PES with maximum specific power, while solid lines are PES with peak efficiency. Colored circles indicate the fuel mass fraction of the PES at that point. Other colored symbols represent PES weight. Diagonal dotted lines are of constant endurance.

5.3 Effect of mission profile and fuel cell/battery hybridization.

Since a typical vehicle mission involves periods of high power operation during locomotion and periods of lower power operation associated with data gathering or waiting, hybridizing the fuel cell system with a battery is natural. The challenge is selecting the optimum battery-fuel cell combination. While a formal optimization is beyond the scope of this thesis, some insight can be gained by considering how battery-fuel cell systems would be configured to support various missions. The DMFC system was chosen for this case study due to higher power level demands associated with the vehicle's functionality.

Two types of missions (illustrated in Figure 31) were considered for an arbitrary flying vehicle with the properties listed in Table 5. The first type has the vehicle flying to its destination, performing its required functions, and then flying back to its origin. The second type has the vehicle stop in three places (following a square flight path), before returning to its origin. Power is taken from the battery when the vehicle is in flight. Transient time required for a power level change was assumed to be 1 minute so the vehicle can land or perch with a safe deceleration and the total mission time is held constant at 60 minutes for all missions. Obviously, these parameters will vary widely depending on the mission but these choices are satisfactory for the purpose of demonstrating the advantages of a hybrid system. A total of 5 missions with different power profiles were investigated.

Table 5 Hybrid Vehicle Properties

Vehicle Mass	Max 225 g
Payload Mass	Max=80 g
Fuel Mass Fraction	Max = 1
Vehicle Speed	5 mph
Propeller Length	20 cm
Flight Power Requirement	30 W (η_{Prop}=0.4)
Stationary Power Requirement	10 W
Sensor Power	2 W
Transmit Power	3 W
Computation Power	5 W

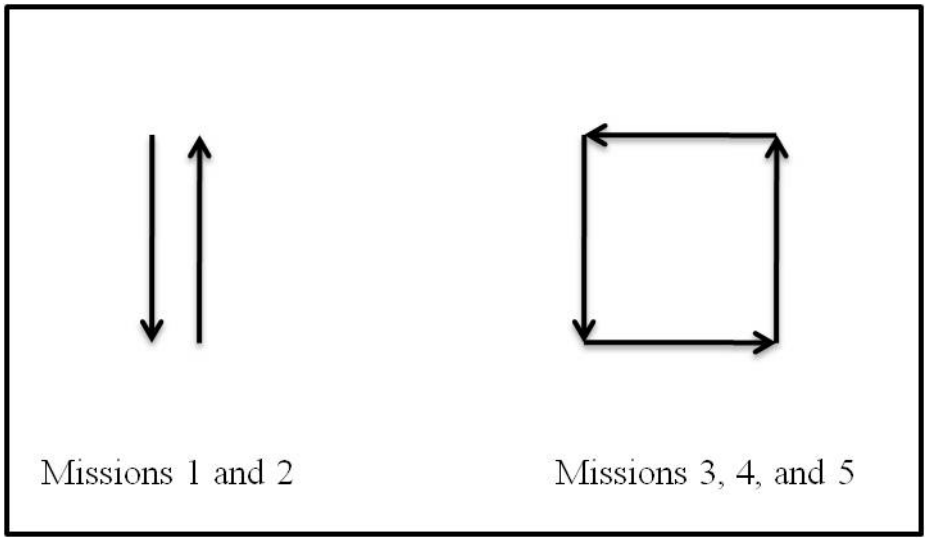

Figure 31: Flight path of hovering UAV for the different missions under consideration. Missions 2, 4, and 5 involve battery recharging.

Figure 32 shows the power profiles associated with the 5 missions under consideration. Mission 1 is the fly in/fly out scenario and uses two batteries to power the airborne legs. Mission 2 is the same, except that the fuel cell recharges the battery after landing at its destination so that only one battery is required. Mission 3 is the baseline for the square path where four batteries are used to fly the four airborne legs. Mission 4 uses two batteries that are recharged at the second stop after both have been depleted. Mission 5 uses only one battery and recharges it at each stop.

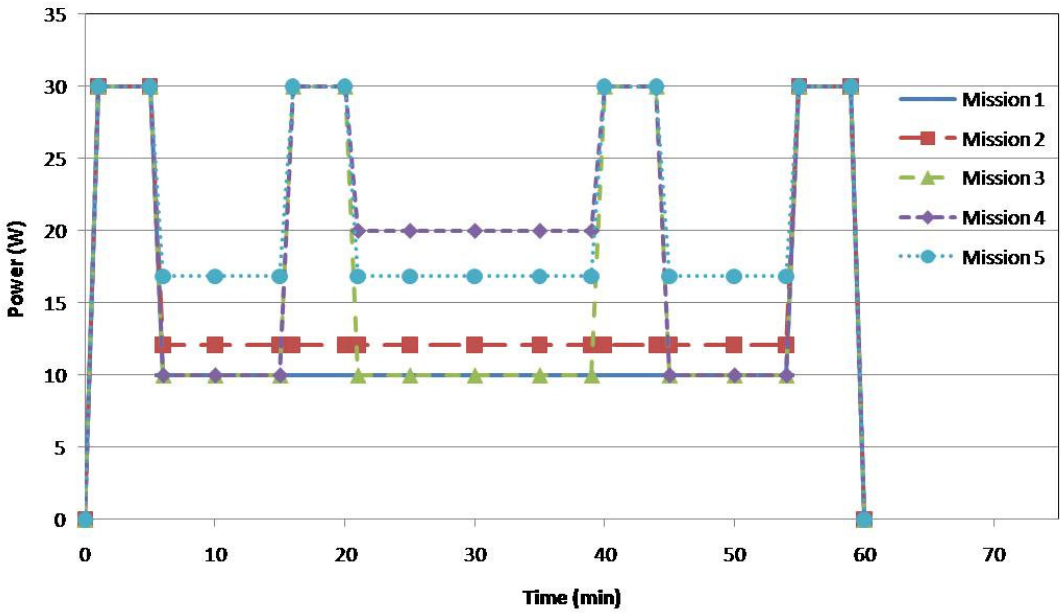

Figure 32: Mission profiles of a battery/ fuel cell hybrid power system for a flying micro vehicle. Higher power levels at non-flight conditions correspond to battery recharging.

Table 6 summarizes the results. The first row gives the energy required to complete the missions. The next two rows give the weights of a PES that utilizes only batteries. The weights of a hybrid battery/FC PES follow, as well as the fuel cell efficiency. PES weight reduction is the entire weight of the power system (battery+ FC PES) divided by the weight of a battery-only system. Previous results (Figure 18) indicated that increasing the number of cells in the fuel cell stack increases its efficiency. The hybrid PES could be enlarged by increasing the amount of cells in the FC stack in order to attain peak efficiency. Increasing the number of cells in the stack until the mass of the hybrid PES system equaled the mass of the battery only PES results in an efficiency increase of about 8%. This difference in efficiency reduces the amount of fuel necessary for the mission by about 1 gram, but the increase in PES

weight is 10 or more grams. Because of the low fuel savings, the PES system used for the results in Table 6 had the minimal amount of fuel cells in the stack (performing at peak system power density).

As can be seen from the table, the PES and vehicle weight reduction are considerable for each mission - even those with no recharging. A power system under mission profile 5 could have its weight reduced by almost half. Even without recharging, the power system mass can be reduced by a fourth. Because a fuel cell system is used in conjunction with a battery, the vehicle mass will be lighter, or the mass "saved" can be used towards a greater payload. This advantage is shown in the last row of the table. For mission 5, the payload weight could almost be doubled due to the mass savings with the hybrid PES. The battery is well suited for flight power; however, recharging one battery with the fuel cell system is the best option for both types of missions because the total and power system mass are smallest. Less mass in the power system leads to better sensing and computing technologies that can be incorporated into the vehicle. A direct methanol fuel cell system coupled with a battery has the potential to meet the needs of the U.S. Army's future fleet of mini flying vehicles.

Table 6: Hybrid system performance evaluation

		Mission 1	Mission 2	Mission 3	Mission 4	Mission 5
Total Energy Required (J)		47400		59400		
Battery Only PES	Battery weight (g)	121.5		152.3		
	Vehicle weight (g)	191.5		222.3		
Battery/FC Hybrid PES	Battery weight (g)	32.3	16.0	63.1	30.8	15.6
	Fuel cell PES (g)	52.2	57.3	52.3	74.6	69.3
	Total vehicle weight (g)	154.4	143.1	185.2	175.2	154.8
	Fuel cell efficiency	29.41%	28.85%	29.41%	32.12%	29.19%
Benefits	FC PES weight reduction	69.58%	60.31%	75.72%	69.16%	55.76%
	Vehicle weight reduction	80.68%	74.79%	83.35%	78.85%	69.67%
	Payload weight increase	52.95%	69.08%	52.95%	67.27%	96.49%

Chapter 6: Conclusions and Future Work.

6.1 Summary/Conclusions.

The U.S. Army is developing miniature (<500g) robotic sensor platforms to explore and monitor harsh/dangerous environments. At present, the range and endurance of these vehicles is severely limited by their battery-based power systems which have relatively low specific energy. Miniature fuel cells consuming high energy density fuels could improve range and endurance by an order of magnitude or more provided suitable levels of overall system-level efficiency can be achieved at small-scale. The objective of this thesis was to identify promising fuel cell technologies appropriate for implementation in sub 500g systems and to develop quantitative methodologies for evaluating miniature fuel cell performance.

A literature survey was conducted to identify the fuel cell technologies that are best suited for powering small autonomous vehicles. It focused on ammonia, methanol, ethanol, and sodium borohydride fuels. A ranking system was developed to assess relative suitability for U.S. Army applications. The survey provided insights into the important advantages and disadvantages of each technology, but did not identify a clear winner. A more quantitative analysis that accounted for the parasitic losses associated with the overall balance of plant (pumps, blowers, power conditioning, etc.) and system weight or size was necessary.

Two types of systems were selected for this focus. The sodium borohydride alkaline fuel cell was selected because it scored highest in the literature survey - partially because of the high energy density of the fuel. The direct methanol system

was selected for the balance of plant's simplicity and the MEAs relatively high power density for a low temperature fuel cell.

A methodology was developed for predicting overall system-level performance of fuel cell power and energy systems. It is unique in that it accounts for how balance of plant losses scale with the physical size of the fuel cell system. This is found to be essential in order to evaluate the suitability of various fuel cell technologies for vehicles of different scales. The methodology was applied to three different types of miniature fuel cell systems: a direct methanol fuel cell system, a direct methanol fuel cell system with water recovery at the anode, and an alkaline $NaBH_4$ fuel cell system.

The results showed that a 150 g, 10 W direct methanol fuel cell system is approximately 15.9% efficient, can achieve system specific power around 100 mW/g, and can maintain it for 1 hour. A 150 g, 10 W direct methanol system with water recovery at the anode achieved slightly lower specific power (5 mW/g difference) but was more efficient (25.3%) and could operate much longer (7.5 hours) because pure methanol fuel could be used instead of a dilute methanol-water mixture. The specific power of a 200 g, 10W $NaBH_4$-based fuel cell system was much less than 100 mW/g because the fuel cell stack must be larger to produce the necessary current. However, the endurance of the 200 g $NaBH_4$ system is also approximately 7.5 hours. This is because of the high energy density of $NaBH_4$. At power levels less than 10W, the $NaBH_4$ power and energy system also offers better specific power than the direct methanol systems because the DMFC BOP mass is a higher percentage of the overall system mass due to the small stack size. With all three cases, the system specific power can be improved by decreasing the number of cells in the stack and decreasing

the fuel mass fraction at the expense of reduced endurance.

A case study of 5 lightweight flying vehicle missions was used to investigate the impact of mission on fuel cell system configuration and integration with a battery. Only direct methanol systems with anode recirculation were considered. The study concluded that sizing the battery to meet the power/energy demands of a single flight leg and using the fuel cell to recharge after each leg is beneficial because it maximizes the amount of energy stored in the fuel instead of the batteries. Incorporating a fuel cell can reduce the weight of the overall power and energy system by as much as 55.76%. This corresponds to a 30% decrease in vehicle mass. If weight reduction is not the goal, the payload mass could be almost doubled enabling greatly expanded operational capabilities.

6.2 Future work.

Future work would focus on applying this modeling methodology to other types of fuels and fuel cells so as to expand the ability to quantitatively rate the performance of different fuel cell systems at different scales. New fuels of particular interest include ethanol, ammonia, and H_2 generated by liquid hydrocarbon reformers. Once multiple fuels and their corresponding systems have been modeled, a more extensive comparison could be made of different fuel cell types based on power, mass, volume, and efficiency requirements. Also, because the overall and BOP efficiencies were higher than typical systems, better estimates of motor, inverter, and membrane efficiencies should be obtained and used to determine the effect they have on the performance shown. Long-term future work would include choosing a system

that outperforms the others for a particular vehicle and mission and fabricating and testing the system to determine functionality and performance.

Appendices

A. Endurance of a hovering vehicle:

Power requirement to hover (Leishman p. 63):

$$P = \frac{1}{\eta_p}\sqrt{\frac{(mg)^3}{2\rho A}} \tag{A-1}$$

Where m is the vehicle mass, g is the acceleration due to gravity, η_p is the propulsive efficiency of the rotor, ρ is the density of the air and A is the disc area. The power to hover can also be written in terms of the mass flow rate of the fuel, the heating value of the fuel (Q_R) and the overall thermal efficiency of powerplant:

$$P = \eta_{th}\dot{m}_f Q_R \tag{A-2}$$

Equating A-1 and A-2 and recognizing that $\dot{m}_f = dm/dt$ gives:

$$\frac{dm}{dt} = \frac{1}{\eta_p\eta_{th}}\left(\frac{g}{Q_R}\right)\sqrt{\frac{mg}{2\rho A}}dt \tag{A-3}$$

This is an ODE that can be solved directly by integration:

$$\int_M^{M+m_f}\frac{dm}{m^{-3/2}} = \int_0^{\tau}\frac{1}{\eta_p\eta_{th}}\left(\frac{g}{Q_R}\right)\sqrt{\frac{g}{2\rho A}}dt \tag{A-4}$$

In this equation, M is the empty weight of the vehicle, m_f is the weight of the fuel, and τ is the hover time. Integrating gives:

$$-2m^{-1/2}\Big|_M^{M+m_f} = \frac{1}{\eta_p\eta_{th}}\left(\frac{g}{Q_R}\right)\sqrt{\frac{g}{2\rho A}}\Bigg|_0^{\tau} \tag{A-5}$$

Solving for τ gives:

$$\tau = 2\eta_p\eta_{th}\left(\frac{Q_R}{g}\right)\sqrt{2\rho\left(\frac{A}{Mg}\right)}\left[1-\frac{\sqrt{M}}{\sqrt{M+m_f}}\right] \tag{A-6}$$

Introducing the fuel mass fraction ($\zeta = m_f/M$) gives:

$$\boxed{\tau = \eta_p\eta_{th}\left(\frac{Q_R}{g}\right)\sqrt{8\rho\left(\frac{A}{Mg}\right)}\left[1-\sqrt{\frac{1}{1+\zeta}}\right]} \tag{A-7}$$

The quantity in parenthesis inside the square root is the disc loading.

B. Survey Data Collection

Fuel Cell Research

Type	Fuel & concentration	Oxidizer	Electrolyte	Catalysts	Max Power Density (mW/cm^2)	Current Density at Max Power (mA/cm^2)	Temperature (Celsius)	# electrons per reaction for current	(mV)	I at Pmax i2 (mA/cm^2)	FP efficiency	FC efficiency	BOP efficiency	mdot (fuel)	size	Reference
Direct Alkaline Fuel Cell for multiple liquid fuels	ethanol (2M)	air	liquid potassium hydroxide (KOH) (3M)	A-Pt-Ru C-Mn02	16	26	25	2	600	17	1			1 ml/min	~424 cm^3	A. Verma, S. Basu, J. Power Sources 174 (2007) 180-185.
																Q. Wang, G.Q. Sun, L. Cao, L.H. Jiang, G.X. Wang, S.L. Wang, S.H. Yang, Q. Xin, J. Power Sources 177 (2008) 142–147
Direct Ethanol Fuel Cell	ethanol (1.5M)	oxygen	Nafion 115	A1-Pt5n3/C A2-Pt/Ru C-??	96	200	90		670	100	1			1 ml/min		
Direct Ethanol Fuel Cell	ethanol (2M)	oxygen	Nafion 117	A-Pt-Sn-Ru/C C-Pt/C	50	180	80		480	90	1			10 ml/min		S. Rousseau, C. Coutanceau, C. Lamy, J-M. Leger, J. Power Sources 158 (2006) 18-24
Direct Alkaline Fuel Cell for multiple liquid fuels	ethanol (2M)	air	liquid potassium hydroxide (KOH) (3M)	A-Pt-black C-Mn02	14.5	~19	65	12??	700	15	1			1 ml/min	~424 cm^3	A. Verma, S. Basu, J. Power Sources 168 (2007) 200-210.
Direct Ethanol Alkaline Medium Fuel Cell	ethanol (1M) +KOH (.5M)	oxygen	anion exchange membrane poly(vinyl alcohol)/titanium oxide composite polymer membrane	A-Pt/Ru C-Pt	58	200	25	4	500	75	1			4 ml/min		N. Fujiwara, Z. Siroma, S. Yamazaki, T. Ioroi, H. Senoh, K. Yasuda, J. Power Sources 185 (2008) 621-626
Direct Methanol Alkaline Membrane Fuel Cell	ethanol (2M) +KOH (4M)	air	A-Pt/Ru C-Mn02		8	35.68	25		600	17	1					C.C. Yang, S.J. Chiu, K.T. Lee, W.C. Chien, C.T. Lin, C.A. Huang, J. Power Sources 184 (2008) 44-51
Direct Ethanol Alkaline Membrane Fuel Cell	ethanol (2M) +NaOH (6M)	oxygen	Nafion 117	A-Ni/Ru/C C-N4Co/C	40	~85	60	12	590	46	1					A. Tsiakaras, M. Tarasevich, B. Efremov, N. Kapustina, and P. Mazin. Doklady Physical Chemistry 415 (2007) 234-236

Fuel Cell Research

Type	Fuel & concentration	Oxidizer	Electrolyte	Catalysts	Max Power Density (mW/cm^2)	Current Density at Max Power (mA/cm^2)	Temperature (Celsius)	# electrons per reaction for current	(mV)	I at Pmax /2 (mA/cm^2)	FP efficiency	FC efficiency	BOP efficiency	mdot (fuel)	size	Reference
Direct Methanol Alkaline Membrane Fuel Cell	methanol (1M)	air	ADP hydroxide ion conducting membrane (cross-linked fluorinated polymer)	A-carbon supported Pt/Ru C-carbon supported Pt	16	45	60	6	525	13	1			12.65 ml/min		K. Scott, E. Yu, G. Vlachogiannopoulos, M. Shivare, N. Duteanu, J. Power Sources 175 (2008) 452-457.
Direct Methanol Fuel Cell - membrane anode/substrate cathode	Methanol (1M)	air	Nafion 115	A-PtRu/C C-Pt/C	85	~280	50	6	400	160	1					J. Park, J. Lee, J. Kim, S. Han, I. Song, J. Power Sources 179 (2008) 1-8
Direct Methanol Fuel Cell - membrane anode/substrate cathode	Methanol (1M)	air	Nafion 115	A-PtRu/C C-Pt/C	120	~330	60	6	430	230	1					J. Park, J. Lee, J. Kim, S. Han, I. Song, J. Power Sources 179 (2008) 1-8
Direct Methanol Fuel Cell - membrane anode/substrate cathode	Methanol (1M)	air	Nafion 115	A-PtRu/C C-Pt/C	130	~340	70	6	450	240	1					J. Park, J. Lee, J. Kim, S. Han, I. Song, J. Power Sources 179 (2008) 1-8
Membraneless laminar flow fuel cell	methanol (1M)	air	KOH (1M)	A-Pt/Ru C-Pt	17.2	~55	25		400	35	1					R. Jayashree, D. Egas, J. Spendelow, D. Natarajan, L. Markoski, P. Kenis, Electrochem. and Solid State Letters 9 (2006) A252-A256
Direct Methanol Fuel Cell	Methanol (1M)	air	Nafion 115	A-Pt/Ru C-Pt	140	~430	80	6	370	300	1			5 ml/min		S. Hwang, H. Joh, M. A. Scibioh, S. Lee, S. Kim, T. Lee, H. Ha, J. Power Sources 183 (2008) 226-231
Direct Methanol Alkaline Membrane Fuel Cell	methanol (1M)	oxygen	anion exchange membrane	A-Pt/Ru C-Pt	7.57	~40	80	6	320	160	1			5 ml/min		H. Bunazawa, Y. Yamazaki, J. Power Sources 182 (2008) 48-51

Fuel Cell Research

Type	Fuel & concentration	Oxidizer	Electrolyte	Catalysts	Max Power Density (mW/cm^2)	Current Density at Max Power (mA/cm^2)	Temperature (Celsius)	# electrons per reaction for current	(mV)	I at Pmax /2 (mA/cm^2)	FP efficiency	FC efficiency	BOP efficiency	mdot (fuel)	size	Reference
Direct Methanol Fuel Cell	Methanol (1M)	oxygen	Nafion 117	A-Pt-Ru/C nano C-Pt black	62	300	60	6	300	180	1					K. Jeng, C. Chien, N Hsu, S. Yen, S. Chiou, S. Lin, W. Huang, J. Power Sources, 160 (2006) 97-104
Direct Alkaline Fuel Cell for multiple liquid fuels	methanol (2M)	air	liquid potassium hydroxide (KOH) (3M)	A-Pt 40wt%, Ru 20wt% C-Mn02	15.8	26.5	25	6	700	23	1			1 ml/min	~424 cm^3	A. Verma, S. Basu, J. Power Sources 174 (2007) 180-185.
Direct Alkaline Fuel Cell for multiple liquid fuels	methanol (2M)	air	liquid potassium hydroxide (KOH) (3M)	A-Pt-black C-Mn02	24.3	~27	65	6	750	20	1			1 ml/min	~424 cm^3	A. Verma, S. Basu, J. Power Sources 168 (2007) 200-210.
Direct Alkaline Fuel Cell for multiple liquid fuels	methanol (2M)	air	liquid potassium hydroxide (KOH) (5M)	A-Pt/C/Ni C-MnO2/C/Ni	31.5	44	60	6	750	35	1			1 ml/min	~424 cm^3	A. Verma, A. K. Jha, S. Basu, J. Fuel Cell Science and Tech. 2 (2005) 234-237
Direct Methanol Fuel Cell	Methanol (5M)	oxygen	modified PVI/Pd Nafion 115	A-PtRu/C C-Pt/C	75	~325	30	6	420	86	1			.6 ml/min		A. Tian, J. Kim, J. Shi, K. Kim, J. Power Sources 183 (2008) 1-7
Direct Methanol Fuel Cell	Methanol (5M)	oxygen	PPO-MMT	A-Pt C-PtRu	125	~500	70	6	350	320	1					M. Hasani-Sadrabadi, S. Emami, H. Moaddel, J. Power Sources 183 (2008) 551-556
Direct Methanol Fuel Cell	Methanol (5M)	oxygen	modified PVI/Pd Nafion 115	A-PtRu/C C-Pt/C	130	~525	60	6	410	120	1			.6 ml/min		A. Tian, J. Kim, J. Shi, K. Kim, J. Power Sources 183 (2008) 1-7
Membraneless laminar flow fuel cell	methanol (10mM)	oxygen	KOH (1M)	A-Pt C-Au	46	153.3	90		420	75	1					J. Hayes, A. Engstrom, C. Friesen, J. Power Sources 183 (2008) 257-259

Fuel Cell Research

Type	Fuel & concentration	Oxidizer	Electrolyte	Catalysts	Max Power Density (mW/cm^2)	Current Density at Max Power (mA/cm^2)	Temperature (Celsius)	# electrons per reaction for current	(mV)	I at Pmax /2 (mA/cm^2)	FP efficiency	FC efficiency	BOP efficiency	mdot (fuel)	size	Reference
Direct Methanol Alkaline Membrane Fuel Cell	methanol (1M)+ NaOH(.5M)	oxygen	anion exchange membrane	A-Pt/Ru C-Pt	58.9	~170	80	6	300	175	1			5 ml/min		H. Bunazawa, Y. Yamazaki, J. Power Sources 182 (2008) 48-51
Direct Methanol Alkaline Membrane Fuel Cell	methanol (2M) +KOH (4M)	air	poly(vinyl alcohol)/titanium oxide composite polymer membrane	A-Pt/Ru C-Mn02	9.25	33.57	25		400	20	1					C.C. Yang, S.J. Chiu, K.T. Lee, W.C. Chien, C.T. Lin, C.A. Huang, J. Power Sources 184 (2008) 44-51
Direct Methanol Alkaline Membrane Fuel Cell	methanol (2M) +KOH (8M)	air	poly(vinyl alcohol)/ hydroxyapatite composite polymer membrane	A-Pt/Ru C-Mn02	11.48	52.2	25	6	300	30	1					C.C. Yang, S.J. Chiu, C.T. Lin, J. Power Sources 177 (2008) 40-49
Direct L-ascorbic acid Fuel Cell	L-ascorbic acid (vitamin C) (.5M)	oxygen	Nafion 117	A-Carbon Black C-Pt Black	15	~60	25	2			1			4 ml/min		N. Fujiwara, S. Yamazaki, Z. Siroma, T. Ioroi, K. Yasuda, Electrochem. Communications 8 (2006) 720–724
Direct Alkaline Fuel Cell for multiple liquid fuels	Sodium Borohydride (2M)	air	liquid potassium hydroxide (KOH) (5M)	A-Pt/C/Ni C-MnO2/C/Ni	24.1	35.3	60	8	750	20	1			1 ml/min	~424 cm^3	A. Verma, A. K. Jha, S. Basu, J. Fuel Cell Science and Tech. 2 (2005) 234-237
Direct Alkaline Fuel Cell for multiple liquid fuels	Sodium Borohydride (2M)	air	liquid potassium hydroxide (KOH) (3M)	A-various Pt loadings C-Mn02	20	30	25	8	750	21	1			1 ml/min	~424 cm^3	A. Verma, S. Basu, J. Power Sources 174 (2007) 180-185.
Direct Alkaline Fuel Cell for multiple liquid fuels	Sodium Borohydride (2M)	air	liquid potassium hydroxide (KOH) (2M)	A-Pt-black C-Mn02	22.5	~28	25	8	750	23	1			1 ml/min	~424 cm^3	A. Verma, S. Basu, J. Power Sources 168 (2007) 200-210.

C. Pressure/current reference relation.

The MEA is assumed to be square and fed by a series of parallel channels (as opposed to the single serpentine channel used by Hwang et. al [47]). The number of channels (n_{chan}) is given by:

$$n_{chan} = \frac{L - w}{w + w_{rib}} \tag{C-1}$$

where L is the channel length, w is the channel width, and w_{rib} is the width of the channel ribs. The hydraulic diameter (D_h) of each channel is given by:

$$D_h = \frac{4A}{P} \tag{C-2}$$

where A is the cross-sectional area and P is the perimeter of the cross-section.

Eq. 4.3 and 4.4 give the relationship between current density (current divided by the area) and the molar fuel flow rate. Knowing the concentration of the fuel enables one to compute the total mass flow rate of the fuel-water mixture. This mass flow rate is converted to a volume flow rate assuming that the density of the fuel-water mixture is approximately the density of water alone. This is a reasonable assumption at the small methanol concentrations considered here.

Another assumption is made as to how much air flow is required on a mole basis for each mole of anode flow. The assumption is necessary because the amount of air is unknown, as it is also used for cooling the stack. This value was estimated by

running the program at different pressure references, and observing the change in air flow.

The Reynolds number of the flows at the cathode and anode are computed using the volume flow rates:

$$\mathrm{Re}_L = \frac{\rho \dot{V} D_h}{\mu A} \tag{C-3}$$

In this expression, ρ is the density of the fluid, and μ is the dynamic viscosity. Since all values of Re_L obtained are well below 2300, the flows in both the anode and cathode are laminar enabling one to estimate the pressure drop using [95]:

$$\Delta P_L = \frac{64}{\mathrm{Re}_L} \frac{L}{D_h} \frac{\rho}{2} \left(\frac{\dot{V}}{A} \right)^2 \tag{C-4}$$

Eq. C-4 is used to find the pressure drops across the anode and cathode flows at the maximum and minimum current densities the model uses (i.e. for DMFC 50 mA/cm^2 and 500 mA/cm^2). The pressure drop through an electrode is given by interpolating between the maximum and minimum pressure value.

D. Fan Performance Data

Manufacturer/Product Number	vol (mm^3)	weight (g)	Power rating	Max Air flow	Range to cover
Oriental Motor/MDS410-12H	17640	25	1.92	6.35	5.2
EBMPapst/405FH	16000	18.1	0.9	5.3	4.3
RedCloud/RDH3010B	9000	8.5	1.2	4.47	2.5
RedCloud/RDH2510B	6250	7	1.2	2.67	1.9
Indek/KDC050210MB8P	6250	7.5	0.6	2	1.25
Indek/KDC052008HB8P	3200	5	0.55	1.3	0.85
Risun/RFA1804D	1296	1.7	0.225	0.9	0.6
Risun/RFA1804D	1296	1.7	0.1056	0.65	0.3
JaroThermal/AD1502LX-471(X)	900	1.9	0.2	0.32	

E. Ragone plot data.

				No Circulation MeOH				With Recirculation MeOH				With Recirculation NaBH4															
MeOH			Power (W)	10		10		10		10		10															
QR uncirc	2914 J/g		Cells	12		60		13		60		66		100		Hr	0.027778	0.277778	2.777778	27.77778	DARPA DMFC	3600					
QR recirc	13323 J/g		Efficiency	0.15959		0.2978		0.25346		0.38624		0.26171		0.36546		Min	1.666667	16.66667	166.6667	1666.667		3600					
NaBH4	33000 J/g		PD_max (W/g)	0.39058		0.08781		0.32138		0.08761		0.07801		0.05222		dt	100	1000	10000	100000		3600					
				ED	PD	ED	PD	ED	PD	ED	PD	ED	PD	ED	PD												
z	1/1+z	z/1+z	Pd*Ed	(J/g)	(W/g)	(J/g)	(W/g)	(J/g)	(W/g)	(J/g)	(W/g)	(J/g)	(W/g)	(J/g)	(W/g)												
0	1	0	0	0.0001	0.39058	0.0001	0.08781	0.0001	0.32138	0.0001	0.08761	0.0001	0.07801	0.0001	0.05222	100	1	0.1	0.01	0.001	A123 battery					
0.2	0.833333	0.166667	0.138888889	77.50754	0.325483	144.6315	0.073175	562.8079	0.267817	857.6459	0.073008	1439.405	0.065008	2010.03	0.043517	500	5	0.5	0.05	0.005		ED	PD				
0.4	0.714286	0.285714	0.204081633	132.8701	0.278986	247.3398	0.062721	964.8136	0.229557	1470.25	0.062579	2467.551	0.055721	3445.766	0.0373	1000	10	1	0.1	0.01		(J/g)	(W/g)			
0.6	0.625	0.375	0.234375	174.392	0.244113	325.421	0.054881	1266.318	0.200863	1929.703	0.054756	3238.661	0.048756	4522.568	0.032638	5000	50	5	0.5	0.05		390	3.3			
0.8	0.555556	0.444444	0.24691358	206.6868	0.216989	385.6841	0.048783	1500.821	0.178544	2287.056	0.049672	3838.413	0.043339	5360.08	0.029011	10000	100	10	1	0.1						
1	0.5	0.5	0.25	232.5226	0.19529	433.8946	0.043905	1688.424	0.16069	2572.938	0.043805	4318.215	0.039005	6030.09	0.02611												
1.2	0.454545	0.545455	0.247933884	253.6611	0.177536	473.3396	0.039914	1841.917	0.146082	2806.841	0.039823	4710.78	0.035459	6578.28	0.023736		Cell #	zeta	100	150	200	250					
1.4	0.416667	0.583333	0.243055556	271.2764	0.162742	506.2104	0.036588	1969.828	0.133908	3001.761	0.036504	5037.918	0.032504	7035.105	0.021758	nonrecirc	12	36	1.777778	3.166667	4.555556	5.944444					
1.6	0.384615	0.615385	0.236686391	286.1817	0.150223	534.0241	0.033773	2078.06	0.123608	3166.693	0.033696	5314.726	0.030004	7421.649	0.020085		60	130.9	-0.22606	0.145913	0.527684	0.909855					
1.8	0.357143	0.642857	0.229591837	298.9577	0.139493	557.8645	0.031361	2170.831	0.114779	3308.063	0.031289	5551.991	0.027861	7752.973	0.01865	recirc	13	42	1.380952	2.571429	3.761905	4.952381					
2	0.333333	0.666667	0.222222222	310.0302	0.130193	578.5261	0.02927	2251.232	0.107127	3430.584	0.029203	5757.62	0.026003	8040.12	0.017407		60	134	-0.25373	0.119403	0.492537	0.865672					
3	0.25	0.75	0.1875	348.7839	0.097645	650.8419	0.021953	2532.636	0.080345	3859.407	0.021903	6477.323	0.019503	9045.135	0.013055	NaBH4	66	161.1	-0.37927	-0.0689	0.241465	0.551831					
4	0.2	0.8	0.16	372.0362	0.078116	694.2314	0.017562	2701.478	0.064276	4116.7	0.017522	6909.144	0.015602	9648.144	0.010444		100	219.5	-0.54442	-0.31663	-0.08884	0.138952					
5	0.166667	0.833333	0.138888889	387.5377	0.065097	723.1577	0.014635	2814.04	0.053563	4288.23	0.014602	7197.025	0.013002	10050.15	0.008703												
6	0.142857	0.857143	0.12244898	398.6102	0.055797	743.8193	0.012544	2894.441	0.045911	4410.75	0.012516	7402.654	0.011144	10337.3	0.00746		Qr		100	150	200	250					
7	0.125	0.875	0.109375	406.9146	0.048823	759.3156	0.010976	2954.742	0.040173	4502.641	0.010951	7556.876	0.009751	10552.66	0.006528	nonrecirc	12	465.0453	297.629	353.4344	381.3371	398.0787					
8	0.111111	0.888889	0.098765432	413.3736	0.043398	771.3682	0.009757	3001.642	0.035709	4574.112	0.009734	7676.827	0.008668	10720.16	0.005802		60	867.7892	-268.147	110.4985	299.8212	413.4148					
9	0.1	0.9	0.09	418.5407	0.039058	781.0103	0.008781	3039.163	0.032138	4631.288	0.008761	7772.787	0.007801	10854.16	0.005222	recirc	13	3376.848	1958.572	2431.33	2667.71	2809.537					
10	0.090909	0.909091	0.082644628	422.7684	0.035507	788.8993	0.007983	3069.861	0.029216	4678.069	0.007965	7851.3	0.007092	10963.8	0.004747		60	5145.876	-1749.6	548.8934	1698.139	2387.686					
100	0.009901	0.990099	0.009802096	460.4409	0.003867	859.1972	0.000869	3343.413	0.003182	5094.926	0.000867	8550.921	0.000772	11940.77	0.000517	NaBH4	66	8636.43	-5276.86	-639.096	1679.786	3071.115					
1000	0.000999	0.999001	0.000998003	464.5807	0.00039	866.9223	8.77E-05	3373.474	0.000321	5140.735	8.75E-05	8627.802	7.79E-05	12048.13	5.22E-05		100	12060.18	-14441.9	-5587.88	-1175.87	1471.342					
																	Pd		100	150	200	250					
																nonrecirc	12	0.39058	0.140609	0.093739	0.070304	0.056244					
																	60	0.08781	0.114943	0.076629	0.057472	0.045977					
																recirc	13	0.32138	0.13498	0.089986	0.06749	0.053992					
																	60	0.08761	0.117397	0.078265	0.058699	0.046959					
																NaBH4	66	0.07801	0.125674	0.083783	0.062837	0.05027					
																	100	0.05222	0.114623	0.076415	0.057311	0.045849					

				No Circulation MeOH				With Recirculation MeOH				With Recirculation NaBH4											
MeOH			Power (W)	5		5		5		5		5		5									
QR uncirc	2914	J/g	Cells	7		55		7		55		37		65		Hr	0.027778	0.277778	2.777778	27.77778			3600
QR recirc	13323	J/g	Efficiency	0.17593		0.27207		0.2043		0.3529		0.22835		0.33534		Min	1.666667	16.66667	166.6667	1666.667			3600
NaBH4	33000	J/g	PD_max (W/g)	0.27911		0.053		0.25842		0.05423		0.07588		0.04299		dt	100	1000	10000	100000	DARPA DMFC		3600
				ED	PD	ED	PD	ED	PD	ED	PD	ED	PD	ED	PD	ED	PD	PD	PD	PD			
z	1/1+ζ	ζ/1+ζ	Pd*Ed	(J/g)	(W/g)	(J/g)	(W/g)	(J/g)	(W/g)	(J/g)	(W/g)	(J/g)	(W/g)	(J/g)	(W/g)	(J/g)	(W/g)	(W/g)	(W/g)	(W/g)		A123 battery	
0	1	0	0	0.0001	0.27911	0.0001	0.053	0.0001	0.25842	0.0001	0.05423	0.0001	0.07588	0.0001	0.04299	100	1	0.1	0.01	0.001		ED	PD
0.01	0.990099	0.009901	0.00980296	5.075842	0.276347	7.849624	0.052475	26.9494	0.255861	46.55135	0.053693	74.60941	0.075129	109.5665	0.042564	500	5	0.5	0.05	0.005		(J/g)	(W/g)
0.1	0.909091	0.090909	0.082644628	46.60546	0.253736	72.07382	0.048182	247.4444	0.234927	427.4261	0.0493	685.05	0.068982	1006.02	0.039082	1000	10	1	0.1	0.01		390	3.3
0.2	0.833333	0.166667	0.138888889	85.44334	0.232592	132.1353	0.044167	453.6482	0.21535	783.6145	0.045192	1255.925	0.063233	1844.37	0.035825	5000	50	5	0.5	0.05			
0.4	0.714286	0.285714	0.204081633	146.4743	0.199364	226.5177	0.037857	777.6825	0.184586	1343.339	0.038736	2153.014	0.0542	3161.777	0.030707	10000	100	10	1	0.1			
0.6	0.625	0.375	0.234375	192.2475	0.174444	297.3045	0.033125	1020.708	0.161513	1763.133	0.033894	2825.831	0.047425	4149.833	0.026869								
0.8	0.555556	0.444444	0.24691358	227.8489	0.155061	352.3609	0.029444	1209.728	0.143567	2089.639	0.030128	3349.133	0.042156	4918.32	0.023883		Cell #	zeta	100	150	200	250	
1	0.5	0.5	0.25	256.33	0.139555	396.406	0.0265	1360.944	0.12921	2350.843	0.027115	3767.775	0.03794	5533.11	0.021495	nonrecirc	7	26	2.846154	4.769231	6.692308	8.615385	
1.2	0.454545	0.545455	0.247933884	279.6327	0.126868	432.4429	0.024091	1484.667	0.117464	2564.556	0.02465	4110.3	0.034491	6036.12	0.019541		55	120.9	-0.17287	0.240695	0.65426	1.067825	
1.4	0.416667	0.583333	0.243055556	299.0517	0.116296	462.4737	0.022083	1587.769	0.107675	2742.651	0.022596	4395.738	0.031617	6455.295	0.017913	recirc	7	30.5	2.278689	3.918033	5.557377	7.196721	
1.6	0.384615	0.615385	0.236686391	315.4831	0.10735	487.8843	0.020385	1675.009	0.099392	2893.346	0.020858	4637.262	0.029185	6809.982	0.016535		55	120.7	-0.1715	0.242751	0.657001	1.071251	
1.8	0.357143	0.642857	0.229591837	329.5672	0.099682	509.6648	0.018929	1749.786	0.092293	3022.513	0.019368	4844.282	0.0271	7113.999	0.015354	NaBH4	37	93.5	0.069519	0.604278	1.139037	1.673797	
2	0.333333	0.666667	0.222222222	341.7733	0.093037	528.5413	0.017667	1814.593	0.08614	3134.458	0.018077	5023.7	0.025293	7377.48	0.01433		65	148.5	-0.3266	0.010101	0.346801	0.683502	
3	0.25	0.75	0.1875	384.495	0.069778	594.609	0.01325	2041.417	0.064605	3526.265	0.013558	5651.663	0.01897	8299.665	0.010748								
4	0.2	0.8	0.16	410.128	0.055822	634.2496	0.0106	2177.511	0.051684	3761.349	0.010846	6028.44	0.015176	8852.976	0.008598			Qr	100	150	200	250	
5	0.166667	0.833333	0.138888889	427.2167	0.046518	660.6767	0.008833	2268.241	0.04307	3918.072	0.009038	6279.625	0.012647	9221.85	0.007165	nonrecirc	7	512.66	379.3684	423.7989	446.0142	459.3434	
6	0.142857	0.857143	0.12244898	439.4229	0.039873	679.5531	0.007571	2333.048	0.036917	4030.017	0.007747	6459.043	0.01084	9485.331	0.006141		55	792.812	-165.698	153.8055	313.5571	409.4081	
7	0.125	0.875	0.109375	448.5775	0.034889	693.7105	0.006625	2381.653	0.032303	4113.976	0.006779	6593.606	0.009485	9682.943	0.005374	recirc	7	2721.889	1891.713	2168.438	2306.801	2389.818	
8	0.111111	0.888889	0.098765432	455.6978	0.031012	704.7218	0.005889	2419.457	0.028713	4179.277	0.006026	6698.267	0.008431	9836.64	0.004777		55	4701.687	-973.249	918.3961	1864.219	2431.712	
9	0.1	0.9	0.09	461.394	0.027911	713.5308	0.0053	2449.7	0.025842	4231.518	0.005423	6781.995	0.007588	9959.598	0.004299	NaBH4	37	7535.55	489.8108	2838.391	4012.68	4717.254	
10	0.090909	0.909091	0.082644628	466.0546	0.025374	720.7382	0.004818	2474.444	0.023493	4274.261	0.00493	6850.5	0.006898	10060.2	0.003908		65	11066.22	-5367.12	110.6622	2849.552	4492.885	
100	0.009901	0.990099	0.00980296	507.5842	0.002763	784.9624	0.000525	2694.94	0.002559	4655.135	0.000537	7460.941	0.000751	10956.65	0.000426								
1000	0.000999	0.999001	0.000998003	512.1479	0.000279	792.02	5.29E-05	2719.17	0.000258	4696.99	5.42E-05	7528.022	7.58E-05	11055.16	4.29E-05			Pd	100	150	200	250	
																nonrecirc	7	0.27911	0.072569	0.048379	0.036284	0.029027	
																	55	0.053	0.064077	0.042718	0.032039	0.025631	
																recirc	7	0.25842	0.078818	0.052545	0.039409	0.031527	
																	55	0.05423	0.065456	0.043637	0.032728	0.026182	
																NaBH4	37	0.07588	0.070948	0.047299	0.035474	0.028379	
																	65	0.04299	0.06384	0.04256	0.03192	0.025536	

				No Circulation MeOH																
MeOH			Power (W)	5		5		15		15		25		25						
QR uncirc	2914	J/g	Cells	7		55		18		65		28		75		Hr	0.027778	0.277778	2.777778	27.77778
QR recirc	13323	J/g	Efficiency	0.17593		0.27207		0.1985		0.3034		0.17932		0.30184		Min	1.666667	16.66667	166.6667	1666.667
NaBH4	33000	J/g	PD_max (W/g)	0.27911		0.053		0.40188		0.11808		0.47755		0.16842		dt	100	1000	10000	100000

				ED	PD	ED	PD	ED	PD	ED	PD	ED	PD	ED	PD	ED	PD	PD	PD	PD
z	1/1+ζ	ζ/1+ζ	Pd*Ed	(J/g)	(W/g)	(J/g)	(W/g)	(J/g)	(W/g)	(J/g)	(W/g)	(J/g)	(W/g)	(J/g)	(W/g)	(J/g)	(W/g)	(W/g)	(W/g)	(W/g)
0	1	0	0	0.0001	0.27911	0.0001	0.053	0.0001	0.40188	0.0001	0.11808	0.0001	0.47755	0.0001	0.16842	100	1	0.1	0.01	0.001
0.01	0.990099	0.009901	0.00980296	5.075842	0.276347	7.849624	0.052475	5.72702	0.397901	8.753541	0.116911	5.173648	0.472822	8.708532	0.166752	500	5	0.5	0.05	0.005
0.1	0.909091	0.090909	0.082644628	46.60546	0.253736	72.07382	0.048182	52.58445	0.365345	80.37342	0.107345	47.5035	0.434136	79.96016	0.153109	1000	10	1	0.1	0.01
0.2	0.833333	0.166667	0.138888889	85.44334	0.232592	132.1353	0.044167	96.40483	0.3349	147.3513	0.0984	87.08975	0.397958	146.5936	0.14035	5000	50	5	0.5	0.05
0.4	0.714286	0.285714	0.204081633	146.4743	0.199364	226.5177	0.037857	165.2654	0.287057	252.6022	0.084343	149.2967	0.341107	251.3034	0.1203	10000	100	10	1	0.1
0.6	0.625	0.375	0.234375	192.2475	0.174444	297.3045	0.033125	216.9109	0.251175	331.5404	0.0738	195.9519	0.298469	329.8357	0.105263					
0.8	0.555556	0.444444	0.24691358	227.8489	0.155061	352.3609	0.029444	257.0796	0.223267	392.9367	0.0656	232.2393	0.265306	390.9163	0.093567		Cell #	zeta	100	150	200	250
1	0.5	0.5	0.25	256.33	0.139555	396.406	0.0265	289.2145	0.20094	442.0538	0.05904	261.2692	0.238775	439.7809	0.08421	5	7	26	2.846154	4.769231	6.692308	8.615385
1.2	0.454545	0.545455	0.247933884	279.6327	0.126868	432.4429	0.024091	315.5067	0.182673	482.2405	0.053673	285.021	0.217068	479.761	0.076555		55	120.9	-0.17287	0.240695	0.65426	1.067825
1.4	0.416667	0.583333	0.243055556	299.0517	0.116296	462.4737	0.022083	337.4169	0.16745	515.7294	0.0492	304.8141	0.198979	513.0777	0.070175	15	18	46.9	1.132196	2.198294	3.264392	4.33049
1.6	0.384615	0.615385	0.236686391	315.4831	0.10735	487.8843	0.020385	355.9563	0.154569	544.0662	0.045415	321.5621	0.183673	541.2688	0.064777		65	140.9	-0.29028	0.064585	0.419446	0.774308
1.8	0.357143	0.642857	0.229591837	329.5672	0.099682	509.6648	0.018929	371.8472	0.143529	568.3549	0.042171	335.9176	0.170554	565.4326	0.06015	25	28	66.7	0.49925	1.248876	1.998501	2.748126
2	0.333333	0.666667	0.222222222	341.7733	0.093037	528.5413	0.017667	385.6193	0.13396	589.4051	0.03936	348.359	0.159183	586.3745	0.05614		75	160.7	-0.37772	-0.06658	0.244555	0.555694
3	0.25	0.75	0.1875	384.495	0.069778	594.609	0.01325	433.8218	0.10047	663.0807	0.02952	391.9039	0.119388	659.6713	0.042105							
4	0.2	0.8	0.16	410.128	0.055822	634.2496	0.0106	462.7432	0.080376	707.2861	0.023616	418.0308	0.09551	703.6494	0.033684			Qr	100	150	200	250
5	0.166667	0.833333	0.138888889	427.2167	0.046518	660.6767	0.008833	482.0242	0.06698	736.7563	0.01968	435.4487	0.079592	732.9681	0.02807	5	7	512.66	379.3684	423.7989	446.0142	459.3434
6	0.142857	0.857143	0.12244898	439.4229	0.039873	679.5531	0.007571	495.7963	0.057411	757.8065	0.016869	447.8901	0.068221	753.9101	0.02406		55	792.812	-165.698	153.8055	313.5571	409.4081
7	0.125	0.875	0.109375	448.5775	0.034889	693.7105	0.006625	506.1254	0.050235	773.5942	0.01476	457.2212	0.059694	769.6165	0.021053	15	18	578.429	307.1458	397.5735	442.7874	469.9157
8	0.111111	0.888889	0.098765432	455.6978	0.031012	704.7218	0.005889	514.1591	0.044653	785.8734	0.01312	464.4786	0.053061	781.8327	0.018713		65	884.1076	-361.6	53.63586	261.2538	385.8246
9	0.1	0.9	0.09	461.394	0.027911	713.5308	0.0053	520.5861	0.040188	795.6968	0.011808	470.2846	0.047755	791.6056	0.016842	25	28	522.5385	174.0053	290.183	348.2719	383.1252
10	0.090909	0.909091	0.082644628	466.0546	0.025374	720.7382	0.004818	525.8445	0.036535	803.7342	0.010735	475.035	0.043414	799.6016	0.015311		75	879.5618	-533.894	-62.7421	172.8339	314.1795
100	0.009901	0.990099	0.00980296	507.5842	0.002763	784.9624	0.000525	572.702	0.003979	875.3541	0.001169	517.3648	0.004728	870.8532	0.001668							
1000	0.000999	0.999001	0.000998003	512.1479	0.000279	792.02	5.29E-05	577.8511	0.000401	883.2244	0.000118	522.0165	0.000477	878.6831	0.000168			Pd	100	150	200	250
																5	7	0.27911	0.072569	0.048379	0.036284	0.029027
																	55	0.053	0.064077	0.042718	0.032039	0.025631
																15	18	0.40188	0.188482	0.125654	0.094241	0.075393
																	65	0.11808	0.166375	0.110916	0.083187	0.06655
																25	28	0.47755	0.318526	0.212351	0.159263	0.12741
																	75	0.16842	0.270651	0.180434	0.135325	0.10826

				Recirculation MeOH																	
MeOH			Power (W)	5		5		15		15		25		25							
QR uncirc	2914	J/g	Cells	7		55		19		65		29		75		Hr	0.027778	0.277778	2.777778	27.77778	
QR recirc	13323	J/g	Efficiency	0.2043		0.3529		0.26231		0.39322		0.24471		0.39637		Min	1.666667	16.66667	166.6667	1666.667	
NaBH4	33000	J/g	PD_max (W/g)	0.25842		0.05423		0.35081		0.11606		0.35489		0.16467		dt	100	1000	10000	100000	
				ED	PD	ED	PD	ED	PD	ED	PD	ED	PD	ED	PD	ED	PD	PD	PD	PD	
z	1/1+ζ	ζ/1+ζ	Pd*Ed	(J/g)	(W/g)	(J/g)	(W/g)	(J/g)	(W/g)	(J/g)	(W/g)	(J/g)	(W/g)	(J/g)	(W/g)	(J/g)	(W/g)	(W/g)	(W/g)	(W/g)	
0	1	0	0	0.0001	0.25842	0.0001	0.05423	0.0001	0.35081	0.0001	0.11606	0.0001	0.35489	0.0001	0.16467	100	1	0.1	0.01	0.001	
0.01	0.990099	0.009901	0.00980296	26.9494	0.255861	46.55135	0.053693	34.60155	0.347337	51.87	0.114911	32.27991	0.351376	52.28552	0.16304	500	5	0.5	0.05	0.005	
0.1	0.909091	0.090909	0.082644628	247.4444	0.234927	427.4261	0.0493	317.7051	0.318918	476.2609	0.105509	296.3883	0.322627	480.0761	0.1497	1000	10	1	0.1	0.01	
0.2	0.833333	0.166667	0.138888889	453.6482	0.21535	783.6145	0.045192	582.4594	0.292342	873.145	0.096717	543.3786	0.295742	880.1396	0.137225	5000	50	5	0.5	0.05	
0.4	0.714286	0.285714	0.204081633	777.6825	0.184586	1343.339	0.038736	998.5018	0.250579	1496.82	0.0829	931.5061	0.253493	1508.811	0.117621	10000	100	10	1	0.1	
0.6	0.625	0.375	0.234375	1020.708	0.161513	1763.133	0.033894	1310.534	0.219256	1964.576	0.072538	1222.602	0.221806	1980.314	0.102919						
0.8	0.555556	0.444444	0.24691358	1209.728	0.143567	2089.639	0.030128	1553.225	0.194894	2328.387	0.064478	1449.009	0.197161	2347.039	0.091483		Cell #	zeta	100	150	200	250
1	0.5	0.5	0.25	1360.944	0.12921	2350.843	0.027115	1747.378	0.175405	2619.435	0.05803	1630.136	0.177445	2640.419	0.082335	5	7	30.5	2.278689	3.918033	5.557377	7.196721
1.2	0.454545	0.545455	0.247933884	1484.667	0.117464	2564.556	0.02465	1906.231	0.159459	2857.565	0.052755	1778.33	0.161314	2880.457	0.07485		55	120.7	-0.1715	0.242751	0.657001	1.071251
1.4	0.416667	0.583333	0.243055556	1587.769	0.107675	2742.651	0.022596	2038.608	0.146171	3056.008	0.048358	1901.825	0.147871	3080.489	0.068613	15	19	55.5	0.801802	1.702703	2.603604	3.504505
1.6	0.384615	0.615385	0.236686391	1675.009	0.099392	2893.346	0.020858	2150.619	0.134927	3223.92	0.044638	2006.321	0.136496	3249.746	0.063335		65	146.5	-0.31741	0.023891	0.365188	0.706485
1.8	0.357143	0.642857	0.229591837	1749.786	0.092293	3022.513	0.019368	2246.629	0.125289	3367.845	0.04145	2095.889	0.126746	3394.824	0.058811	25	29	92	0.086957	0.630435	1.173913	1.717391
2	0.333333	0.666667	0.222222222	1814.593	0.08614	3134.458	0.018077	2329.837	0.116937	3492.58	0.038687	2173.514	0.118297	3520.558	0.05489		75	167.5	-0.40299	-0.10448	0.19403	0.492537
3	0.25	0.75	0.1875	2041.417	0.064605	3526.265	0.013558	2621.067	0.087703	3929.153	0.029015	2445.203	0.088723	3960.628	0.041168							
4	0.2	0.8	0.16	2177.511	0.051684	3761.349	0.010846	2795.805	0.070162	4191.096	0.023212	2608.217	0.070978	4224.67	0.032934			Qr	100	150	200	250
5	0.166667	0.833333	0.138888889	2268.241	0.04307	3918.072	0.009038	2912.297	0.058468	4365.725	0.019343	2716.893	0.059148	4400.698	0.027445	5	7	2721.889	1891.713	2168.438	2306.801	2389.818
6	0.142857	0.857143	0.12244898	2333.048	0.036917	4030.017	0.007747	2995.505	0.050116	4490.46	0.01658	2794.518	0.050699	4526.432	0.023524		55	4701.687	-973.249	918.3961	1864.219	2431.712
7	0.125	0.875	0.109375	2381.653	0.032303	4113.976	0.006779	3057.912	0.043851	4584.011	0.014508	2852.737	0.044361	4620.733	0.020584	15	19	3494.756	1555.166	2201.696	2524.961	2718.92
8	0.111111	0.888889	0.098765432	2419.457	0.028713	4179.277	0.006026	3106.45	0.038979	4656.773	0.012896	2898.019	0.039432	4694.078	0.018297		65	5238.87	-2436.07	122.2403	1401.398	2168.892
9	0.1	0.9	0.09	2449.7	0.025842	4231.518	0.005423	3145.281	0.035081	4714.983	0.011606	2934.244	0.035489	4752.754	0.016467	25	29	3260.271	260.8217	1260.638	1760.547	2060.491
10	0.090909	0.909091	0.082644628	2474.444	0.023493	4274.261	0.00493	3177.051	0.031892	4762.609	0.010551	2963.883	0.032263	4800.761	0.01497		75	5280.838	-3564.57	-616.098	858.1361	1742.676
100	0.009901	0.990099	0.00980296	2694.94	0.002559	4655.135	0.000537	3460.155	0.003473	5187	0.001149	3227.991	0.003514	5228.552	0.00163							
1000	0.000999	0.999001	0.000998003	2719.17	0.000258	4696.99	5.42E-05	3491.265	0.00035	5233.636	0.000116	3257.014	0.000355	5275.562	0.000165			Pd	100	150	200	250
																5	7	0.25842	0.078818	0.052545	0.039409	0.031527
																	55	0.05423	0.065456	0.043637	0.032728	0.026182
																15	19	0.35081	0.1947	0.1298	0.09735	0.07788
																	65	0.11606	0.170028	0.113352	0.085014	0.068011
																25	29	0.35489	0.326499	0.217666	0.163249	0.1306
																	75	0.16467	0.275822	0.183882	0.137911	0.110329

				Recirculation NaBH4																
MeOH			Power (W)	5		5		7.5		7.5		10		10						
QR uncirc	2914	J/g	Cells	37		65		53		80		66		100		Hr	0.027778	0.277778	2.777778	27.77778
QR recirc	13323	J/g	Efficiency	0.22835		0.33534		0.26639		0.35114		0.26171		0.36546		Min	1.666667	16.66667	166.6667	1666.667
NaBH4	33000	J/g	PD_max (W/g)	0.075879		0.04299		0.0768		0.05026		0.07801		0.05223		dt	100	1000	10000	100000
				ED	PD	ED	PD	ED	PD	ED	PD	ED	PD	ED	PD	ED	PD	PD	PD	PD
z	1/1+ζ	ζ/1+ζ	Pd*Ed	(J/g)	(W/g)	(J/g)	(W/g)	(J/g)	(W/g)	(J/g)	(W/g)	(J/g)	(W/g)	(J/g)	(W/g)	(J/g)	(W/g)	(W/g)	(W/g)	(W/g)
0	1	0	0	0.0001	0.075879	0.0001	0.04299	0.0001	0.0768	0.0001	0.05026	0.0001	0.07801	0.0001	0.05223	100	1	0.1	0.01	0.001
0.01	0.990099	0.009901	0.00980296	74.60941	0.075128	109.5665	0.042564	87.03832	0.07604	114.7289	0.049762	85.50921	0.077238	119.4077	0.051713	500	5	0.5	0.05	0.005
0.1	0.909091	0.090909	0.082644628	685.05	0.068981	1006.02	0.039082	799.17	0.069818	1053.42	0.045691	785.13	0.070918	1096.38	0.047482	1000	10	1	0.1	0.01
0.2	0.833333	0.166667	0.138888889	1255.925	0.063233	1844.37	0.035825	1465.145	0.064	1931.27	0.041883	1439.405	0.065008	2010.03	0.043525	5000	50	5	0.5	0.05
0.4	0.714286	0.285714	0.204081633	2153.014	0.054199	3161.777	0.030707	2511.677	0.054857	3310.749	0.0359	2467.551	0.055721	3445.766	0.037307	10000	100	10	1	0.1
0.6	0.625	0.375	0.234375	2825.831	0.047424	4149.833	0.026869	3296.576	0.048	4345.358	0.031413	3238.661	0.048756	4522.568	0.032644					
0.8	0.555556	0.444444	0.24691358	3349.133	0.042155	4918.32	0.023883	3907.053	0.042667	5150.053	0.027922	3838.413	0.043339	5360.08	0.029017		Cell #	zeta	100	150	200
1	0.5	0.5	0.25	3767.775	0.03794	5533.11	0.021495	4395.435	0.0384	5793.81	0.02513	4318.215	0.039005	6030.09	0.026115	5	37	93.5	0.069519	0.604278	1.139037
1.2	0.454545	0.545455	0.247933884	4110.3	0.03449	6036.12	0.019541	4795.02	0.034909	6320.52	0.022845	4710.78	0.035459	6578.28	0.023741		65	148.5	-0.3266	0.010101	0.346801
1.4	0.416667	0.583333	0.243055556	4395.738	0.031616	6455.295	0.017913	5128.008	0.032	6759.445	0.020942	5037.918	0.032504	7035.105	0.021763	7.5	53	125.5	-0.20319	0.195219	0.593625
1.6	0.384615	0.615385	0.236686391	4637.262	0.029184	6809.982	0.016535	5409.766	0.029538	7130.843	0.019331	5314.726	0.030004	7421.649	0.020088		80	178	-0.4382	-0.1573	0.123596
1.8	0.357143	0.642857	0.229591837	4844.282	0.0271	7113.999	0.015354	5651.274	0.027429	7449.184	0.01795	5551.991	0.027861	7752.973	0.018654	10	66	161.1	-0.37927	-0.0689	0.241465
2	0.333333	0.666667	0.222222222	5023.7	0.025293	7377.48	0.01433	5860.58	0.0256	7725.08	0.016753	5757.62	0.026003	8040.12	0.01741		100	219.5	-0.54442	-0.31663	-0.08884
3	0.25	0.75	0.1875	5651.663	0.01897	8299.665	0.010748	6593.153	0.0192	8690.715	0.012565	6477.323	0.019503	9045.135	0.013058						
4	0.2	0.8	0.16	6028.44	0.015176	8852.976	0.008598	7032.696	0.01536	9270.096	0.010052	6909.144	0.015602	9648.144	0.010446			Qr	100	150	200
5	0.166667	0.833333	0.138888889	6279.625	0.012647	9221.85	0.007165	7325.725	0.0128	9656.35	0.008377	7197.025	0.013002	10050.15	0.008705	5	37	7535.55	489.8108	2838.391	4012.68
6	0.142857	0.857143	0.12244898	6459.043	0.01084	9485.331	0.006141	7535.031	0.010971	9932.246	0.00718	7402.654	0.011144	10337.3	0.007461		65	11066.22	-5367.12	110.6622	2849.552
7	0.125	0.875	0.109375	6593.606	0.009485	9682.943	0.005374	7692.011	0.0096	10139.17	0.006283	7556.876	0.009751	10552.66	0.006529	7.5	53	8790.87	-2241.67	1435.842	3274.599
8	0.111111	0.888889	0.098765432	6698.267	0.008431	9836.64	0.004777	7814.107	0.008533	10300.11	0.005584	7676.827	0.008668	10720.16	0.005803		80	11587.62	-9038.34	-2163.02	1274.638
9	0.1	0.9	0.09	6781.995	0.007588	9959.598	0.004299	7911.783	0.00768	10428.86	0.005026	7772.787	0.007801	10854.16	0.005223	10	66	8636.43	-5276.86	-639.096	1679.786
10	0.090909	0.909091	0.082644628	6850.5	0.006898	10060.2	0.003908	7991.7	0.006982	10534.2	0.004569	7851.3	0.007092	10963.8	0.004748		100	12060.18	-14411.9	-5587.88	-1175.87
100	0.009901	0.990099	0.00980296	7460.941	0.000751	10956.65	0.000426	8703.832	0.00076	11472.89	0.000498	8550.921	0.000772	11940.77	0.000517						
1000	0.000999	0.999001	0.000998003	7528.022	7.58E-05	11055.16	4.29E-05	8782.088	7.67E-05	11576.04	5.02E-05	8627.802	7.79E-05	12048.13	5.22E-05			Pd	100	150	200
																5	37	0.075879	0.070947	0.047298	0.035473
																	65	0.04299	0.06384	0.04256	0.03192
																7.5	53	0.0768	0.096384	0.064256	0.048192
																	80	0.05026	0.089463	0.059642	0.044731
																10	66	0.07801	0.125674	0.083783	0.062837
																	100	0.05223	0.114645	0.07643	0.057322

Bibliography

[1] United States Army Research Laboratory (ARL) Micro Autonomous Systems and Technology (MAST) Collaborative Technology Alliance (CTA) Final Program Announcement (PA) W911NF-06-R-0006. September 2006.

[2] A. Mitsos, B. Chachuat, P. Barton. What is the design objective for portable power generation: Efficiency or energy density? *J. Power Sources* 164 (2007) 678-687.

[3] J.D. Holladay, E.O. Jones, R.A. Dagle, G.G. Xia, C. Cao, Y. Wang. High efficiency and low carbon monoxide micro-scale methanol processors, *J. Power Sources* 131 (2004) 69-72.

[4] F. Bohorquez, P. Samuel, J. Sirohi, D. Pines, L. Rudd, R. Perel. Design, analysis and hover performance of a rotary wing micro air vehicle. *J. Amer. Helicopter Soc*. 48 (2003) 80-90.

[5] S. Menon. Performance measurement and scaling in small internal combustion engines, Master Thesis 2006.

[6] S. Yao, X. Tang, C. Hsieh, Y. Alyousef, M. Vladimer, Gary K. Fedder, C. Amon. Micro-electro-mechanical systems (MEMS)-based micro-scale direct methanol fuel cell development, *Energy* 31 (2006) 636-649.

[7] National Renewable Energy Laboratory. Go/No-Go recommendation for sodium borohydride for on-board vehicle hydrogen storage. NREL/MP-150-42220 November 2007.

[8] S. Menon, N. Moulton, C.P. Cadou. Development of a Dynamometer for Measuring Small Internal-Combustion Engine Performance, *J. Propulsion and Power* 23 (2007) 194-202.

[9] D. Chrenko, S. Lecoq, E. Herail, D. Hissel, M.C. Pe´ra. Static and dynamic modeling of a diesel fed fuel cell power supply, *Inter. J. Hydrogen Energy* 35 (2010) 1377-1389.

[10] P. Bubna, D. Brunner, J. Gangloff Jr., S. Advani, A. Prasad. Analysis, operation and maintenance of a fuel cell/battery series-hybrid bus for urban transit applications, *J. Power Sources* 195 (2010) 3939-3949.

[11] S. Yu, J. Han, S.M. Lee, Y.D. Lee, K.Y. Ahn. A Dynamic Model of PEMFC System for the Simulation of Residential Power Generation, *J. Fuel Cell Sci and Tech* 7 (2010) #061009.

[12] J. Hu, J. Pearlman, G.S. Jackson, C. Tesluk. Evaluating the impact of enhanced anode CO tolerance on performance of proton-exchange-membrane fuel cell systems fueled by liquid hydrocarbons, *J. Power Sources* 195 (2010) 1926-1935.

[13] J.B. Pearlman, A. Bhargav, E.B. Shields, G.S. Jackson, P.L. Hearn. Modeling Efficiency and Water Balance in PEM Fuel Cell Systems with Liquid Fuel Reforming and Hydrogen Membranes, *J. Power Sources* 185 (2008) 1056-1065.

[14] E. D. Doss, R. Kumar, R. K. Ahluwalia, M. Krumpelt. Fuel processors for automotive fuel cell systems: a parametric analysis. *J. Power Sources* 102 (2001) 1-15.

[15] R. K. Ahluwalia, E. D. Doss, R. Kumar. Performance of high-temperature polymer electrolyte fuel cell systems. *J. Power Sources* 117 (2003) 45-60.

[16] T. Brown, J. Brouwer, G. S. Samuelsen, F. Holcomb, J. King. Dynamic first principles model of a complete reversible fuel cell system, *J. Power Sources* 182 (2008) 240–253.

[17] A. Mitsos, I. Palou-Rivera, P.I. Barton. Alternatives for Micropower Generation Processes, *Industrial & Engineering Chemistry Research* 43 (2004) 74-84.

[18] V.B. Oliveira, D.S. Falcão, C.M. Rangel, A.M.F.R. Pinto. Heat and Mass Transfer Effects in a Direct Methanol Fuel Cell: A 1D Model, *Inter. J. of Hydrogen Energy* 33 (2008) 3818-3828.

[19] L. Xianglin, H. Yaling, Y. Benhao, M. Zheng, L. Xiaoyue. Exergy Flow and Energy Utilization of Direct Methanol Fuel Cells based on a Mathematic Model, *J. Power Sources* 178 (2008) 344-352.

[20] N. Benavides, P. Chapman. Mass Optimal Design Methodology for DC-DC Converters in Low-Power Portable Fuel Cell Applications, *IEEE Trans. Power Electronics* 23 (2008) 1545-1555.

[21] A. Klerke, C. H. Christensen, J. Nørskov, T. Vegge. Ammonia for hydrogen storage: challenges and opportunities, *J. Mater. Chem*. 18 (2008) 2304–2310.

[22] X. Zhang, J. Yan, S. Han, H. Shioyama, K. Yasuda. A high performance anion exchange membrane-type ammonia borane fuel cell, *J. Power Sources* 182 (2008) 515-519.

[23] C. Ponce de Leon, F. Walsh, D. Pletcher, D. Browning, J. Lakeman. Direct borohydride fuel cells, *J. Power Sources* 155 (2006) 172-181.

[24] T. Umegaki, J. Yan, X. Zhang, H. Shioyama, N. Kuriyama, Q. Xu. Boron- and nitrogen-based chemical hydrogen storage materials, *Inter. J. Hydrogen Energy* 34 (2009) 2303-2311.

[25] Q. Zhang, G. Smith, Y. Wu. Catalytic hydrolysis of sodium borohydride in an integrated reactor for hydrogen generation, *Inter. J. Hydrogen Energy* 32 (2007) 4731-4735.

[26] L. Arana, S. Schaevitz, A. Franz, M. Schmidt, K. Jensen. A microfabricated suspended-tube chemical reactor for thermally efficient fuel processing, *J. Microelectromechanical Systems* 12 (2003) 600-612.

[27] B. Chachuat, A. Mitsos, P. Barton. Optimal design and steady-state operation of micro power generation employing fuel cells, *Chemical Engineering Science* 60 (2005) 4535 – 4556.

[28] J.C. Ganley, F.S. Thomas, E.G. Seebauer, and R.I. Masel. A priori catalytic activity correlations: the difficult case of hydrogen production from ammonia, *Catal. Lett*. 96 (2004) 117–122.

[29] J. Ganley, E. Seebauer, R. Masel. Porous anodic alumina microreactors for production of hydrogen from ammonia, *AIChE J*. 50 (2004) 829–834.

[30] J. Ganley, E. Seebauer, R. Masel. Development of a microreactor for the production of hydrogen from ammonia, *J. Power Sources* 137 (2004) 53–61.

[31] R.Z. Sørensen, A. Klerke, U. Quaade, S. Jensen, O. Hansen, and C. H. Christensen. Promoted Ru on high-surface area graphite for efficient miniaturized production of hydrogen from ammonia, *Catal. Lett*. 112 (2006) 77-81.

[32] N. Sifer, K. Gardner. An analysis of hydrogen production from ammonia hydride hydrogen generators for use in military fuel cell environments, *J. Power Sources* 132 (2004) 135–138.

[33] F. Uribe, S. Gottesfeld, T. Zawodzinski Jr. Effect of ammonia as potential fuel impurity on proton exchange membrane fuel cell performance, *J. Electrochem.l Soc*. 149 (3) (2002) A2930A296.

[34] A. Casanovas, M. Saint-Gerons, F. Griffon, J. Llorca. Autothermal generation of hydrogen from ethanol in a microreactor, *Inter. J. Hydrogen Energy* 33 (2008) 1827-1833.

[35] D. Behrens, I. Lee, C.M. Waits. Catalytic combustion of alcohols for microburner applications, *J. Power Sources* 195 (2010) 2008-2013

[36] M. Lee, M. Werhahn, D. Hwang, N. Hotz, R. Greif, D. Poulikakos, C. Grigoropoulos. Hydrogen production with a solar steam-methanol reformer and colloid nanocatalyst, *Inter. J. Hydrogen Energy* 35 (2010) 118-126.

[37] J. Jang, Y. Huang, C. Cheng. The effects of geometric and operating conditions on the hydrogen production performance of a micro methanol steam reformer, *Chem. Eng. Science* 65 (2010) 5495-5506

[38] C. Jung, A. Kundu, B. Ku, J. Gil, H. Lee, J. Jang. Hydrogen from aluminum in a flow reactor for fuel cell applications, *J. Power Sources* 175 (2008) 490–494.

[39] B. Bae, B. Kho, T. Lim, I. Oh, S. Hong, H. Ha. Performance evaluation of passive DMFC single cells, *J. Power Sources* 158 (2006) 1256-1261.

[40] G.G.M. Fournier, I.W. Cumming, K. Hellgardt. High performance direct ammonia solid oxide fuel cell, *J. Power Sources* 162 (2006) 198-206

[41] N. Fujiwara, Z. Siroma, S. Yamazaki, T. Ioroi, H. Senoh, K. Yasuda. Direct ethanol fuel cells using an anion exchange membrane, *J. Power Sources* 185 (2008) 621-626.

[42] H. Kim. Passive direct methanol fuel cells fed with methanol vapor, *J. Power Sources* 162 (2006) 1232-1235.

[43] S. Eccarius, X. Tian, F. Krause, C. Agert. Completely passive operation of vapor-fed direct methanol fuel cells for portable power applications, *J. Micromech. Microeng*. 18 (2008) #104010.

[44] Q. Ye, T.S. Zhao. A natural-circulation fuel delivery system for direct methanol fuel cells, *J. Power Sources* 147 (2005) 196-202.

[45] K. Jeng, C. Chien, N Hsu, S. Yen, S. Chiou, S. Lin, W. Huang. Performance of direct methanol fuel cell using carbon nanotube-supported Pt–Ru anode catalyst with controlled composition, *J. Power Sources*, 160 (2006) 97-104.

[46] M. Hasani-Sadrabadi, S. Emami, H. Moaddel. Preparation and characterization of nanocomposite membranes made of poly(2,6-dimethyl-1,4-phenylene oxide) and montmorillonite for direct methanol fuel cells, *J. Power Sources* 183 (2008) 551-556.

[47] A. Tian, J. Kim, J. Shi, K. Kim. Poly(1-vinylimidazole)/Pd-impregnated Nafion for direct methanol fuel cell applications, *J. Power Sources* 183 (2008) 1-7.

[48] J. Park, J. Lee, J. Kim, S. Han, I. Song. Stable operation of air-blowing direct methanol fuel cells with high performance, *J. Power Sources* 179 (2008) 1-8.

[49] S. Hwang, H. Joh, M. A. Scibioh, S. Lee, S. Kim, T. Lee, H. Ha. Impact of cathode channel depth on performance of direct methanol fuel cells, *J. Power Sources* 183 (2008) 226-231.

[50] S. Rousseau, C. Coutanceau , C. Lamy, J.-M. Leger. Direct ethanol fuel cell (DEFC): Electrical performances and reaction products distribution under operating conditions with different platinum-based anodes, *J. Power Sources* 158 (2006) 18-24.

[51] Q. Wang, G.Q. Sun, L. Cao, L.H. Jiang, G.X. Wang, S.L. Wang, S.H. Yang, Q. Xin. High performance direct ethanol fuel cell with double-layered anode catalyst layer, *J. Power Sources* 177 (2008) 142–147.

[52] C. Pan, H. Wu, C. Wang, B. Wang, L. Zhang, Z. Cheng, P. Hu, W. Pan, Z. Zhou, X. Yang, J. Zhu. Nanowire-Based High-Performance ‘‘Micro Fuel Cells’’: One Nanowire, One Fuel Cell, *Adv. Mater*. 20 (2008) 1644–1648.

[53] A. Verma, S. Basu. Direct alkaline fuel cell for multiple liquid fuels: Anode electrode studies, *J. Power Sources* 174 (2007) 180-185.

[54] K. Scott, E. Yu, G. Vlachogiannopoulos, M. Shivare, N. Duteanu. Performance of a direct methanol alkaline membrane fuel cell, *J. Power Sources* 175 (2008) 452-457.

[55] Y. Wang, L. Li, L. Hu, L. Zhuang, J. Lu, B. Xu. A feasibility analysis for alkaline membrane direct methanol fuel cell: thermodynamic disadvantages versus kinetic advantages, *Electrochem. Communications* 5 (2003) 662-666.

[56] A. Verma, A. K. Jha, S. Basu. Evaluation of an alkaline fuel cell for multifuel system, *J. Fuel Cell Science and Tech*. 2 (2005) 234-237.

[57] A. Verma, S. Basu. Experimental evaluation and mathematical modeling of a direct alkaline fuel cell, *J. Power Sources* 168 (2007) 200-210.

[58] H. Bunazawa, Y. Yamazaki. Influence of anion ionomer content and silver cathode catalyst on the performance of alkaline membrane electrode assemblies (MEAs) for direct methanol fuel cells (DMFCs), *J. Power Sources* 182 (2008) 48-51.

[59] C.C. Yang, S.J. Chiu, C.T. Lin. Electrochemical performance of an air-breathing direct methanol fuel cell using poly(vinyl alcohol)/ hydroxyapatite composite polymer membrane, *J. Power Sources* 177 (2008) 40-49.

[60] C.C. Yang, S.J. Chiu, K.T. Lee, W.C. Chien, C.T. Lin, C.A. Huang. Study of poly(vinyl alcohol)/titanium oxide composite polymer membranes and their application on alkaline direct alcohol fuel cell, *J. Power Sources* 184 (2008) 44-51.

[61] R. Jayashree, D. Egas, J. Spendelow, D. Natarajan, L. Markoski, P. Kenis. Air breathing laminar flow-based direct methanol fuel cell with alkaline electrolyte, *Electrochem. and Solid State Letters* 9 (2006) A252-A256.

[62] R. Jayashree, L. Gancs, E. Choban, A. Primak, D. Natarajan, L. Markoski, P. Kenis. Air-Breathing Laminar Flow-Based Microfluidic Fuel Cell. *J. Am. Chem. Soc.* 127 (2005) 16758-16759.

[63] J. Hayes, A. Engstrom, C. Friesen. Orthogonal flow membraneless fuel cell, *J. Power Sources* 183 (2008) 257-259.

[64] A. Y. Tsivadze, M. R. Tarasevich, B. N. Efremov, N. A. Kapustina, and P. V. Mazin. A fuel cell with a cation-exchange membrane for direct oxidation of ethanol in an alkaline medium, *Physical Chemistry* 415 (2007) 234-236.

[65] N. Maffei, L. Pelletier, J.P. Charland, A. McFarlan. An intermediate temperature direct ammonia fuel cell using a proton conducting electrolyte, *J. Power Sources* 140 (2005) 264-267.

[66] L. M. Zhang, W. S. Yang. Direct ammonia solid oxide fuel cell based on thin proton-conducting electrolyte, *J. Power Sources* 179 (2008) 92-95.

[67] J. Ganley. An intermediate-temperature direct ammonia fuel cell with a molten alkaline hydroxide electrolyte, *J. Power Sources* 178 (2008) 44–47.

[68] C. Rice, S. Ha, R. Masel, P. Waszczuk, A. Wieckowski, T. Barnard. Direct formic acid fuel cells, *J. of Power Sources* 111 (2002) 83-89.

[69] Y. Rhee, S. Ha, R. Masel. Crossover of formic acid through Nafion® membranes, *J. Power Sources* 117 (2003) 35-38.

[70] P. Waszczuk, T. Barnard, C. Rice, R. Masel, A. Wieckowski. A nanoparticle catalyst with superior activity for electrooxidation of formic acid + Erratum, *Electrochemistry Communications* 4 (2002) 599-603.

[71] C. Rice, S. Ha, R. Masel, A. Wieckowski. Catalysts for direct formic acid fuel cells, *J. Power Sources* 115 (2003) 229-235.

[72] M. Zhao, C. Rice, R. Masel, P. Waszczuk, A. Wieckowski. Kinetic study of electro-oxidation of formic acid on spontaneously-deposited Pt/Pd nanoparticles - CO tolerant fuel cell chemistry, *J. Electrochem. Soc*. 151 (2004) A131-A136.

[73] S. Ha, C. Rice, R. Masel, A. Wieckowski. Methanol conditioning for improved performance of formic acid fuel cells, *J. Power Sources* 112 (2002) 655-659.

[74] S. Ha, B. Adams, R. Masel. A miniature air breathing direct formic acid fuel cell, *J. Power Sources*, 128 (2004) 119-124.

[75] Y. Zhu, S. Ha, R. Masel. High power density direct formic acid fuel cells, *J. Power Sources* 130 (2004) 8-14.

[76] S. Ha, Z. Dunbar, R. Masel. Characterization of a high performing passive direct formic acid fuel cell. *J. Power Sources* 158 (2006) 129-136.

[77] Y. Zhu, Z. Khan, R. Masel. The behavior of palladium catalysts in direct formic acid fuel cells, *J. Power Sources* 139 (2005) 15-20.

[78] R. Larsen, J. Zakzeski, R. Masel. Unexpected activity of palladium on vanadia catalysts for formic acid electro-oxidation, *Electrochem. Solid State Lett*. 8 (2005) A291–A293.

[79] S. Ha, R. Larsen, R. Masel. Performance characterization of Pd/C nanocatalyst for direct formic acid fuel cells, *J. Power Sources* 144 (2005) 28-34.

[80] R. Larsen, S. Ha, J. Zakzeski, R. Masel. Unusually active palladium-based catalysts for the electrooxidation of formic acid, *J. Power Sources* 157 (2006) 78-84.

[81] S. Gold, K. Chu, C. Lu, M. Shannon, R. Masel. Acid loaded porous silicon as a proton exchange membrane for micro-fuel cells, *J. Power Sources* 135 (2004) 198-203.

[82] K. Chu, S. Gold, V. Subramanian, C. Lu, M. Shannon, R. Masel. A nanoporous silicon membrane electrode assembly for on-chip micro fuel cell applications, *J. Microelectromechanical Systems* 15 (2006) 671-677.

[83] K. Chu, M. Shannon, R. Masel. An improved miniature direct formic acid fuel cell based on nanoporous silicon for portable power generation, *J. Electrochem. Soc.* 153 (2006) A1562-A1567.

[84] K. Chu, M. Shannon, R. Masel. Porous silicon fuel cells for micro power generation. *J. Micromech. Microeng.* 17 (2007) S243–S249.

[85] C. Miesse, W. Jung, K. Jeong, J. Lee, J. Lee, J. Han, S. Yoon, S. Nam, T. Lim, S. Hong. Direct formic acid fuel cell portable power system for the operation of a laptop computer, *J. Power Sources* 162 (2006) 532–540.

[86] N. Fujiwara, K. Yasuda, T. Ioroi, Z. Siroma, Y. Miyazaki, and T. Kobayashi. Direct Polymer Electrolyte Fuel Cells Using L-Ascorbic Acid as a Fuel, *Electrochem. and Solid-State Letters* 6 (2003) A257-A259.

[87] N. Fujiwara, S. Yamazaki, Z. Siroma, T. Ioroi, K. Yasuda. Direct oxidation of L-ascorbic acid on a carbon black electrode in acidic media and polymer electrolyte fuel cells, *Electrochem. Communications* 8 (2006) 720–724.

[88] R. Peterson, B. Paul, T. Palmer, Q.Wu, W. Jost, C. H. Tseng, S. Tiwari, G. Patello, E. Buck, J. Holladay, R. Shimskey, P. Humble, P. MacFarlan and J. Wainright. Radiolytic microscale power generation based on single chamber fuel cell operation, *J. Micromech. Microeng.* 17 (2007) S250–S256.

[89] Y. Cengel, M. Boles. Thermodynamics: An Engineering Approach. McGraw-Hill, 2001.

[90] http://www.micropumps.co.uk/TCSM100range.htm, Webpage accessed on September 10, 2009.

[91] http://scm.asianproducts.com/manufacturer/index.php?op=product&item_ id=P11973436037337577&cno=A11141394990710142, Webpage accessed on July 24, 2009.

[92] http://www.jarothermal.com/web-settings/catalog/AD/1.pdf, Webpage accessed on July 24, 2009.

[93] http://www.russellind.com/Conco/indek/fans/k/ kd2008.htm, Webpage accessed on July 24, 2009.

[94] *http://www.a123systems.com/a123/products*, Webpage accessed on February 24, 2010.

[95] Y. Cengel, J. Cimbala. Fluid Mechanics: Fundamentals and Applications. McGraw-Hill, 2006